The Effect of Frosting on the Performance of Domestic Refrigerator-Freezer Finned Tube Evaporator Coils

R. W. Rite and R. R. Crawford

ACRC TR-01 August 1990

For additional information:

Air Conditioning and Refrigeration Center
University of Illinois
Mechanical & Industrial Engineering Dept.
1206 West Green Street
Urbana, IL 61801

(217) 333-3115

Prepared as part of ACRC Project 02
Effect of Frost Formation on Evaporator Performance in Domestic Refrigerator Freezers
R. R. Crawford, Principal Investigator

The Air Conditioning and Refrigeration Center was founded in 1988 with a grant from the estate of Richard W. Kritzer, the founder of Peerless of America Inc. A State of Illinois Technology Challenge Grant helped build the laboratory facilities. The ACRC receives continuing support from the Richard W. Kritzer Endowment and the National Science Foundation. The following organizations have also become sponsors of the Center.

Acustar Division of Chrysler
Amana Refrigeration, Inc.
Brazeway, Inc.
Carrier Corporation
Caterpillar, Inc.
Delphi Harrison Thermal Systems
E. I. du Pont de Nemours & Co.
Eaton Corporation
Electric Power Research Institute
Ford Motor Company
Frigidaire Company
General Electric Company
Lennox International, Inc.
Modine Manufacturing Co.
Peerless of America, Inc.
U. S. Army CERL
U. S. Environmental Protection Agency
Whirlpool Corporation

For additional information:

Air Conditioning & Refrigeration Center
Mechanical & Industrial Engineering Dept.
University of Illinois
1206 West Green Street
Urbana IL 61801

217 333 3115

THE EFFECT OF FROSTING ON THE PERFORMANCE OF DOMESTIC REFRIGERATOR-FREEZER FINNED TUBE EVAPORATOR COILS

Raymond Walter Rite, M.S.

Department of Mechanical and Industrial Engineering
University of Illinois at Urbana-Champaign, 1990

ABSTRACT

The effect of frost formation on the performance of a domestic refrigerator-freezer evaporator coil was investigated. A low temperature evaporator test facility was developed to closely simulate refrigerator-freezer conditions. The rate of frost deposition on the evaporator was determined to be constant with respect to time for a ten-hour testing period over a range of air inlet temperatures and relative humidities, refrigerant temperatures, and airflow rates. Higher humidities and air inlet temperatures and lower refrigerant temperatures were found to increase the frosting rate significantly. Varying the airflow rate was found to slightly affect the frosting rate. Increasing the airflow rate increased the frosting rate a small amount, while decreasing the airflow rate decreased the frosting rate an equally small amount. However, it appears that the actual correlation between airflow rate and frosting rate is not this straight-forward, but is, instead, the result of the influences of the mass transfer coefficient, the evaporator surface temperature, and the air moisture capacity. How these factors balance one another determines the actual relationship between frost rate and airflow rate. In addition to these findings, it was found that the UA-value of the evaporator increased as frost was deposited on the coil while a constant airflow rate was maintained through the coil. The increase at the highest frosting rates was on the order of 40% but was accompanied by an exponentially increasing air side pressure drop.

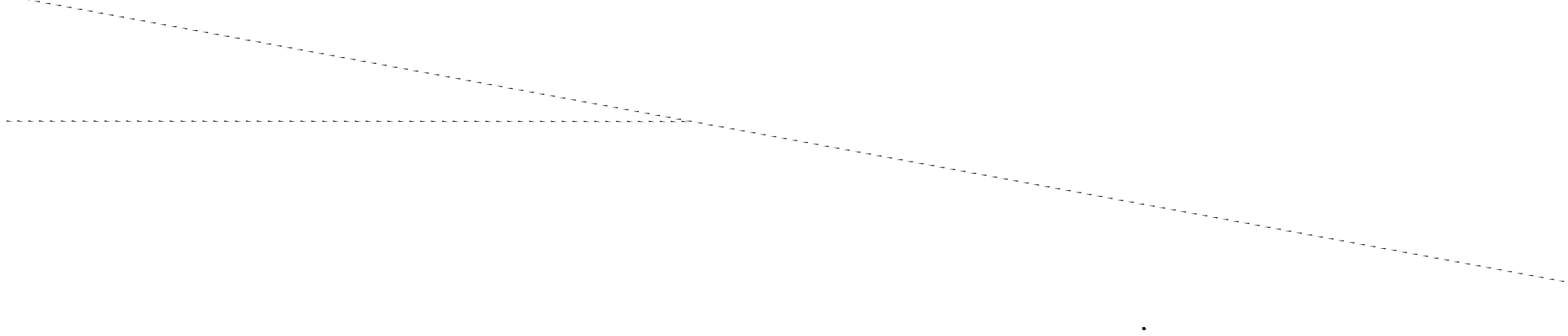

TABLE OF CONTENTS

Page

LIST OF TABLES

LIST OF FIGURES

Chapter 1

INTRODUCTION

1.1 Objectives

Condensation occurs on any surface exposed to moist air whenever the temperature of that surface is below the dew point of the moist air that it is in contact with. If this dew point is below 32 F (0 C), the condensate will freeze and a layer of frost will form on the surface. This process occurs continually on the evaporator coil of any refrigerator-freezer or freezer, and can occur on the evaporator of a heat pump during winter months. The purpose of the following study is to evaluate the effect of this frost on the performance of the evaporator and to determine how various environmental conditions affect the growth rate of this frost. Automatic defrost domestic refrigerator-freezer evaporators in particular will be the focus of this work. Although many studies of the effects of frosting on various heat exchangers and surfaces (i.e. flat plates, annuli, and cylinders) have been done, this will be one of the first studies of evaporators that are extensively used in domestic refrigerator-freezers with relatively low air velocities. In addition, in contrast to previous studies on a variety of heat exchangers which largely dealt with single-phase flow on both sides of the heat exchanger, this work entails two-phase flow on the low temperature side of the exchanger. The reason for incorporating this added level of complexity into the overall system is a desire to operate the evaporator for these studies in as close a manner to their actual operation in the field as is possible. It is hoped that by doing this the results will more closely correlate with actual refrigerator-freezer performance.

The evaluation of frost's effect on evaporator coil performance will involve quantitatively studying the change in the overall heat transfer coefficient of the coil and its air side pressure drop as frost forms under a variety of conditions. In addition, the influence of these various conditions

(e.g., evaporator air and refrigerant inlet temperatures, relative humidity and airflow rate) on the rate of frost formation will also be quantitatively examined. The determination of how all three of these parameters change should allow for a much better understanding of how frosting affects refrigerator performance and the optimization of the evaporator coil defrost procedure.

1.2 Background

The evaporator frost study is part of a continuing research effort in all areas of refrigeration and air conditioning by the faculty and students in the Department of Mechanical and Industrial Engineering at the University of Illinois, Urbana-Champaign under the auspices of the Air Conditioning and Refrigeration Center (ACRC). The ACRC is a National Science Foundation industry-university cooperative research center which was formed in November of 1989.

Many of the components that are part of the present evaporator frosting facility were originally used in a finned tube evaporator evaluation study done by O'Neill (1988). O'Neill, using basically the same evaporators that will be studied here, determined effectivenesses and overall heat transfer coefficients for the non-frosted coils under a number of conditions. After the successful completion of that work, further modifications were undertaken by Heflin (1989) in order to adapt the set-up for two-phase flow and frosting studies. This author continued the modifications begun by Heflin to the point that the facility is now capable of providing the data on frosting that is to be presented in the following chapters.

Chapter 2

LITERATURE REVIEW

2.1 Introduction

A great deal of research has been done on the formation of frost on surfaces that are cooled to temperatures that are less than or equal to the frost point of the humid air flowing over it. This research includes studies of simple surface geometries as well as entire heat exchangers. The simple surfaces include flat plates, annuli, and cylinders. Among the flat plate work are papers by Barron and Han (1965), Yamakawa, Takahashi, and Ohtani (1972), Jones and Parker (1975), Hayashi, Aoki, and Yuhara (1977), Schulte and Howell (1982), O'Neal and Tree (1984), and Sami and Duong (1989). Annuli were studied by Beatty, Finch, and Schoenborn (1951), Kamei, Mizushina, Kifune, and Koto (1952), Chen and Rohsenow (1964), and Marinyuk (1980). Lastly, frosting on cylindrical surfaces was examined by Chung and Algren (1958), Stoecker (1960), Schneider (1978), and Parish and Sepsy (1972). An extensive review of all of these papers may be found in Heflin (1989).

In addition to the research on simple geometries, extensive work has also been done on actual heat exchangers. The emphasis of this literature review will be on these papers, specifically the ones dealing with finned tube heat exchanger coils. However, in later chapters some further reference will be made to some of the flat plate and cylindrical studies listed above. This reference will be in regard to, first of all, the properties of frost that were experimentally determined in these studies, specifically thermal conductivity and density. How these two properties vary with various parameters such as air temperature, surface temperature, air velocity, and relative humidity will play a crucial role in the explanation of the experimental results that will be presented in Chapter 6. Secondly, two of the simple geometry studies will be used for comparison purposes with the data

generated in this study. This can be justified based on the fact that the evaporator geometry basically involves a conglomeration of cylindrical tubes and flat plates

2.2 Frosting of Finned Tube Heat Exchangers

The majority of frost research that has been done on finned tube heat exchangers has been limited to heat exchangers with inlet air temperatures at or above freezing. Most often the heat exchangers have been evaporators for heat pumps. This means that the air side temperatures that the evaporator is exposed to are significantly higher than the temperatures encountered in this study and, of course, the corresponding refrigerant inlet temperatures are also higher. Also, the airflow rates tend to be substantially higher than the 40 to 80 cfm (ft^3/min) (17 to 34 L/s) examined here. Despite these differing conditions, however, an examination of the literature is still worthwhile for the purpose of seeing if the results found at these higher temperatures correlate with the lower temperature results from this study. If they do correlate well, obviously the original results are valid over a wider temperature and airflow rate range than originally thought.

One of the first heat exchanger frosting studies was done by Stoecker (1957). In this study two finned coils were examined. One had a fin spacing of nine per inch (2.8 mm/fin) and the other had a spacing of four per inch (6.4 mm/fin). Two types of tests were run on both coils. In one the airflow was kept constant by opening a damper, in the other the flow rate was allowed to decrease as the coil became increasingly blocked with frost. In the first set of tests, airflow rates of 540, 960, and 1450 cfm (250, 450, and 683 L/s) were maintained through the coil. For a face area of 21.5 x 21.0 in. (0.546 x 0.533 m), this corresponds to 172 ft/min (52 m/min), 306 ft/min (93 m/min), and 462 ft/min (141 m/min), respectively. The entering air temperature was maintained at 32 F (0 C) with 72% relative humidity, and the glycol-water temperature inside the tubes was 16 F (-8.9 C).

Stoecker found that at the early stages of frost formation the overall heat transfer coefficient, U, of the coil based on the log-mean-temperature-difference between the air and the refrigerant and on the air side surface area of the frost-free coil increases until 2.0-3.0 lb_m (0.9-1.4 kg) of frost are accumulated and then begins to decrease. It was conjectured that the initial increase may be due to the extended surface area afforded by the initial frost or the increase in air velocity over the surface due to the decreased passage areas. The decrease in the U value after further accumulation of frost was not found to be significant, however, even up to 7.0 lb_m (3.2 kg) of frost accumulation.

In the second set of tests, the airflow rate started out at 1370 cfm (647 L/s) and was reduced to 540 cfm (250 L/s) with 6.5 lb_m (2.9 kg) of frost on the coil. It was found that the refrigerant temperature had to be decreased by approximately 9.0 F (-13 C) with the 6.5 lb_m of frost in order to maintain the original refrigeration capacity of one ton. This represents a significant reduction in heat transfer.

A comparison of the performance of the 9 fins per inch (fpi) coil and the 4 fpi coil showed that at light frost accumulations the 9 fpi coil had greater capacity than the 4 fpi coil. After large amounts of frost are deposited, the 4 fpi coil showed better performance because less blockage occurred in this coil.

Wagner (1963) studied a plate finned tube heat exchanger under frosting conditions. Air face velocities across the coil for this study ranged from 42 to 117 ft/min (13 to 35.7 m/min) which corresponds to 25 to 70 cfm (12 to 33 L/s) given a face area of 0.595 ft^2 (0.0553 m^2). The inlet air temperature was 70 F (21 C) and the inlet relative humidity ranged from 29 to 86%. The single phase refrigerant inlet temperature was maintained at 0 F (-18 C). Wagner's results were similar to Stoecker's in that there was an initial increase in the heat transfer coefficient as frosting commenced and then a gradual, small decrease in the coefficient as more and more frost accumulated on the coil while airflow was kept constant. Wagner also found that an increase in velocity increased the rate

of frost formation and the heat transfer coefficient between the air and refrigerant. An increase in humidity at a fixed velocity also was found to increase both the frost formation rate and the heat transfer coefficient. Overall, the frost had the most significant effect on the pressure drop through the coil. The sharp increase in pressure drop translates into a decrease in airflow if that parameter was not artificially maintained constant by means of a damper.

Production-type air conditioning coils were studied under frosting conditions by Gates, Sepsy, and Huffman (1967). The coils that were tested had fin densities varying from 2 to 16 fpi (13 to 1.6 mm/fin)with from one to six tube rows. Coil face velocities of between 110 and 770 fpm (33.5 and 235 m/min) were maintained through the coils. The airflow rate through the coil was maintained constant during the frosting process. The results of the first part of their study showed that once again the increase in the pressure drop across the coil was the parameter most affected by the frosting process. In addition, heat transfer coefficients were found to increase with air velocity and decrease as the humidity ratio of the incoming air stream was increased.

In the second part of the air conditioning coil study, Huffman and Sepsy (1967), dimensionless correlations relating heat transfer and pressure loss to frost formation are provided. It was found that the number of tube rows had only a slight effect on the heat transfer but a significant effect on the pressure drop. The heat transfer dimensionless parameter and the pressure loss parameter decreased with increasing fin pitch.

Lotz (1967) examined a coil with a fin spacing of 2.5 fpi (10.2 mm/fin). In this study the entering air temperature to the coil was varied between 32 F (0 C) and -4 F (-20 C) and the relative humidity was varied between 45 and 80%. The airflow rate through the coil was maintained between 0.6 and 4.5 cfm (0.3 to 2.2 L/s). As in Stoecker's original study, the heat transfer coefficients were found to increase initially as frosting began and then decrease due to the

insulating effect of the frost layer. Lotz conjectured that the reason for the initial increase was due to the roughness that was added to the surfaces by the first growth of ice crystals.

Although the air side heat transfer coefficient changed, the pressure drop through the coil was found to be the most affected parameter by frost build up. This fact led Lotz to recommend that pressure drop be the controlling factor in the determination of defrost time.

Sanders (1975) undertook an extensive examination of the frost formation process. In his work, the frosting of air coolers as well as frost formation on a flat plate geometry were analyzed experimentally. The experimental conditions examined included air velocities of 10 ft/s (3.0 m/s), 20 ft/s (6.0 m/s), and 26 ft/s (8.0 m/s), air temperatures of 14 F (-10 C), 23 F (-5.0 C), and 30 F (-1.0 C) and dew point temperatures of 20 F (-6.6 C) and 26 F (-3.5 C). Sanders found that the Nusselt number was substantially larger under frosted conditions than for a clean coil and that the Nusselt number increased with increasing Reynolds number for both cases at approximately the same rate. He attributed this larger Nusselt number to the roughness of the frosted surface. It was also shown that the ratio of the Nusselt number with frost to the Nusselt number with a clean surface increases as the frost thickness increases up to a certain point. After this point the ratio remains constant.

Another aspect of frosting that Sanders considered was the effect of air velocity, air temperature, and humidity on the rate of frost formation. He found that initially a higher velocity resulted in a thicker layer of frost, but over longer time periods the growth rate of the frost diminished and was eventually surpassed by the growth rate at lower velocities. Higher air temperatures resulted in lower frost growth rates and higher humidities resulted in higher frost growth rates.

A third frosting parameter that Sanders examined was the effect of the same three parameters discussed above (air velocity, air temperature, and humidity) on the density of the frost that is formed. He found that the density of the frost was greater for greater air velocities. Lower air temperatures and higher dew points (i.e., higher humidities) resulted in lower frost densities.

In addition to the experimental results provided by Sanders, there is also a rather thorough literature review of previous frosting studies. Some of the key results that are given here include the finding that as the density of the frost increases its thermal conductivity also increases. Also, Sanders found that there is considerable disagreement among researchers as to whether air velocity has an effect on frosting rate. Some work has shown a relation between the two while other work has not. It appears that there is a relation at low Reynolds numbers but that there is no relation at higher Reynolds numbers.

Frosting and defrosting effects on coil heat transfer were discussed by Niederer (1976). Niederer studied finned tube air coolers with 5/8 in. (16 mm) O. D. tubes, 1 3/4 in. (45 mm) on centers and staggered 12 tubes in the face, and 8 rows in the direction of the airflow with a fin length of 102 in. (2.59 m). Air coolers with four different fin patterns were examined. These patterns included a heat exchanger with 6 fpi (4.2 mm/fin), 4 fpi (6.4 mm/fin), and two with a variable number of fins. Ammonia was used as the refrigerant in the cooler and the evaporator was run in a flooded condition so as to maintain a constant refrigerant temperature of 20 F (-6.7 C) throughout the heat exchanger. The air inlet temperature was maintained at 32 F (0.0 C) with a relative humidity of 85%. The airflow through the coil was allowed to vary as frost collected on the coil. The result that Niederer found was that the increase in the heat transfer coefficient on the air side of the coil due to the initial frost formation was more than offset by the reduced airflow through the coil. This led to a reduction in air cooler heat transfer capacity. Niederer also concluded that the reduction in airflow was more apparent for the closer fin spacing heat

exchangers than the wider fin spacing exchangers and the variable fin spacing coils were less affected than the constant fin spacing coils for the same amount of accumulated frost.

Gatchilov and Ivanova (1979) studied the frosting of extended surface air coolers with copper tubes and aluminum fins. Three different fin spacings for the same counterflow heat exchanger configuration were looked at: 0.30 in. (7.5 mm), 0.39 in. (10 mm) and 0.59 in. (15 mm). The environmental conditions that were set included inlet air relative humidities of 74 and 88%, an inlet air temperature of 32 F (0 C) and air velocities of between approximately 300 ft/min (91 m/min) to 1500 ft/min (457 m/min). The mean temperature difference between the air and the brine filled coil was maintained at approximately 13 F (7.0 C). The main emphasis of Gatchilov and Ivanova's work was on characterizing the effect of humidity and air velocity on frost thickness, roughness, and density. They found that over a ten-hour test period the frost thickness increased more rapidly with higher air relative humidities and higher air velocities. The surface roughness of the frost was found to be greater with higher humidities and velocities. The surface roughness is important because it influences both the pressure drop across the coil (higher friction factor) and the heat transfer coefficients on the outer tube surfaces. The density of the frost was found to increase with time, velocity, and relative humidity.

Barrow (1985) undertook an analytical study of the frosting process on plane wall surfaces and surfaces with straight fins. The two geometries that were chosen were designed to be a useful representation of the heat transfer surfaces on heat pump evaporator coils. Through this analysis, Barrow arrived at several conclusions. Comparing the insulating effect of the frost in the plane surface case with its effect when there are fins on the surface, Barrow found that the insulating effect is much less apparent when there are fins. The reason for this is that the high conductivity of the fin core material is the controlling parameter for heat transfer through the fins with the frost having a negligible influence. Therefore, the surface geometry of the fins as well as their thermal properties are important in the assessment of the effects of frosting.

Another conclusion that he came to was that the insulating effect of frost does not completely explain the reduction in heat transfer capacity of frosted evaporators. This capacity reduction is mainly due to the reduction in airflow through the coil due to the blockage of the coil. Once this premise is accepted, it can be seen that the thickness of the frost is much more important than its density or thermal conductivity as far as heat transfer is concerned. However, the thermal properties of the frost are important for predicting the growth rate of the frost.

Tantakitti and Howell (1986) developed a computer simulation model of a heat pump system under frosting conditions. The model was used to assess the effect of frosting on overall system performance in terms of its coefficient of performance (COP). It was found that the reduction in COP was directly related to the relative humidity of the inlet air flowing through the coil. At 90% relative humidity, the COP was reduced by approximately 5 percent within 60 minutes of compressor run time while at 100% inlet relative humidity the COP was reduced by over 10 percent in 46 minutes. This reduction in performance was accredited to the increased rate of frost formation precipitated by the higher humidities.

Kondepudi and O'Neal (1989) and (1990) studied frosting in heat pump evaporators with a variety of fin configurations: flat, wavy, and louvered. The following testing conditions were considered:

air velocity: 130 fpm (39.6 m/min), 200 fpm (61.0 m/min)
fin spacing: 10 fpi, 18 fpi (2.54 mm/fin, 1.4 mm/fin)
relative humidity: 65%, 80%
air inlet temperature: 32 F (0.0 C)
refrigerant temperature: <10 F (-12 C)

It was found that the louvered fins had a slightly higher frosting rate than either the wavy or flat fins and a significantly higher pressure drop. The louvered fin heat exchanger also proved to have a larger overall heat transfer coefficient than either of the other two and retained this advantage even

with an accumulation of frost. Unlike previous researchers' findings, Kondepudi and O'Neal did not find any detrimental effect on the heat transfer coefficient, enthalpy change, or effectiveness due to frost formation for the fifty-minute test duration. The tests were limited to fifty minutes because heat exchanger blockage at that point was so extensive that a constant airflow across the coil could not be maintained. Two additional findings that were made were that the frosting rate increased as relative humidity increased and as air velocity increased.

Three computer simulation models of the evaporator portion of a heat pump system under dry, wet, and frosted conditions were developed by Oskarsson, Krakow, and Lin (1990). The models consist of a detailed finite element model, a three-region model, and a parametric model. All of the models utilize a number of coefficients derived empirically by various researchers. The coefficients that were used involve heat transfer coefficients for the refrigerant and air sides of the exchanger as well as frost growth rate coefficients and pressure drop factors for both the refrigerant side and the frosted air side. One important point that must be mentioned is that no attempt was made to modify the air side heat transfer coefficient to account for the apparent augmentation provided by the initial frost formation as described by many researchers previously cited.

The finite element model which divides the evaporator into approximately fifty sections was determined to be the most accurate although it did require an extremely long time to run. It was used as a benchmark along with some experimental data to verify the accuracy of the other two models. The three-region model divides the evaporator into only three parts (two-phase region, transitional region, and superheated region), neglects the refrigerant side pressure drop, and assumes that no dehumidification of the air takes place in the superheated section of the evaporator. Although it was very fast computationally compared with the finite element model, it was found to give results in very good agreement with the finite element model. The last model, the parametric model, was determined to be satisfactory but required that different coefficients be put into the

model depending on whether the coil was dry, wet, or frosted. This model uses two parameters, the coil characteristic and the coil enthalpy effectiveness, to describe the coil performance. Data generated by the three-region model were used to develop the coefficients needed to define the coil characteristic and the effectiveness.

Senshu, Yasuda, Oguni, and Ishibane (1990) also considered the performance of heat pumps under frosting conditions. In the experimental section of their work, Senshu et al. studied the frosting of a cross-finned tube heat exchanger in an air duct with R-22 (Chlorodifluoromethane) evaporating inside of the tubes. While holding the inlet air temperature, relative humidity, and air inlet velocity constant and varying the refrigerant temperature, they found that the amount of frost on the coil increased linearly with time, and the frost formation rate became greater the more the refrigerant temperature was lowered. This indicates that the frost formation rate is constant with respect to time. They also found that if all parameters except air velocity are held constant, the frost formation rate will decrease as the air velocity is increased. This is contradictory to the results of other researchers that have been presented previously. Another result that they found which contradicts the findings of several of the other researchers is that the air side heat transfer coefficient was not found to change significantly as frost formed on the heat exchanger. Unlike the other researchers who noticed an initial increase in the overall UA-value as the frost grew on the coil and then a decrease, the results here show an essentially constant heat transfer coefficient. This discrepancy is probably due to the fact that the test times presented were not very long (~1 hour) and only a very small amount of frost had been deposited on the coil.

Based on the experimental results given above, a theoretical treatment of the performance of the heat pump evaporator under frosting conditions was then provided. This analysis was then used to develop a computer simulation model of an entire system. The results provided by the model were found to be in good agreement with experimental data from an actual heat pump.

A summary of the experimental research discussed above is shown in Table 2.2.1. In the table, fpi is the number of fins per inch that the heat exchangers that were tested had, V_{air} is the air velocity in ft/min, T_{surf} is the surface temperature of the exchanger in degrees Fahrenheit, T_{air} is the air inlet dry bulb temperature in degrees Fahrenheit, and RH is the relative humidity.

2.3 Summary

It can be seen in the preceding paragraphs that there is a substantial body of knowledge on the frosting of heat exchangers. Unfortunately, due to the vast variety of heat exchanger configurations and methods of evaluating the effect of frosting on heat exchanger performance as well as the varying properties of frost with testing conditions and time, it is extremely difficult to coordinate all of the various findings on a common basis. This probably accounts for most of the conflicting results that have been described.

The most difficult of the obstacles discussed above to overcome are the varying properties of the frost. As was shown by Trammell, Little, and Killgore (1968) and Hayashi, Aoki, Adachi, and Hori (1977) for a flat plate, the structure of the frost changes as the relative humidity and velocity of the moist air passing over the cold surface changes and as the temperature of the plate changes. They found that this structural change alters both the density of the frost and the surface architecture. This density alteration changes the thermal conductivity of the frost while the alteration in surface architecture changes the surface roughness. Both of these changes consequently modify the heat transfer coefficients and pressure drops of the heat exchanger, thus affecting coil performance. To summarize briefly the findings of Trammell et al. and Hayashi et al., it was reported that the density increases as the relative humidity and air velocity increases and that the density decreases as the surface temperature decreases. It was shown that the conductivity is directly related to the density although the relationship is not linear. The surface roughness,

Table 2.2.1 Summary of Previous Experimental Research on Heat Exchanger Frosting

Researcher	Experimental Parameters					Effect of Parameter on Frosting Rate				Effect of Parameters on UA			
	fpi	V_{air}	T_{surf}	T_{air}	RH	V_{air}	T_{surf}	T_{air}	RH	V_{air}	T_{surf}	T_{air}	RH
Stoecker	4, 9	172 - 462	16	32	72	----	----	----	----	↑	----	----	-----
Wagner	----	42 - 117	0	70	29 - 86	↑	----	----	↑	↑	----	----	↑
Gates	2-16	110 - 770	----	----	----	----	----	----	----	↑	----	----	↓
Lotz	2.5	200- 1380	–30	5-32	45 - 80	----	----	----	----	----	----	----	----
Sanders	----	600 - 1560	–22- 14	14-30	88 - 95	*	----	↓	↑	↑	----	-----	-----
Niederer	6, 4	----	20	32	85	----	----	----	----	↑	----	----	----
Gatchilov	3, 2.5, 1.5	300 - 1500	19	32	74 - 88	↑	----	----	↑	----	----	----	*
Tantakitti	12	306 - 475	5-20	10 - 35	80 - 100	----	----	↑	↑	----	----	----	----
Kondepudi	10, 18	130 - 200	< 10	32	65, 80	↑	----	-----	↑	↑	----	----	↑
Senshu	12	274	5-32	35	85	↓	↓	----	----	↑	----	----	----

KEY

↑ : As parameter is increased, frosting rate or UA increases

↓ : As parameter is increased, frosting rate or UA decreases

* : Frosting rate or UA initially increases, then decreases as parameter is increased

---- : No information available

however, is inversely related to the density. At low densities there is significant roughening of the surface.

In addition to varying with the environmental conditions, the frost structure may also vary with time. During the frosting process a melting of the outer frost surface will occur if its temperature exceeds the freezing point due to the increase in the thermal resistance of the thickening frost layer. After this melting process, the surface temperature will again drop below the freezing point and the frost layer will resume its growth. The frost that melts into the layer will cause an increase in the density of the underlying frost and, thus, will change its conductivity and possibly its roughness.

Further complicating the frost structure problem highlighted above for flat plates is the complexity added by a heat exchanger. With a heat exchanger, the frost properties will change with all of the parameters noted above for a flat plate as well as location on the heat exchanger and the configuration of the heat exchanger. This makes it extremely difficult to compare frost properties from one heat exchanger to the next.

Chapter 3

EXPERIMENTAL FACILITY

3.1 Overall Facility

The experimental apparatus used for this frosting study was first described by Heflin (1989). Several modifications and additions have been made to the basic system described in Heflin's work in order to facilitate the retrieval of data. Among these changes are the addition of a remotely controlled valve system on the refrigerant side, a remotely controlled conical-type damper on the air side, and humidity generation and measuring systems. A complete description of all of these major changes as well as a complete review of the entire system follows.

The facility used for this study is located at present in the basement of the Mechanical Engineering Laboratory (MEL) on the Urbana-Champaign campus of the University of Illinois. The facility, on which construction was started in the summer of 1988, consists of three main sections: the refrigeration system, the air loop section, and the data acquisition system. Figure 3.1.1 shows a photograph of the entire system and a schematic is provided in Figure 3.1.2. The condensing unit which was used to deliver two-phase refrigerant to the test evaporator is shown in the lower left corner of the photograph. Various refrigerant plumbing lines and electronic controls are located above. Continuing to the right, the second panel of the facility consists of more electronics for data acquisition and control. Lastly, on the far right is the freezer unit in which the air loop test section is contained.

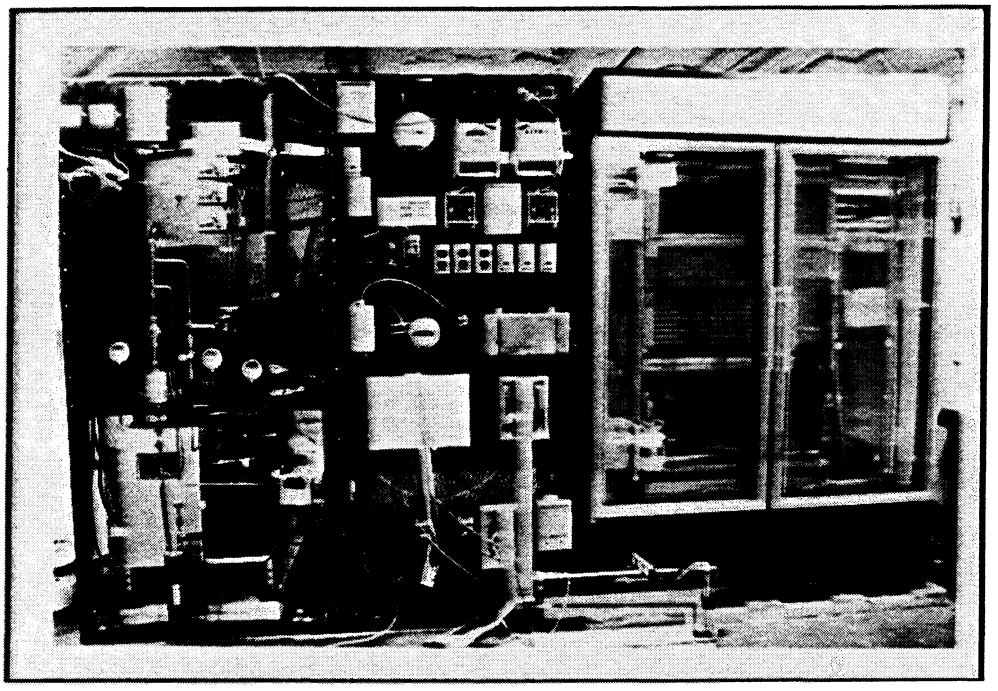

Figure 3.1.1 Photograph of Evaporator Test Facility

3.2 Refrigeration System

The refrigeration system is essentially a typical vapor compression system with a few added components designed to aid the achievement of various test conditions that were desired during the course of this study. The refrigeration system can be separated into two basic sections: the ambient side and the freezer side. As shown in Figures 3.1.1 and 3.1.2, the ambient side includes the compressor, subcoolers, and suction line, while the freezer side includes the main expansion valve and evaporator. The step-by-step description of the system will begin on the ambient side of the system at the compressor.

A detailed schematic of the ambient temperature side of the refrigeration system is shown in Figure 3.2.1. It should be noted that all of the plumbing was done with 3/8 in. (9.53 mm) O. D.

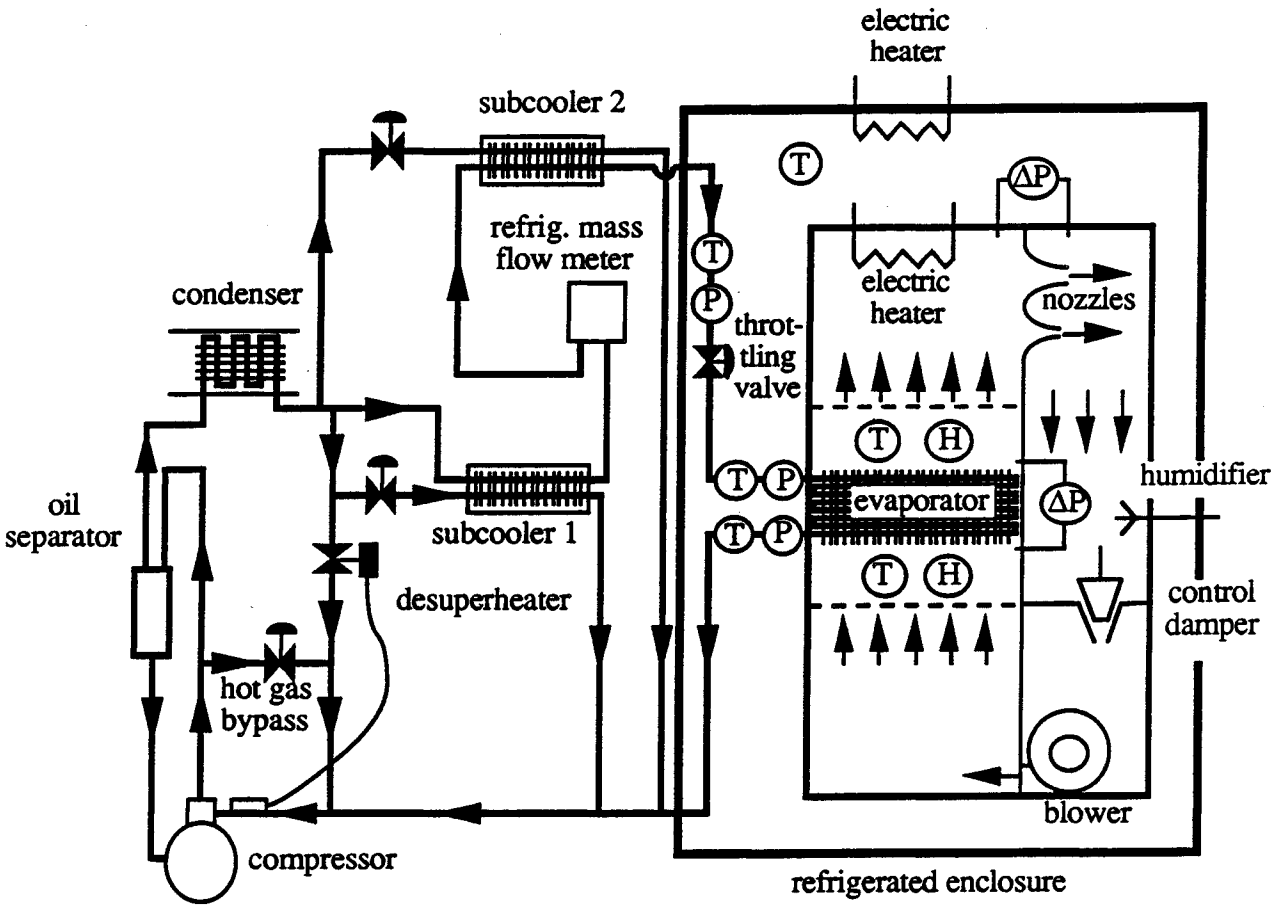

Figure 3.1.2 Schematic of Evaporator Test Facility

soft copper tubing, wall thickness = 0.032 in. (0.813 mm), except the suction line which is 5/8 in.(15.9 mm) O. D., wall thickness= 0.035 in. (0.889 mm). The compressor and condenser were purchased as a single unit from Bohn Heat Transfer. The specific model is designated as a DS1L1AC01 Bohnametic Air Cooled Condensing Unit and consists of a 1 HP, R-12 (dichlorodifluoromethane), reciprocating compressor, air cooled condenser coil, a 1/8 HP fan, and a liquid receiver. The compressor has three ports: inlet (low side) port, outlet (high side) port, and an oil fill port. The low and high side ports were used to isolate the condensing unit during times when work was performed on the rest of the refrigerant lines and for recharging the system when necessary.

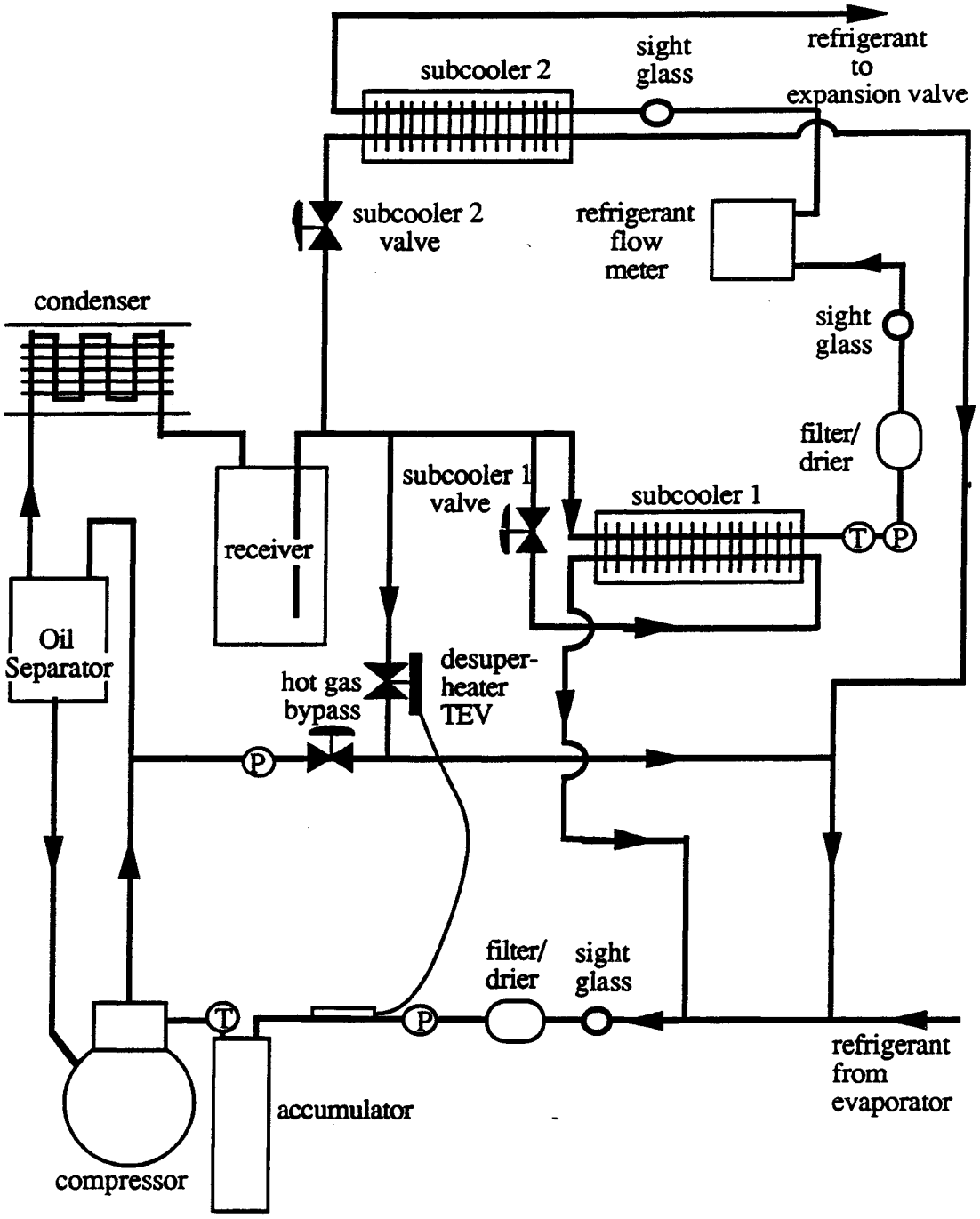

Figure 3.2.1 Ambient Side of Refrigeration System

After leaving the high side port, there are two paths that the refrigerant may take. The majority of the refrigerant proceeds into the Temprite model 501 oil separator shown in the schematic. In

the separator, gravity is used to separate the heavy oil from the light refrigerant vapor. One outlet port of the separator then sends the vapor refrigerant to the air cooled condenser. The other outlet port returns the oil to the compressor through its oil fill port. The second path, that only a proportionally small amount of refrigerant takes, is through a bypass line that circumvents the oil separator and condenser and goes directly to the suction line. The reason for this hot gas bypass is to control the pressure in the evaporator. This is done by regulating the amount of bypass gas with the use of a Hoke model 2331G4B metering valve. Decreasing the amount of bypass flow decreases the evaporator pressure and, consequently, the temperature. A J/B analog pressure gauge (0-500 psi) is attached to the bypass line.

After the condenser, the refrigerant enters the receiver. Upon exit of the receiver, the liquid refrigerant then proceeds down one of four paths. First, a small amount is utilized for coolant, after expansion across a valve, in the second of two subcoolers in the system, marked as subcooler 2 in Figure 3.2.1. The second branch from the main refrigerant line is used for desuperheating of the refrigerant in the suction line. This desuperheating is controlled by a Sporlan BFFE-A-Z Thermostatic Expansion Valve (TEV). The bulb for the TEV is located on the suction line as is a pressure port used for balancing the TEV. The amount of liquid refrigerant flow is then controlled so as to maintain a preset amount of superheat in the suction flow. The third branch from the main line goes to the first subcooler in the system after expansion across a Hoke model 3812F4Y needle valve.

Returning to the main refrigerant line, after all of the relatively small flows are branched out for the various purposes described above, the refrigerant is then sent to subcooler 1 mentioned above. Subcooler 1 consists of an Edwards Engineering tube-in-tube heat exchanger model B-1/2. The plumbing for the subcooler is arranged in a counterflow arrangement such that the main refrigerant flow is in the opposite direction of the refrigerant flow exiting the expansion valve. The purpose of subcooler 1 is to provide a sufficient amount of subcooling to the main flow to insure

that all liquid reaches the mass flow meter which requires a single phase flow (gas or liquid) in order to function properly.

After the main refrigerant line leaves subcooler 1, the temperature is measured with a Taylor 9860 digital thermometer and the pressure is measured by another J/B (0-500 psi) analog gauge. It is then sent through a Sporlan Catch-All Type C-165 dessicant filter-drier and a Sporlan SA-15 sight glass so that a visual check of the refrigerant may be made before it enters the mass flow meter. The visual check is required in order to verify that there are no vapor bubbles in the liquid refrigerant

Following the sight glass the refrigerant then proceeds to the flow meter. As mentioned above the meter that was utilized is a true mass flow meter that operates on the Coriolis principle. This means that the density, viscosity, and other transport properties of the fluid do not have to be considered in order to receive an accurate reading of mass flow. This should allow a very high degree of accuracy. The model of the mass flow meter is a Micro Motion DS006S100. The remote electronics unit which converted the 0 to 1.0 lb_m/min (0 to 0.46 kg/min) mass flow rate registered by the meter to a 0-10 VDC reading is designated as a model RE-01061431. Upon leaving the mass flow meter, another visual check of the refrigerant is made in order to further verify that it is still all liquid and has not flashed to vapor on passing through the flow meter.

The next component is subcooler 2. This subcooler functions in a manner similar to subcooler 1 in that a small amount of refrigerant is branched off the receiver outlet flow, as was described previously, and is expanded across a valve in order to drop the pressure, flash the refrigerant, and, consequently, decrease the temperature. The valve used for this expansion, however, is not a hand valve but is, rather, an electronic linear control valve (ELCV). This valve consists of a 12 VDC stepping motor driving a needle valve and is manufactured by Fujikoki of America. The model KEM-05 valve has six and one-quarter turns from full open to full close and there are ninety-six

steps per turn. The stepping motor is driven by a Sprague integrated circuit UCN5804B. This IC in turn is given commands by either manual control at the panel shown in Figures 3.2.2 and 3.2.3 or by the computer through the digital outputs located on the data acquisition boards which will be further described in the data acquisition section of this paper. The circuit diagram of the ELCV

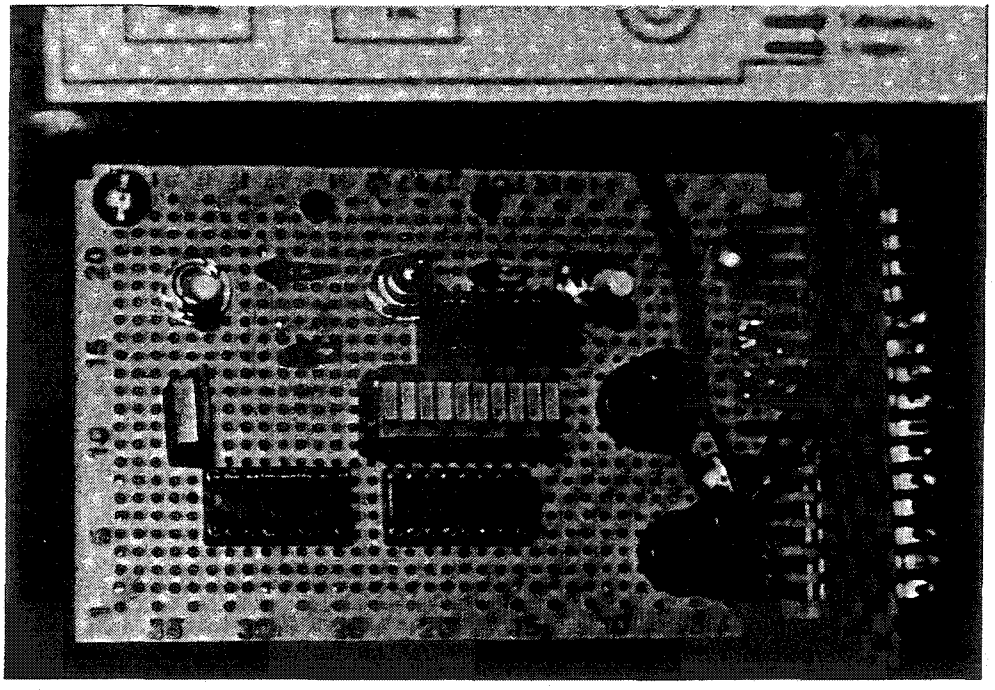

Figure 3.2.2 Photograph of ELCV Control Panel

control module is shown in Figure 3.2.4. It can be seen in the drawing that the two commands input either manually or by the computer, marked as Computer Direction and Computer Input, are for indicating a direction that the stepping motor should take (open or close) and informing the IC how many steps the motor should take, respectively. The number of steps required could be determined by a simple proportional control loop contained in the Turbo Pascal data acquisition program discussed in Section 3.4, but was set manually for all of the work to be shown here.

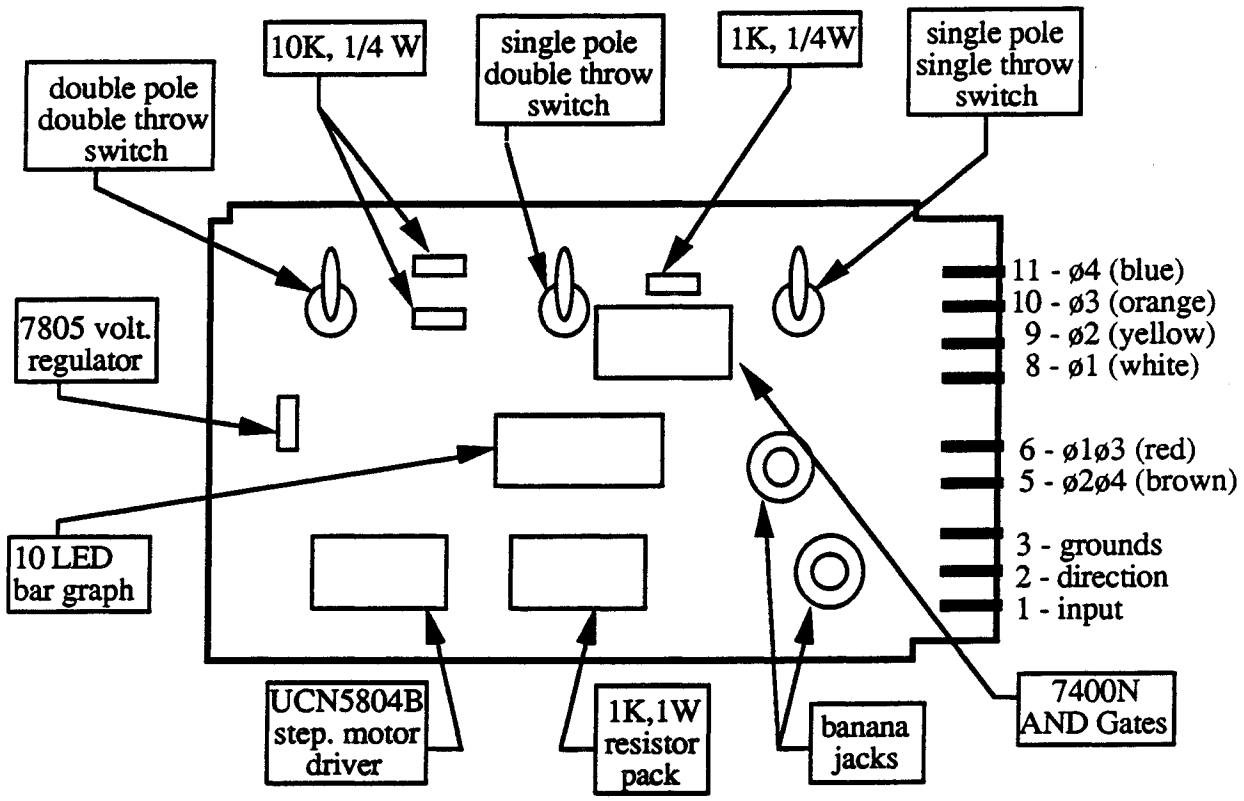

Figure 3.2.3 Schematic of ELCV Control Panel

Subcooler 2 is also a tube-in-tube counterflow heat exchanger as is subcooler 1. However, this heat exchanger was not commercially purchased but was designed and fabricated in-house. It consists of an approximately 9.0 foot (2.7 m), 3/8 in. (9.53 mm) diameter length of soft copper tube inserted in a 5/8 in.(15.9 mm) outer diameter soft copper tube, t_w = 0.032 in. (0.813 mm). The coaxial length of tubing was then wrapped into a helical coil having a diameter of approximately 1.5 ft (0.5 m) with three turns. The necessary connections were then made with the appropriate copper, solder-type fittings modified for this installation.

During initial testing of the facility, it was found that a second subcooler was necessary due to an unusual amount of heat gain through the mass flow meter. By adding this additional subcooler after the flow meter, the amount of subcooling of the liquid refrigerant entering the main expansion

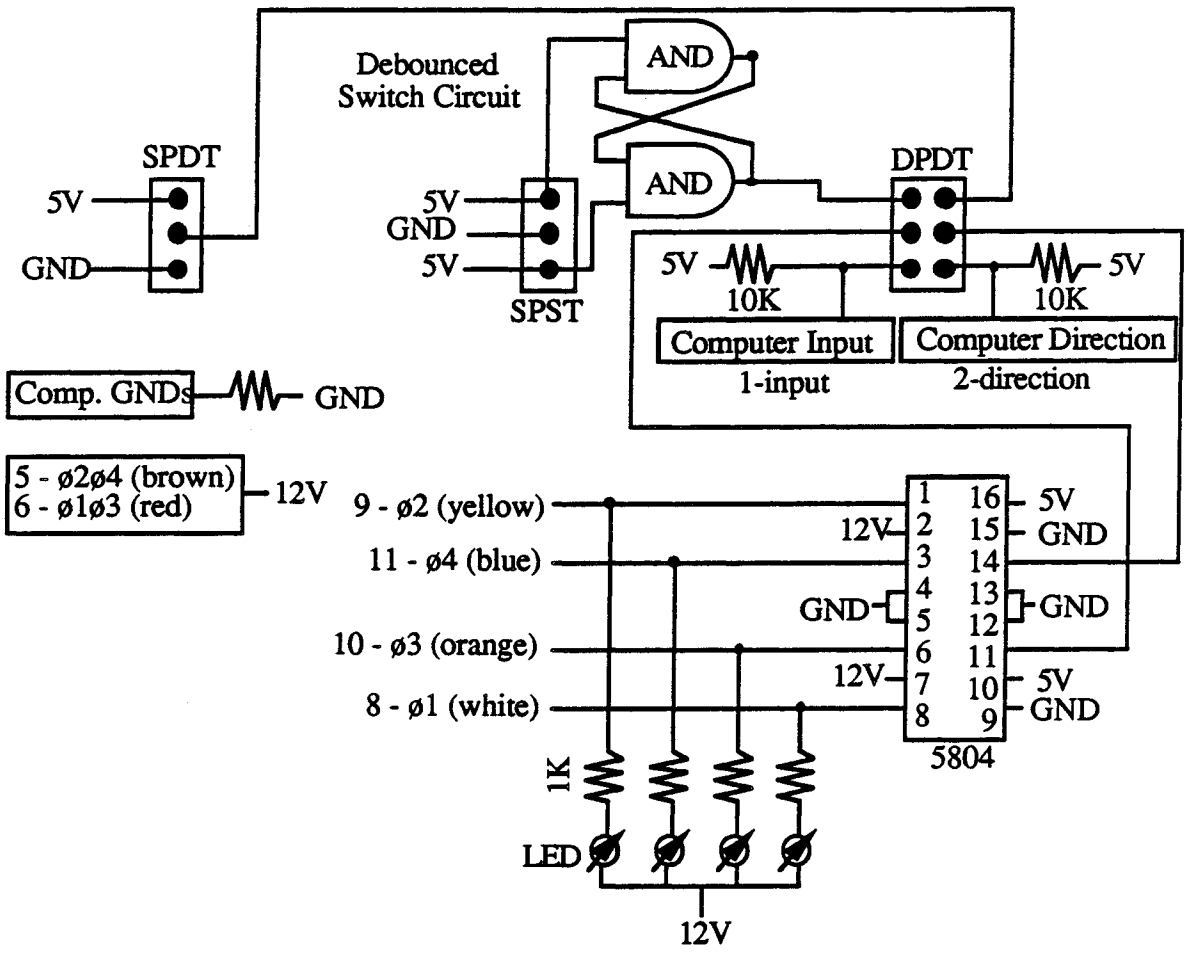

Figure 3.2.4 Circuit Diagram of ELCV Control Panel

valve could than be controlled over a wider range. This allowed a wider latitude on the types of evaporator inlet qualities that could be obtained.

After the second subcooler, the refrigerant pressure and temperature are measured with an Omega PX176 model pressure transducer and a 3.0 in. (76 mm) copper-constantan (Type-T) thermocouple probe, respectively. The refrigerant is then sent through the main expansion valve in order to produce the refrigeration effect in the evaporator. The main expansion valve is a Hoke Milli-Mite metering valve model 1335G4B. A metering valve was chosen in order that more exact control of the relatively low flow rates through the evaporator could be accomplished. Since this

portion of the refrigeration system is located inside of the refrigerated enclosure as shown in Figure 3.2.5 , a remotely controlled actuator had to be used so that the doors of the refrigerated enclosure would not have to be opened in order to adjust the flow rate through the evaporator. A Hoke

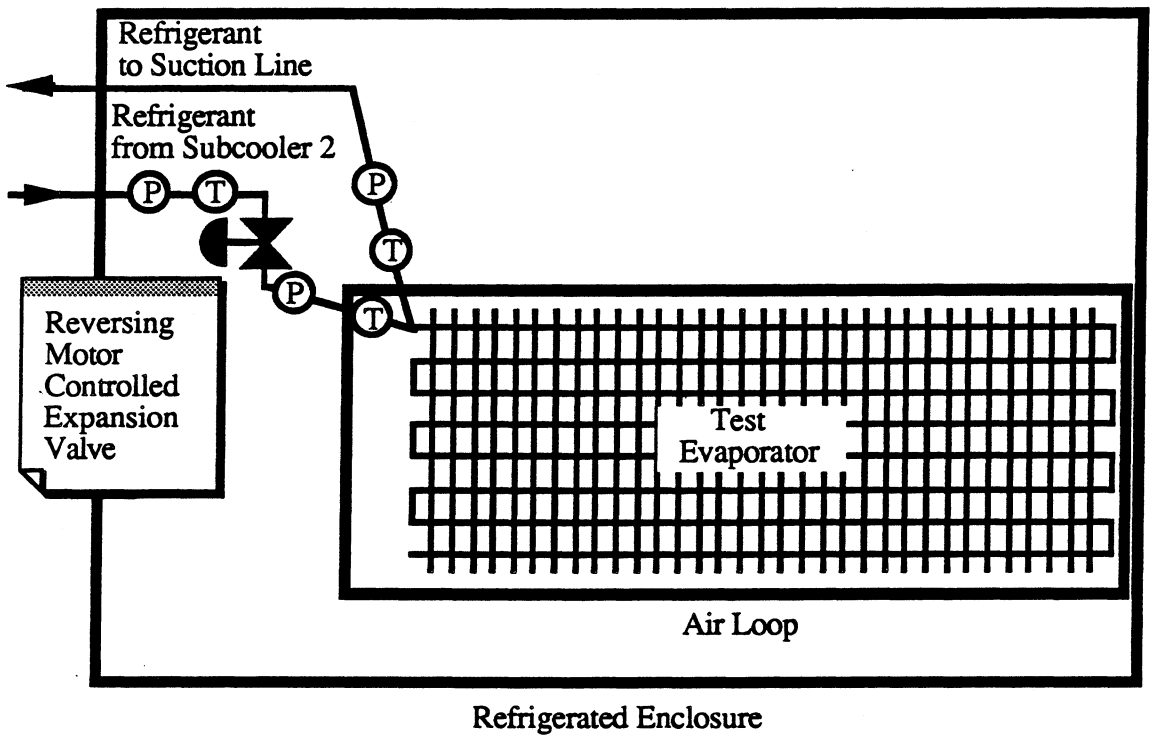

Figure 3.2.5 Schematic of Evaporator and Main Expansion Valve in Refrigerated Enclosure

reversible electro-mechanical valve actuator model 021A2D was chosen for this purpose. This actuator is specifically designed for use with Hoke 1300 series metering valves. The direction and duration of valve operation is controlled by means of a double-throw toggle switch located on the second control panel as shown in the schematic in Figure 3.2.6. A problem with the actuator that became apparent during initial operation of the system at nominal test conditions was a slowing and eventual stoppage of actuation capability as the temperature of the freezer compartment dropped below the freezing point and normal compartment testing temperatures were reached at approximately 0.0 F (-18 C). This problem was found to be due to a water based lubricant used in the actuator motor. The solution that was implemented involved wrapping the motor housing with

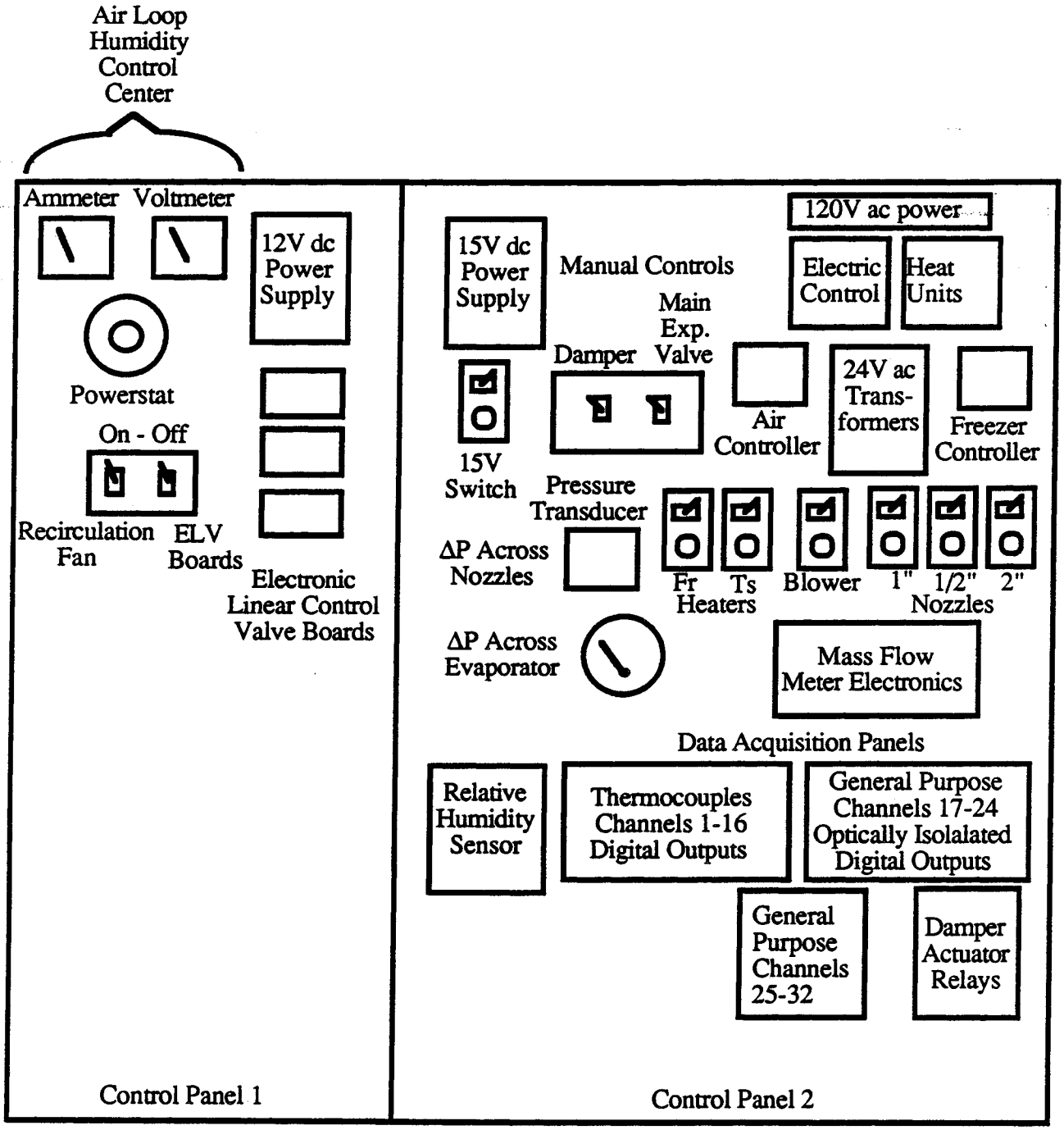

Figure 3.2.6 Schematic of Control Panels 1 and 2

an electrical resistance heater cord with a bi-metal thermostat which would deactivate the heater at 35 F (1.7 C). The motor housing was then insulated with 1 in. (25.4 mm) of Celotex foam insulation. This solution was found to be quite satisfactory.

It should be mentioned that all of the plumbing shown in Figure 3.2.5 is insulated with two layers of 3/8 in. (9.53 mm) thick foam insulation in order to reduce any heat exchange between the refrigerated enclosure and the refrigerant.

On exit of the expansion valve, the refrigerant temperature and pressure are again measured with exactly the same devices as used before the valve, and the flow then proceeds to the evaporator. The evaporator used is a model 162506 currently in production by Peerless of America and is used in top mount, automatic defrost, domestic refrigerator-freezers. As can be seen in the photograph in Figure 3.2.7 and also more clearly in the schematic in Figure 3.2.8, it

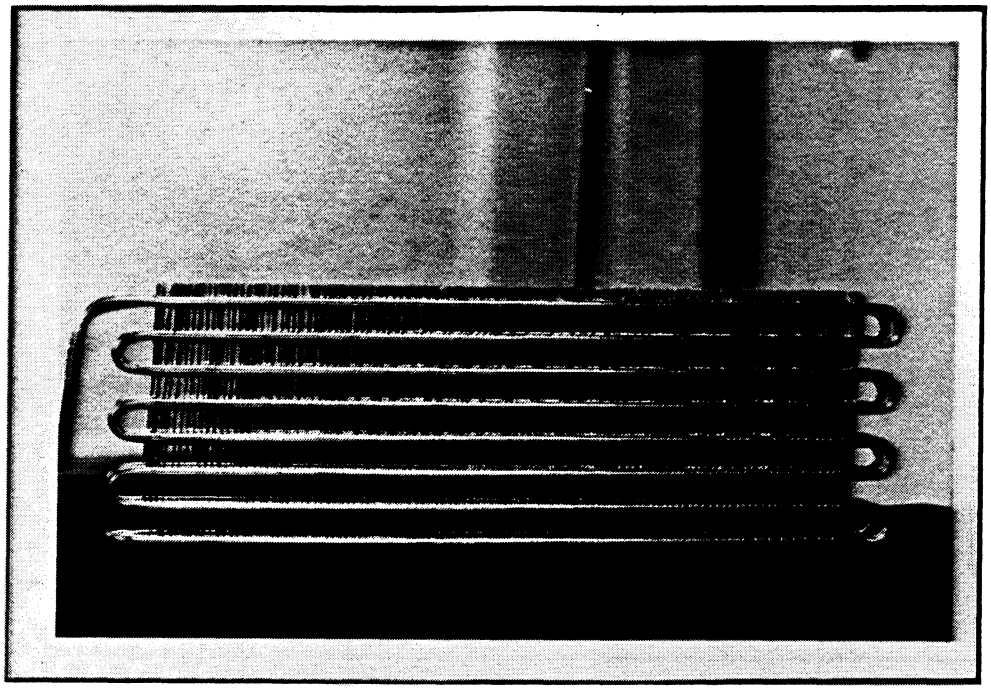

Figure 3.2.7 Photograph of Peerless 162506 Evaporator

employs a parallel-cross/counter-cross geometric flow arrangement. This means that the refrigerant flow enters the evaporator at the top as shown in the figures, flows in a counter-cross relationship to the airflow until it reaches the bottom of the coil. At the bottom of the coil the flow crosses over to the back row of tubes and then flows in a parallel-cross path relative to the airflow until it exits

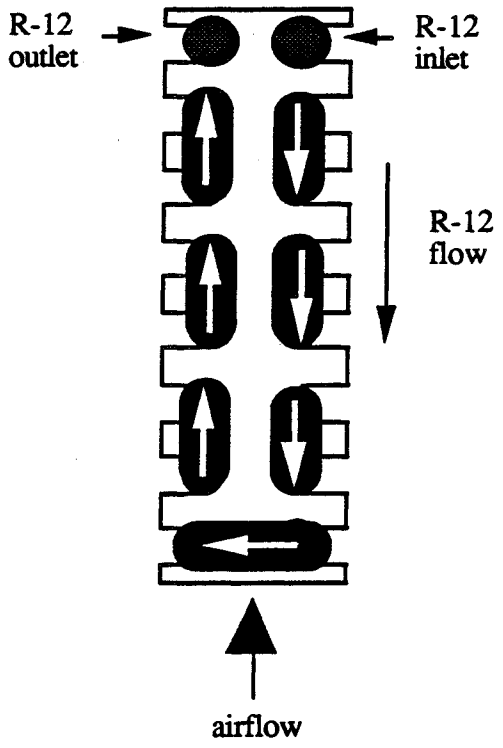

Figure 3.2.8 Evaporator Flow Arrangement (End View)

the evaporator at the top. The overall dimensions of the coil including the end turns are 2.00 x 8.00 x 23.5 in. (50.8 x 203 x 597 mm). Two pieces of Styrofoam were fitted over the turns on either end of the coil, however, so that they did not participate directly in the transfer of heat. The tube stock is 1435 aluminum alloy. The tubes have a 3/8 in. (9.53 mm) O. D. and a wall thickness of 0.028 inches (0.7112 mm). The fins are referred to as offset fins and the tubes are merely forced into them during assembly. There is no metallurgical bonding or expansion of the tube into the fins. This results in a significant contact resistance between the two. The configuration of the

fins is shown in Figure 3.2.9. There are 106 fins or 5 fpi (5.1 mm/fin) made of the same aluminum alloy and 53 of them have overall dimensions of 0.0075 x 2.00 x 8.00 in. (0.19 x 50.8 x 203 mm) while the other 53 have dimensions of 0.0075 x 2 x 7.25 (0.19 x 50.8 x 184 mm) to provide 2.5 fpi (10.2 mm/fin) at the air inlet.

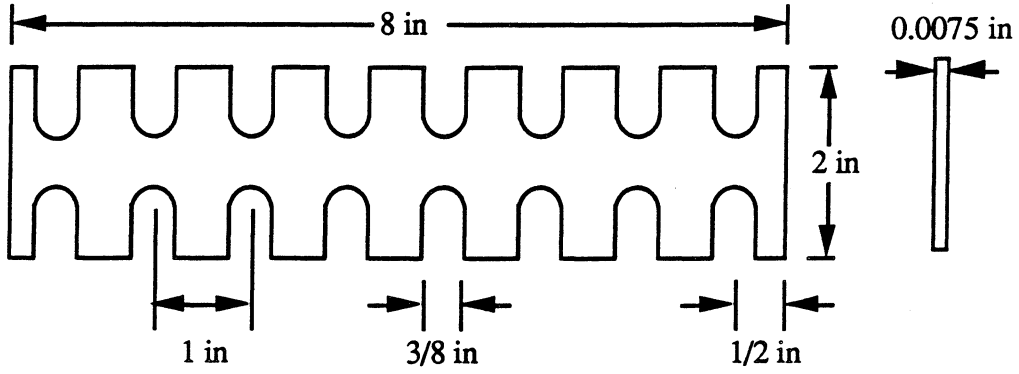

Figure 3.2.9 Evaporator Fin Configuration

After leaving the evaporator, the refrigerant is sent to the suction line where it joins up again with the small flows that were utilized in subcoolers 1 and 2, the hot gas bypass line, and the desuperheater. Located in the suction line are another Sporlan SA-15 sight glass and Sporlan Catch-All Type C-165 filter-drier. After the filter there is a J/B analog pressure gauge (30 in. Hg vac – 350 psi). From this pressure gauge the refrigerant then enters the suction accumulator. The purpose of the accumulator is to ensure that only refrigerant vapor reaches the compressor. Liquid refrigerant is very detrimental to compressor operation and could lead to a catastrophic failure. A Taylor 9860 digital thermometer is situated at the accumulator outlet port. From this port the refrigerant proceeds directly to the low side port of the compressor.

3.3 Air Loop Section

The air loop test section part of the facility can be divided into two components: the refrigerated enclosure and the air loop test area which is located inside the refrigerated enclosure. The purpose of placing the air loop in the refrigerated enclosure was to reduce any infiltration of heat into the evaporator coil from the ambient. By setting the refrigerated enclosure temperature approximately equal to the average temperature of the air passing over the evaporator coil, heat transfer from the enclosure to the refrigerant should be minimized. This should allow for a good balance between the air side energy removal rate and the refrigerant side heat gain rate.

The refrigerated enclosure that was selected for use as an artificial environment for the test section was a 49.0 cubic foot (1.39 m^3) upright freezer produced by True Manufacturing Company, model GDM-49 as shown in Figure 3.3.1. As can be seen in the figure, the evaporator and fans for the freezer are located in the top of the unit and the compressor and condenser are located in the bottom portion. The doors of the freezer are triple-pane glass. The mullion shown in the figure was removed during installation and removal of the test section.

In order to facilitate the maintenance of a constant temperature in the freezer compartment during testing, the normal cycling of the freezer refrigeration system or "on-off" type temperature control was eschewed in favor of running the compressor continuously and using a Johnson Controls, Inc., temperature control system connected to the freezer evaporator defroster. The Johnson system consists of three components: a thermistor, a temperature controller and a heater controller. A rough schematic of the system is shown in Figure 3.3.2. The thermistor is a model TE-1101-1 Duct Sensor, the temperature controller is a Cybertronic controller, and the heater controller is a model DQ-4100-31 Solid State Electric Heater Controller. A complete description with all the details of this system is provided by Heflin (1989).

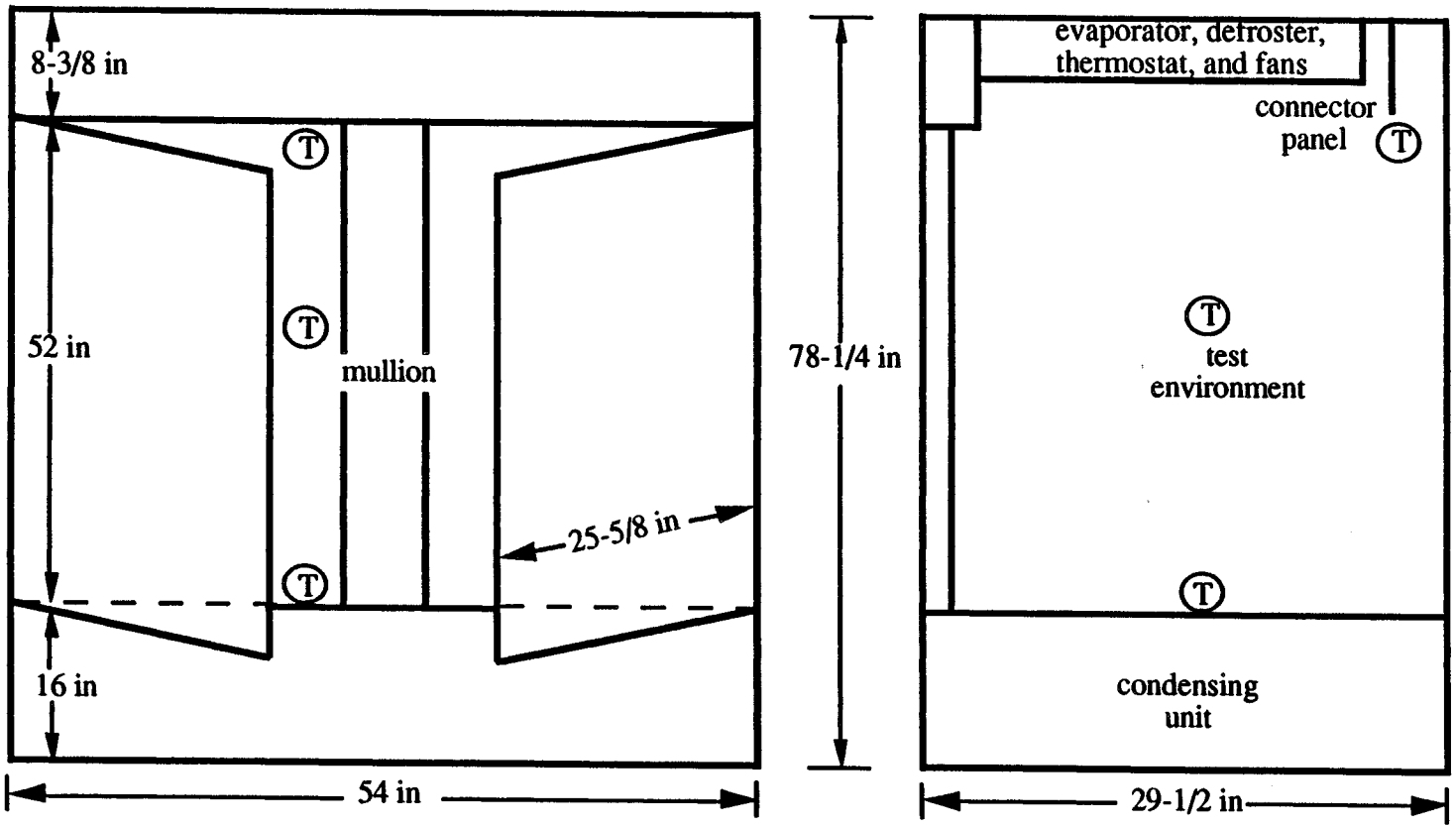

Figure 3.3.1 Refrigerated Enclosure

Proceeding now to the actual air test loop, a detailed schematic is shown in Figure 3.3.3. In the figure, it can be seen that after exiting the Peerless-Windsmith 1/8 HP direct drive pressure blower in the lower right corner, the air enters the lower plenum. Both the lower and upper plenums are constructed of 1/4 in. (1.35 mm) grey PVC board with clear acrylic front sliding doors to allow observation during testing and easy access during down times. The bottom of the

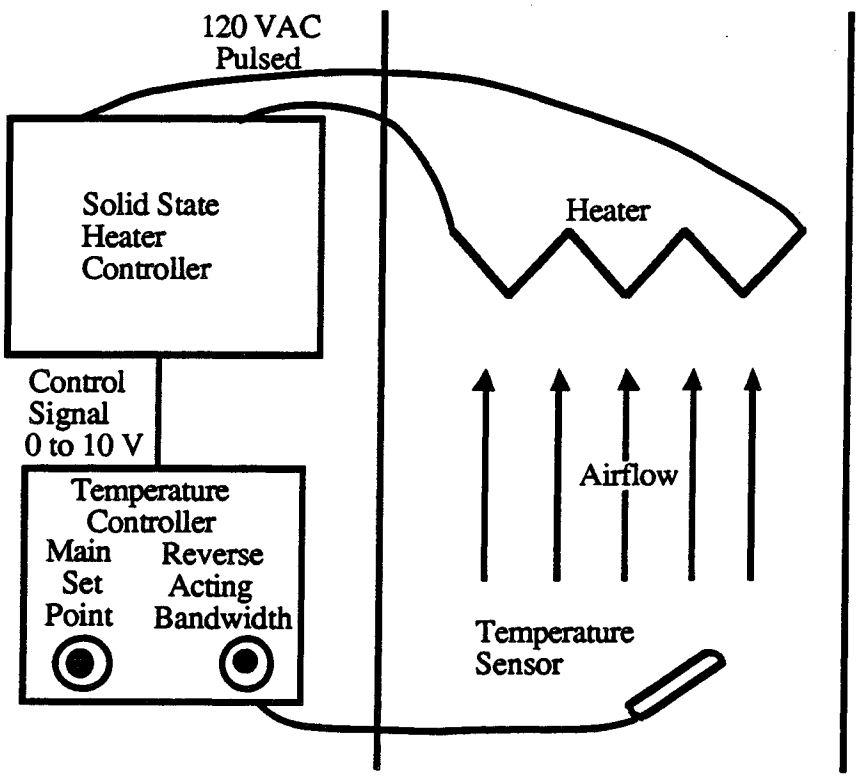

Figure 3.3.2 Schematic of Freezer and Air Loop Temperature Controller

lower plenum is covered with a plastic waterproof liner and has a centrally located 1.00 in. (25.4 mm) diameter drain whole with an RTV silicon plug. The purpose of these two accessories is to allow for easy drainage of the evaporator condensate out of the test section to the freezer drainage pan during the defrosting of the evaporator coil. The overall dimensions of the plenums are 30.0 x 18.0 x 16.0 in. (762 x 457 x 406 mm). In the bottom plenum, temperature and relative humidity

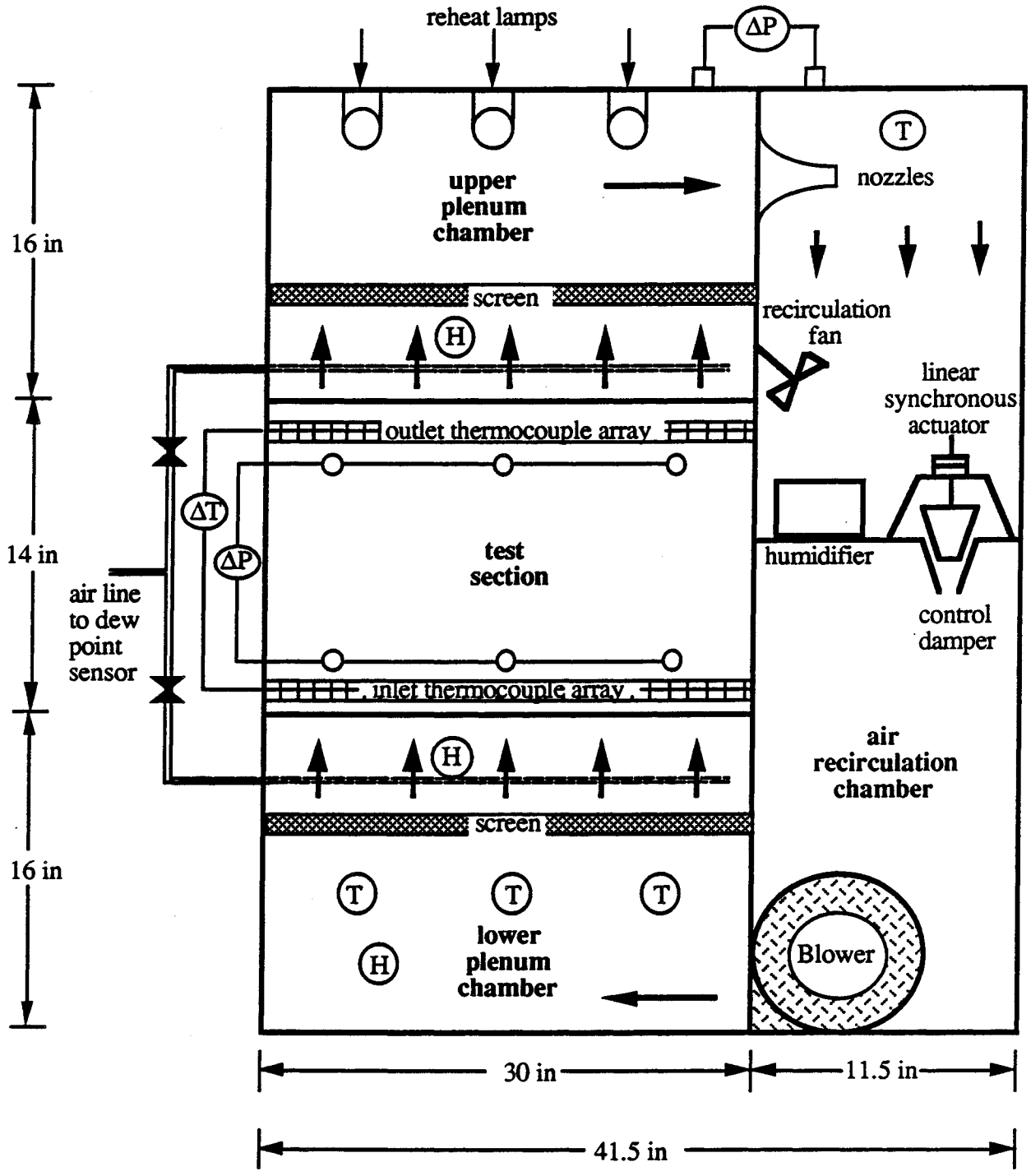

Figure 3.3.3 Schematic of Air Loop

measurements are made. The temperature of the air in the plenum (inlet air to the evaporator) is measured by means of three Type-T thermocouple probes having a length of 12.0 in. (305 mm) inserted into the plenum through the back wall. The probes are equally spaced horizontally and each is located 8 in. (203 mm) from the bottom of the plenum and 11.0 in. (279 mm) from the bottom of the evaporator coil. A mathematical averaging of the three readings is made in order to determine an evaporator inlet temperature. A Rotronic model HT220R capacitance type relative humidity sensor is used to determine the relative humidity at the inlet. This sensor consists of essentially two parts: the humidity transmitter, which is located on control panel 1, and the sensor itself. The transmitter is responsible for converting the signal it receives from the sensor to a 0-10 VDC analog signal which it sends to the general purpose board of the data acquisition system. The sensor probe is connected to the transmitter via a 5.0 ft (1.5 m) long shielded cable. The probe has a length of 9.74 in. (247 mm) and its tip is fitted with a protective silicon dust filter. This filter was found to be necessary due to the relatively high air velocities encountered by the probe during testing.

In addition to the relative humidity sensor in the bottom plenum, a tap drawing in an air sample for a dew point sensor is also located there as shown in Figure 3.3.3. In order to obtain an average moisture measurement, a 22.0 in. (559 mm) piece of soft plastic tubing with two approximately 0.050 in. (1.3 mm) diameter holes every 2.0 in. (51 mm) is attached to the tap line and is tied to the bottom of the thermocouple probe holder to be described presently. The dew point sensor itself is located outside of the freezer unit and is a General Eastern model 1211HX chilled mirror sensor. This type of sensor operates by means of an optical detection of the formation of condensation (dew or frost) on a thermoelectrically cooled metallic mirror surface. Once frost is detected the mirror's temperature is held constant and is measured by means of a platinum resistance thermometer. This temperature is the dew or frost point. The accuracy of this device is given by the manufacturer as +/-0.2 F (+/- 0.1 C). This sensor was used for all humidity measurements on account of its higher accuracy and reliability.

The sample is drawn into the sensor by means of an aquarium air pump whose suction side is connected to the outlet of the sensor. The inlet of the sensor is attached to a tee-shaped configuration of copper tubing which has a plug type shutoff valve on either branch of the tee. One end of the tee enters the air loop at the lower plenum with the inlet manifold described above and the other end enters the top plenum at the evaporator outlet with a manifold exactly the same as the one at the inlet. Soft copper tubing with 1/4 in. (6.4 mm) O. D. and wall thickness of 0.030 in. (0.76 mm) was used for the tap line.

In addition to the temperature and humidity devices, a thermistor for another Johnson Controls temperature and heater controller set-up, exactly the same as the one described during the freezer discussion, is also located in the plenum. The heat sources that are controlled by this system are the three reheat lamps located in the top plenum. The reheat lamps are three, 200 W, light bulbs that were painted with a high temperature black paint in order to prevent any radiation in the visible spectrum from reaching the outlet thermocouple array or the air exiting the evaporator, which would reduce the accuracy of the temperature measurement.

After the lower plenum, the air flows through a 1/16 in. (1.6 mm) metal screen before entering the evaporator section. The purpose of the screen is to insure that there is a uniform flow entering the test section. The test section has dimensions of 20.75 x 14.0 x 2.25 in. (527.0 x 356 x 57.2 mm). The back wall of the evaporator section is made of 1/4 in. (6.35 mm) thick acrylic with a 2 in. (50.8 mm) thick insulation panel. The sides are also made of 1/4 in. (6.35 mm) acrylic and have 1.00 in. (25.4 mm) of insulation. The front of the test section is composed of two layers of 1/4 in. (6.35 mm) clear acrylic panels which are joined together by a 2.0 in. (50.8 mm) rim of 1 in. (25.4 mm) thick Celotex insulation around all four edges. This effectively isolates the test section from the freezer compartment thermally . Clear acrylic was chosen for the front section so that visual observations of the evaporator coil can be made as the frosting process proceeds. Although there was initial concern about the potential for thermal radiation pick up from the room, simple

hand calculations and a comparison of evaporator performance with the clear panel covered by a 1.00 in. (25.4 mm) thick piece of rigid foam insulation and without the cover showed that heat transfer to the evaporator by thermal radiation was negligible.

The temperature change of the air as it passes over the evaporator coil is measured by means of a thermocouple array at the inlet and outlet. This thermocouple array consists of ten Type-T 20 AWG thermocouple wires, soldered at the ends, spaced equally in a horizontal row at the inlet of the evaporator section and ten 2.00 x 2.00 in. (50.8 mm x 50.8 mm) squares of copper screen at the outlet. The wires are housed in 1/8 in. (3.175 mm) diameter, 6.00 in. (152 mm) long tubes that are attached to an aluminum rod approximately 8.00 in. (203 mm) below the evaporator (the dew point sample line discussed previously is attached to the bottom of this rod). The copper screens at the outlet are located 3.0 in. (76 mm) above the evaporator and are glued to two strips of acrylic to form a horizontal row of screens. A schematic of the array is shown in Figure 3.3.4. The array was wired by connecting the constantan lead of each thermocouple pair in the bottom array to its corresponding copper screen at the outlet. The copper lead of each bottom thermocouple was then attached to the adjacent copper screen at the outlet. By connecting the inlet and outlet arrays in this manner the voltage signal is ten times higher than if just one thermocouple is used, thus increasing the accuracy of the measurement and delivering an average temperature difference across the inlet and outlet cross-sectional areas.

In addition to the temperature difference measurement, the pressure drop across the coil is also measured. This measurement is made by means of two sets of pressure taps. The first set is located 1.5 in. (38 mm) below the bottom of the evaporator in the back wall of the evaporator section. It consists of three equally spaced 1/4 in. (6.35 mm) taps connected in parallel with flexible plastic tubing. The second set of taps is located 1 1/2 in. (38 mm) above the top of the evaporator coil and is identical to the first. The system of having three taps in parallel was conceived in order to obtain an average pressure across the full flow area. The pressure differential

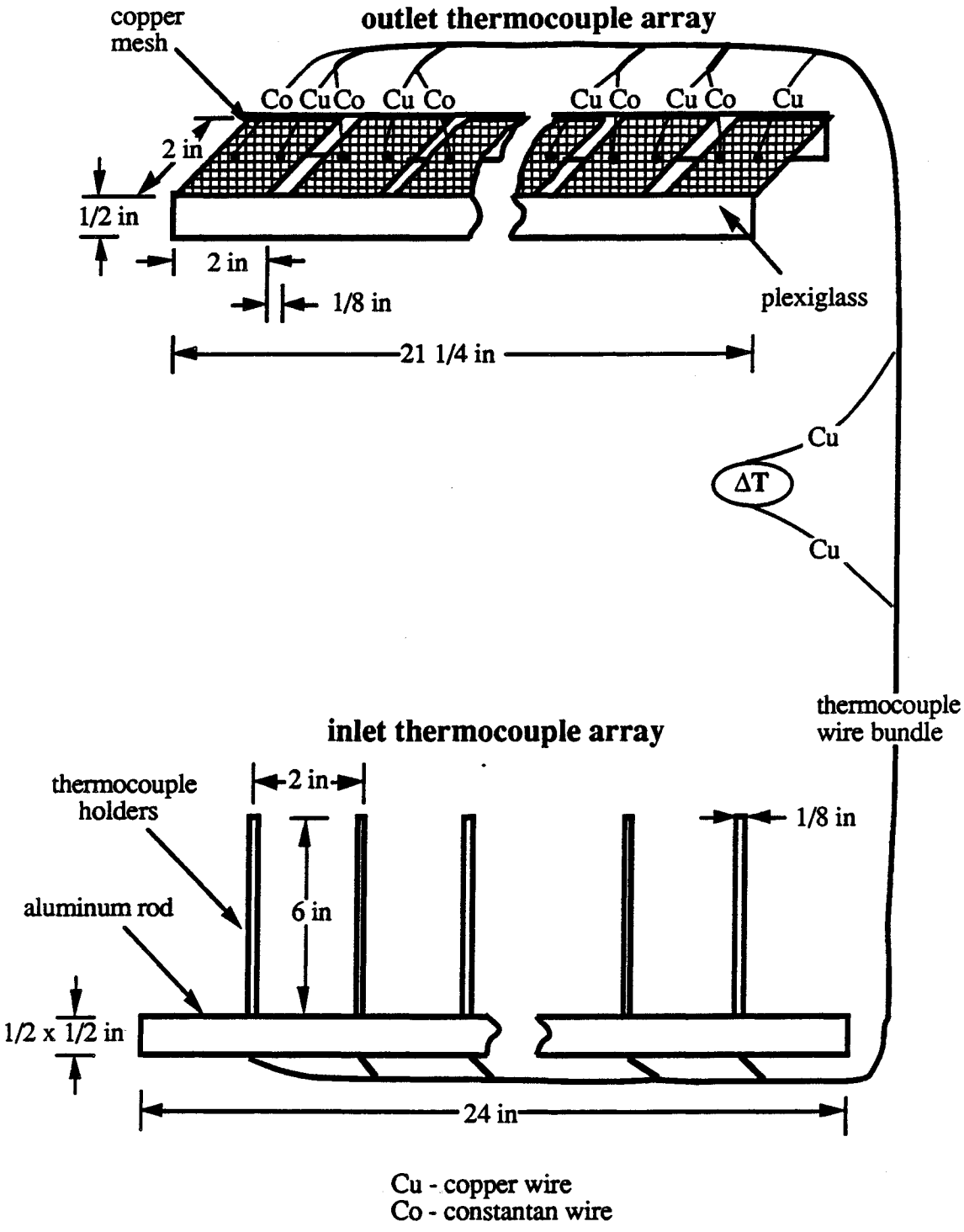

Figure 3.3.4 Evaporator Inlet and Outlet Thermocouple Array

between the two sets of taps is measured with two instruments connected in parallel: a 0-1/2 in. water (0-124 Pa) Dwyer Instruments Magnehelic pressure gauge and a 0-5 in. water (0-1244 Pa) Dwyer Instruments model 424-5 inclined-vertical manometer. Both pressure measuring devices are required because the pressure drop across the evaporator coil ranges from less than 0.010 in. water (2.5 Pa) when the coil is clean to 2.00 in. water (498 Pa) when the coil is essentially blocked with frost at the airflow rates that were tested.

After exiting the evaporator section, another 1/16 in. (1.58 mm) metal screen in the top plenum is used to make the flow uniform. The air exits the top plenum through a system of three nozzles on the right side of the plenum as shown back in Figure 3.3.3. The nozzles have diameters of 1/2 in. (12.7 mm), 1 in. (25.4 mm), and 2.00 in. (50.8 mm). Felt-covered aluminum doors with spring loaded hinges are located over each nozzle. A Guardian Electric Manufacturing Company 120 VAC - 60 Hz continuous duty solenoid actuator is attached to each of these doors so that they may be opened remotely by means of switches located on control panel 2. By varying the number of nozzles that are open and the size of the open ones (as well as the damper setting which will be discussed later) a range of volumetric flow rates from 0 to 100 cfm (0 to 47 L/s) is achievable.

In addition to allowing for a wide range of flow rates, the nozzles provide a means of determining what the flow rate is. This is done by measuring the pressure differential across the nozzles and applying a modified Bernoulli's equation to the flow (Appendix A). The pressure differential is measured between three equally spaced taps 2 1/2 inches (63.5 mm) upstream of the nozzles and three taps 2 1/2 inches (63.5 mm) downstream of the nozzles. Each set of taps is connected in parallel with 1/4 inch (6.35 mm) flexible plastic tubing, just as the evaporator pressure taps are, in order to obtain an average value. A Setra model 261-1, 0-5 in. water (0-1244 Pa), pressure transducer is used to determine the pressure differential between the two sets of taps.

A 12.0 in. (305 mm) Omega Type-T thermocouple probe is also located just downstream of the nozzle outlets.

In the return duct to the blower after the airflow exits the nozzles, it encounters the humidifier. The humidifier consists of a 57.6 in^3 (944 cm^3) cylindrical container with a 3 1/4 in. (82.6 mm) height and a 4 3/4 in. (120.7 mm) diameter filled with water. The water is heated by means of an electrical resistance heater attached to the bottom surface of the container. A ruler is attached to the inside of the container in order to indicate the liquid level. Its outside is covered with 1 in. of Celotex insulation on its sides and bottom in order to minimize the heat gain of the return air. The container is filled with water during system operation through a 5/8 in. (15.9 mm) O. D. polypropylene tube that penetrates both the air loop and the freezer compartment. A 10 3/4 x 15 1/4 in. (273 x 387 mm) clear acrylic sliding door similar to the doors on the lower and upper plenums is located on the return duct to facilitate emptying of the humidifier after testing as well as observation of the level indicator.

The heater at the bottom of the container is used to maintain the water at some temperature above the freezing point that will permit the amount of mass transfer from the water to the air necessary to maintain a prescribed relative humidity. In order to aid the mass transfer, a 2 1/2 in. (63.5 mm) recirculation fan is mounted just above the humidifier. The fan is run off of 12 VDC voltage and consumes 1.7 W. The resistance heater has a maximum power at 120 VAC of 600 W. The amount of voltage applied to the heater is regulated by a Superior Electric Company Powerstat which is located on control panel 1 as was shown in Figure 3.2.6. A Simpson voltmeter and ammeter are used to monitor the voltage and current to the heater.

Located on the same level as the humidifier is the damper. The purpose of this damper is to provide a fine control for the flow rate to complement the coarse control afforded by opening and closing the nozzles as was discussed previously. Also, the damper allows for the maintenance of a

constant airflow across the evaporator as it becomes more blocked with frost without changing the nozzle arrangement.

A conical-type damper was selected because of its large control surface area. This damper consists of a solid wood cone having a top diameter of 4.00 in. (102 mm), a bottom diameter of 2.0 in. (51 mm), and a height of 5 1/4 in. (133 mm) that moves in and out of a 1/32 in. (0.794 mm) thick aluminum sheet fashioned into a cone with approximately the same dimensions. The cone is thoroughly coated with a polyurethane lacquer to prevent moisture absorption. The inside of the aluminum cone is lined with a layer of 1/8 in. (3.2 mm) thick foam in order to provide a good seal.

The movement of the cone in and out of its aluminum mate is achieved by means of a Hurst synchronous linear actuator model SL. This 115 VAC actuator is controlled by either a manual double-throw switch located on control panel 2 or by the data acquisition program. The data acquisition program controls the actuator by means of two of the optically isolated high voltage AC relays on the general purpose data acquisition board. Closing one relay and opening the other causes the actuator to move in one direction while the opposite relay setting reverses the movement of the actuator. It was found, however, during the course of testing that there was a significant amount of current leakage across the solid state relays possibly due to the the low impedance, inductive nature of the load. This leakage necessitated the use of two electro-mechanical relays in series with the solid state relays in order to achieve proper operation of the actuator. The relays that were chosen are Potter & Brumfield model KHU-17A11-24. They are located on the lower right side of control panel 2 as shown in Figure 3.2.6. Following exit of the damper, the air returns immediately to the inlet of the blower.

3.4 Data Acquisition

The data acquisition system consists of a personal computer, a Turbo Pascal data acquisition program, two printers, data acquisition cards, and terminal panels. The computer and one of the printers is housed in a cabinet in front of the test facility as shown in Figure 3.4.1. The other printer is located in an office in another area of MEL and is connected to the computer through a phone line. The terminal panels are mounted on control panel 2 as shown back in Figure 3.2.6 and are connected to the computer via multi-wire ribbon cables. A schematic of the entire data acquisition system is shown in Figure 3.4.2.

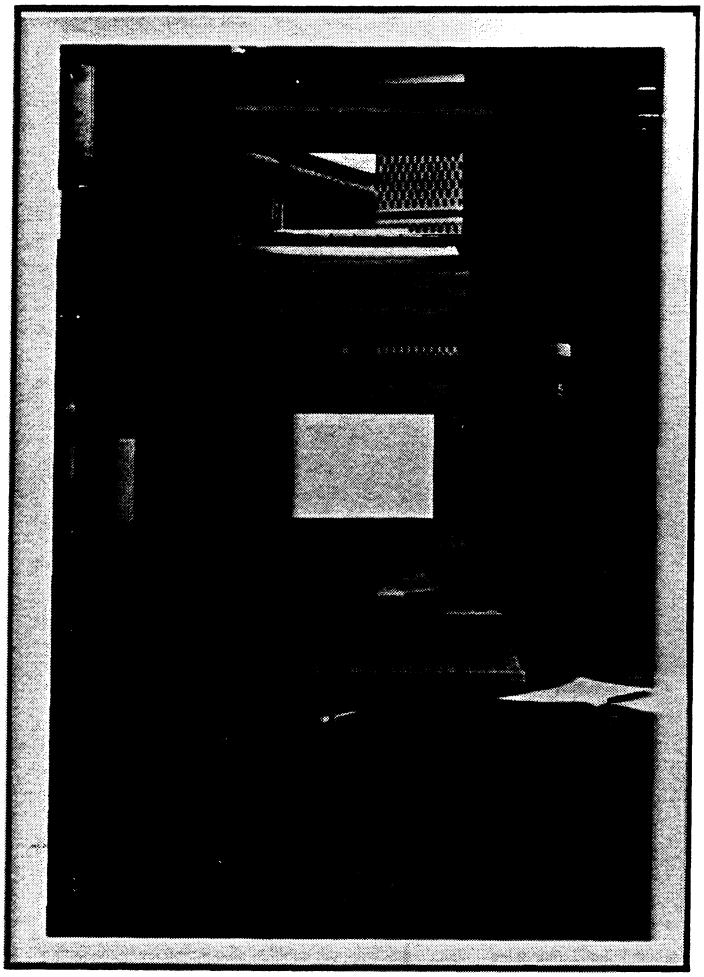

Figure 3.4.1 Photograph of Data Acquisition System

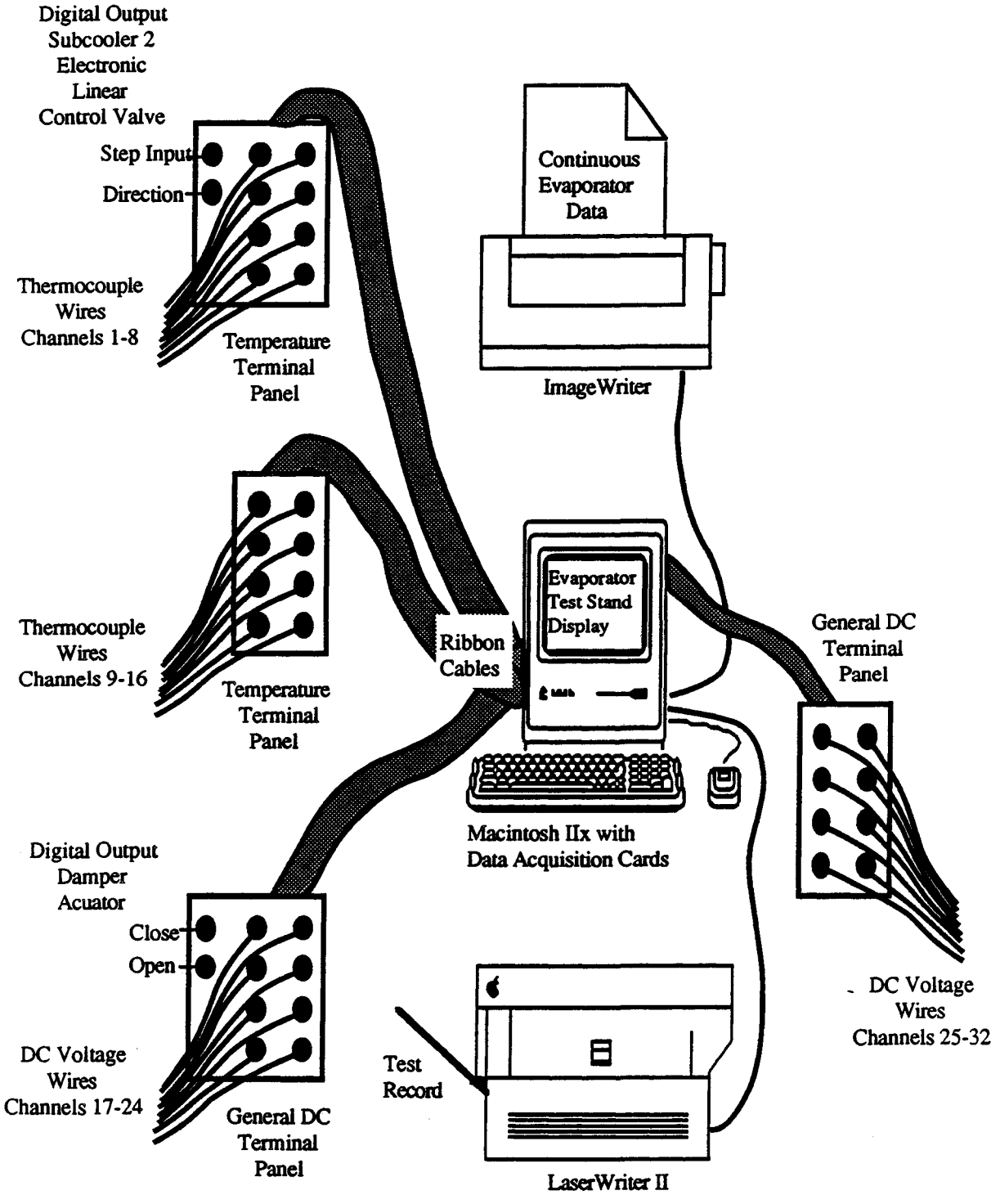

Figure 3.4.2 Schematic of Data Acquisition System

The personal computer used for the data acquisition is an Apple Macintosh IIx. It is used to run the Turbo Pascal program which is responsible for: collecting and processing the data, displaying it on the screen together with a schematic diagram, controlling the expansion valve on subcooler 2 and the damper, and sending a line of data to the Apple ImageWriter II for printing once a minute and a data summary page to the Apple Laser Writer II once every hour. In order to perform these functions, the Macintosh IIx was outfitted with two Strawberry Tree Computers data acquisition cards. The cards work in tandem with four terminal panels each capable of reading eight channels of data. Two of the panels are model T-21 equipped with eight thermocouple channels as well as eight digital inputs/outputs. The other two panels are model T-51s which have eight general purpose DC voltage channels, four optically isolated high voltage DC relays, and four high voltage AC relays. The ACM-16-16 card calibrates and reads the thermocouple temperature panels with 16 bit resolution. The general purpose panels are calibrated and read with ACM2-12-8A cards with 12 bit resolution.

The on-screen display of data consists of a system schematic with temperatures, pressures, and relative humidities situated on the schematic at the locations where they are measured. These measurements are updated every six seconds. There is also a data box on the screen where the air and refrigerant heat loads in Btu/Hr and Watts, the percent difference between the two, the UA-value of the evaporator, the airflow rate in cfm, refrigerant mass flow, evaporator superheat, and evaporator inlet quality are displayed. Figure 3.4.3 shows a photograph of the on-screen display.

The line of data that is sent to the ImageWriter II is made up of the time, air inlet temperature, UA-value, refrigerant inlet temperature, relative humidity before the evaporator measured with the capacitance sensor, the dew point measured with the dew point sensor, the refrigerant temperature before the main expansion valve, the volumetric airflow rate, the air side heat transfer rate, refrigerant mass flow rate, and evaporator inlet refrigerant quality. A sample page of output is presented in Appendix C.

The LaserWriter II one-page summary sheet that is printed contains all of the parameters listed on the screen and on the ImageWriter II output. It consists of the average of ten readings recorded over a one-minute time interval as well as the ten readings themselves. The standard deviations of the data over this one-minute time span are also provided. A sample sheet is presented in Appendix C.

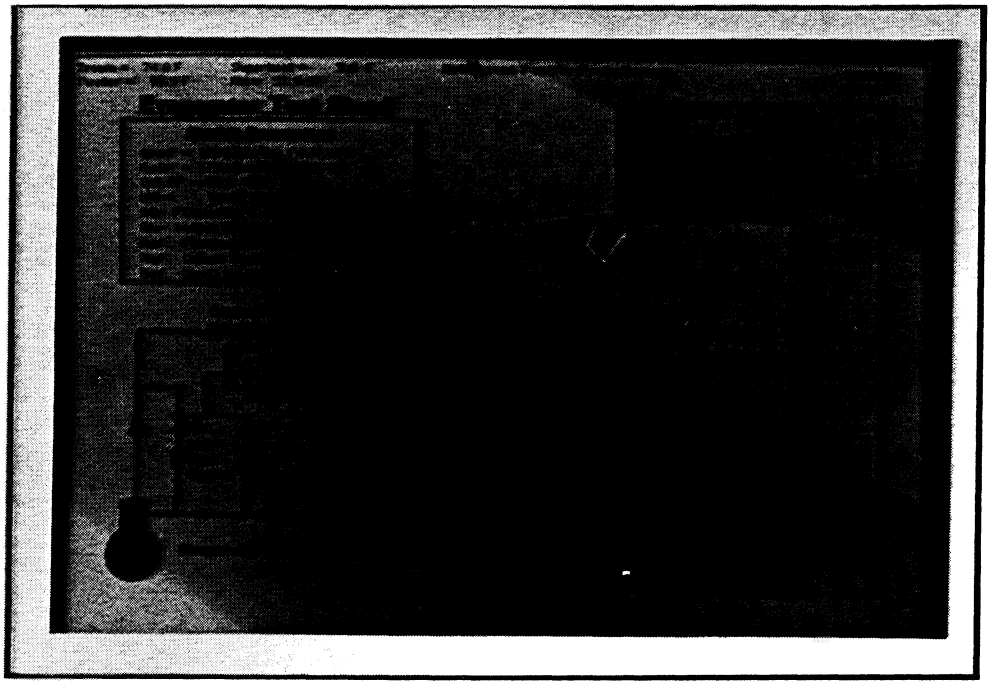

Figure 3.4.3 Photograph of On-screen Data Acquisition Display

In addition to the data acquired by the computer, hand tabulation of humidifier liquid level, evaporator air side pressure drop, and visual observation of the frosting coil was done.

Chapter 4

THEORETICAL ANALYSIS

4.1 Frosting Rate

The rate of frost deposition on the evaporator coil, $\dot{m}_v$, was determined using three methods: the change in the liquid level in the humidifier, the change in the dew point of the air from the inlet of the evaporator to the outlet, and the change in the weight of the coil. The first and the third methods are strictly experimental methods as described in Chapter 5 and require essentially no analytical interpretation of the raw numbers that are measured. The second method, however, does require interpretation.

From the dew point measurements at the inlet and outlet of the evaporator, the inlet and outlet humidity ratios may be calculated. This is done by determining the partial pressure of water at the inlet and outlet of the evaporator. Water partial pressure is determined from the dew point by the following equation from *ASHRAE Handbook – Fundamentals* (1981) which is valid for the temperature range of -148 F to 32 F (-100 C to 0 C):

$$\ln (P_w) = \frac{C_1}{T_{dp}} + C_2 + C_3 T_{dp} + C_4 T_{dp}^2 + C_5 T_{dp}^3 + C_6 T_{dp}^4 + C_7 \ln (T_{dp}) \qquad (4.1.1)$$

where,

T_{dp} = the dew point temperature [K],

P_w = the partial pressure of water [Pa],

C_1 = -5674.5359,

C_2 = 6.3925247,

$C_3 = -0.9677843 \times 10^{-2}$,

$C_4 = 0.62215701 \times 10^{-6}$,

$C_5 = 0.20747825 \times 10^{-8}$,

$C_6 = -0.9484024 \times 10^{-12}$,

and

$C_7 = 4.1635019$.

In equation 4.1.1, it is assumed that the water vapor partial pressure is only a function of temperature and is not affected by the presence of air.

The partial pressure of water is related to the humidity ratio by the following:

$$W = 0.62198 \frac{P_w}{P_{total} - P_w} \qquad (4.1.2)$$

where,

P_{total} = the the total pressure of the moist air [Pa]

and

W = the humidity ratio $[\frac{lb_{m\ water}}{lb_{m\ air}}]$.

The change in the moisture content of the air as it passes over the coil, ΔW, is then determined by:

$$\Delta W = W_{air\ in} - W_{air\ out} \cdot \qquad (4.1.3)$$

This quantity is then related to the frosting rate, $\dot{m}_v$, by multiplying by the mass flow rate of the dry air passing over the coil, $\dot{m}_{air}$, such that

$$\dot{m}_v = \dot{m}_{air}\ \Delta W \quad . \tag{4.1.4}$$

It is assumed that the mass flow rate of the water vapor is negligible compared to the dry air mass flow rate. The methodology for calculation of this flow rate is explained in Appendix A.

Although the frosting rate can be determined directly from the humidifier liquid level measurement as mentioned above, some calculations are required in order to obtain the humidity ratio at the outlet of the evaporator. These calculations involve using equation 4.1.4 to obtain ΔW based on the measured frosting rate, and then plugging this value into equation 4.1.3. It was found that it was necessary to use this procedure to determine W_{out} due to a discrepancy in the outlet dew point measurement. This discrepancy will be further explained in Chapter 6.

4.2 Calculation of Total Evaporator Heat Load

Knowledge of the humidity ratio on each side of the coil may be used to determine the total heat transfer across the coil. Although usually the amount of latent heat transfer is very small compared to the the sensible heat transfer, in this case it was found that the latent heat transfer was about 10 percent of the total heat transfer for many of the test conditions. Therefore, both latent and sensible heat transfer were included in the calculation of air side heat transfer. From *ASHRAE Handbook – Fundamentals* (1981), the total specific enthalpy of the air can be calculated in the inch-pound system of units with the equation:

$$h = 0.240T_{db} + W(1061 + 0.444\ T_{db}) \tag{4.2.1}$$

where,

h = total specific enthalpy of air $[\frac{Btu}{lb_{m\ air}}]$,

T_{db} = the dry bulb temperature [F],

and

W = the humidity ratio $[\frac{lb_{m\ water}}{lb_{m\ air}}]$.

Once the total enthalpy of the air is calculated at both the inlet and outlet, the difference between the two, Δh, is then used to calculate the total heat load, $\dot{Q}$, by multiplying it by the air mass flow such that:

$$\dot{Q} = \dot{m}_{air}\,\Delta h \ . \qquad (4.2.2)$$

Since the evaporator was operated in a flooded condition during all of the test runs and there was no means to measure the evaporator outlet quality, it was not possible to verify the calculation of total evaporator heat load by comparing the air side calculation with a refrigerant side calculation. However, in previous work with the system where superheat was maintained at the outlet, the energy balance of the two sides was within 7%. Therefore, the accuracy of the air side heat load calculation should be acceptably accurate.

4.3 Overall Heat Transfer Coefficient

The average overall heat transfer coefficient, UA, for the evaporator coil under frosting conditions may be represented by:

$$\frac{1}{UA} = \frac{1}{h_{ref}\,A_i} + R_{tubewall} + R_{contact} + R_{frost} + \frac{1}{h_{air}\,\eta\,A_o} \qquad (4.3.1)$$

where,

h_{ref} = the average refrigerant side convective heat transfer coefficient [Btu/hr-ft^2-F],

A_i = the inside surface area of the tube [ft^2],

$R_{tubewall}$ = the thermal resistance of the tube wall [hr-F/Btu],

$R_{contact}$ = the thermal contact resistance between the tube and fin [hr-F/Btu],

R_{frost} = the thermal resistance of the frost layer [hr-F/Btu],

h_{air} = the average air side convective heat transfer coefficient [Btu/hr-ft^2-F],

η = overall thermal efficiency of air side primary and secondary surfaces,

and

A_o = the outside surface area (primary and secondary surfaces) [ft^2].

Since there are no fins on the inside of the coil tube, the efficiency of the surface inside the tube is equal to unity and has been omitted from the equation.

Both the contact resistance and the frost resistance listed in equation 4.3.1 vary as the thickness of the frost on the outer surfaces of the evaporator coil increases. The contact resistance varies due to the filling of the interstitial gaps between fin and tube by the frost. The frost resistance varies due to both the increasing thickness of the frost layer as well as a density change that occurs as the frost grows. Since there is presently no method for determining the variation of these two resistances directly, the UA-value must be determined by other means. The method that was chosen was the log-mean-temperature-difference (LMTD) method.

Using the LMTD method, the total heat transfer from the air to the refrigerant, $\dot{Q}$, for a multi-pass heat exchanger such as the evaporator is defined as

$$\dot{Q} = UA \; F_G \, \Delta T_{lm} \qquad (4.3.2)$$

where,

F_G = the correction factor for a multi-pass heat exchanger.

The ΔT_{lm} in the above equation is defined as the LMTD for a counterflow heat exchanger and the F_G factor is used to correct for the fact that this may not actually be so. However, since the refrigerant side of the heat exchanger is maintained as a two-phase mixture throughout the length of the heat exchanger in this case, a constant temperature is assumed for the refrigerant side. This is not precisely the case due to the fact that there is a finite pressure drop through the heat exchanger. Depending on the refrigerant flow rate this pressure drop was between 1.5 and 3.0 psid (10 and 21 kPa) which corresponds to approximately a 2 F (1 C) drop in refrigerant temperature. Because this difference is relatively small, a constant refrigerant temperature was taken to be a reasonable assumption. Based on this assumption, the geometry of the heat exchanger can now be treated as a straight counterflow exchanger, and, so, F_G is equal to 1.

The ΔT_{lm} for a counterflow heat exchanger with a constant refrigerant side temperature is defined as

$$\Delta T_{lm} = \frac{\Delta T_1 - \Delta T_2}{\ln(\Delta T_1/\Delta T_2)} \tag{4.3.3}$$

where

$$\Delta T_1 = T_{air,\,in} - T_{ref} \tag{4.3.4}$$

and

$$\Delta T_2 = T_{air,\,out} - T_{ref} \,. \tag{4.3.5}$$

For this study the measured refrigerant inlet temperature was used to determine T_{ref}.

Once ΔT_{lm} is determined, UA may be calculated with equation 4.3.2.

Chapter 5

EXPERIMENTAL METHOD

5.1 Start-Up

Before actual test data were recorded, a standard start-up procedure was followed. The first thing that needed to be accomplished was the removal of all moisture from the coil that had been left from the previous test run. It was found that a substantial amount of moisture tended to adhere to the coil after the frost was melted. In order to remove this residual condensate, the blower in the air loop was run for about two hours. The air loop was then opened up to the ambient environment so that the humidity in the air loop would equalize with the humidity in the laboratory. During the winter and spring months when the relative humidity in MEL was below 50%, this process was adequate for obtaining a low enough moisture content in the test section so that frosting on the evaporator coil before water was added to the humidifier was kept to insignificant amounts. However, during the more humid summer months in Urbana-Champaign, an additional step was required in order to remove moisture from the air loop. This step involved placing desiccant in the return duct and running the blower for approximately an hour. After the hour, the desiccant was removed and the air loop was sealed. This proved to be more than adequate in removing sufficient moisture from the air loop.

Once the system was sealed, the refrigeration system for the refrigerated enclosure in which the air loop is located was run for approximately eight hours before the actual test facility refrigeration system was started. The reason for doing this was to allow for a quicker attainment of the test conditions that are required. Since the test condition temperatures of the air loop, 10 to 30 F (-12 to -1.1 C), are well below the ambient temperature range of 70 to 90 F (21 to 32 C), this eight-hour cool-down period with just the refrigerated enclosure operating allowed all of the air in

the loop as well as the hardware to reach temperatures close to the set point temperatures before the test facility was completely activated.

After the cool-down period, the appropriate nozzles were opened in the air loop, the blower was started, and the compressor of the test facility refrigeration system was then started. At start-up the hot gas bypass valve was opened approximately halfway in order to insure that all vapor reached the compressor and no slugging occurred.

5.2 Setting Test Conditions

After a successful start-up was achieved, a series of tuning procedures were then carried out in order to obtain the testing set points. The tuning procedures included: selecting the temperature for the air entering the evaporator and the temperature of the refrigerated enclosure and setting the controller at that temperature, adjusting the air side flow control damper, the main expansion valve, the hot gas bypass valve, and the valves for subcoolers 1 and 2.

The first adjustments that were made were the settings of the air inlet temperature and the refrigerated enclosure temperature. Both of these temperatures are controlled by the heater controllers described in Chapter 3. For the test conditions required for this study, air inlet temperatures of 10 F (-12 C) and 20 F (-6.7 C) were set. In order to minimize the heat transfer between the air loop and the refrigerated enclosure, the enclosure was set at a temperature in between the inlet and outlet temperatures of the air passing over the evaporator coil. Therefore, for the 10 F air inlet temperature, the refrigerated enclosure was set at approximately 3.0 F (-16 C); for the 20 F case, the enclosure was set at 10 F (-12 C); and for the -20 F refrigerant inlet case, the enclosure was set at 1.0 F (-17 C).

The airflow damper was then adjusted after the temperature set points had been preliminarily selected. In addition to using the damper for flow-control purposes, the nozzles were also required to obtain the full range of airflows. For the baseline airflow rate of 40 cfm (18 L/s), the 1 in. and 1/2 in. nozzles were opened. Only the 1 in. nozzle was in operation for the 25 cfm (11 L/s) test run. For the 80 cfm (38 L/s) cases, the 2 in. and 1/2 in. nozzles had to be opened. In order to maintain a constant airflow during the frosting process as was desired for the prescribed testing conditions, the damper was slowly opened as the evaporator becomes more and more blocked.

After the air side was set, attention was then turned to the refrigerant side of the test facility. The first area of concern on this side was the main expansion valve located just before the evaporator. This expansion valve was adjusted so that the desired amount of superheat at the evaporator outlet was achieved. For the present testing, the evaporator was operated in a flooded condition so as to maintain an approximately constant temperature on the refrigerant side for the reasons outlined in Section 4.3.

The second refrigerant side valve that was manipulated was the expansion valve for subcooler 1. This valve was set in order to maintain enough subcooling so that there was no danger of the refrigerant flashing to vapor in the mass flow meter, which has a fairly substantial pressure drop ~10 psid (69 kPa), or anywhere else in the plumbing between subcooler 1 and subcooler 2. Approximately 50 F (28 C) of subcooling was usually maintained at the outlet of subcooler 1.

Once it was assured that there was subcooled liquid in the mass flow meter, the pressure at the inlet of the evaporator and, consequently, the temperature for the two-phase mixture were then set. This was done by regulating the amount of refrigerant that was bypassed around the evaporator. The evaporator inlet pressure is directly related to the amount of bypass. In order to decrease the evaporator pressure the hot gas bypass valve must be throttled down. Decreasing the amount of bypass lowers the evaporator refrigerant temperature. Evaporator pressures of 20.0 psia (138 kPa)

and 16.0 psia (110 kPa) were achieved during testing corresponding to evaporator temperatures of -10 F (-23 C) and -20 F (-29 C), respectively.

The last refrigerant side temperature that needed to be set was the temperature before the main expansion valve. This temperature, as well as the evaporator pressure, determines the quality of the refrigerant entering the evaporator. Its magnitude is determined by the amount of subcooling provided by subcooler 2. The amount of subcooling is controlled by the expansion valve on the subcooler. Opening this valve increases the amount of subcooling. For the present set of tests this temperature was maintained at approximately 30 F (-1.1 C) in order to maintain a quality of 0.11 at the evaporator inlet for an inlet temperature of -10 F (-23 C). An expansion valve inlet temperature of approximately 19 F (-7.2 C) was required for the -20 F (-29 C) evaporator inlet case in order to obtain a 0.11 inlet quality.

After the above adjustments had been made, many of them were repeated usually more than once in order to obtain the required set points. Once the set points were achieved, a sufficient length of time was allowed to pass with the system at these set points so that the attainment of steady-state conditions was assured. At steady-state conditions, frosting was then commenced.

5.3 Frosting Test Procedure

Once the system had obtained steady-state operation, a one page data summary sheet was saved, and water was introduced into the humidifier in the air loop. In order to add water to the humidifier, the air loop blower was momentarily turned off to relieve the air pressure. While the blower was off, 20.3 ounces (600 mL) of water were poured into the humidifier in the return duct through the access port described in Chapter 3. The access port was then closed and the blower was turned back on. The liquid level in the humidifier was also recorded at this time.

The heater in the humidifier and the recirculation fan in the return duct were activated as soon as the water was added. The Powerstat connected to the humidifier heater was used to control the temperature of the water and, consequently, the humidity in the air loop. It usually took between 15 and 20 minutes to achieve the desired relative humidity.

Thirty-five minutes after water was added to the humidifier, the dew point sensor sampling line was switched from the evaporator inlet to the evaporator outlet. After allowing ten minutes for a steady-state reading to be measured, the outlet dew point was then recorded and the sampling line was switched back to the inlet. During the interim, when no inlet dew point measurement was available, the relative humidity sensor was used to verify that the relative humidity at the inlet was being maintained at the desired set point. An hour after the initial addition of moisture into the loop, the data summary page, the pressure drop across the evaporator coil, and the liquid level were recorded. At this time, the photographs of the frosted coil shown in Chapter 6 were also taken.

The entire procedure described in the above paragraph was repeated every hour for the duration of the test run.

5.4 Determination of the Amount of Frost on the Evaporator

In addition to the determination of frosting rate by the change in absolute humidity of the air as it passes over the evaporator which was described in Chapter 4 and the change in the humidifier liquid level described in the previous section, two other methods to verify the rate were also pursued. These consisted of melting the condensate off the coil and collecting and measuring it and weighing the coil with the frost still attached.

For the first method, the collection process was done by opening the bottom plenum of the air loop after the completion of testing and inserting a collection vessel underneath the coil. After an overnight melt of the frost, the water collected was then measured. This method was shown to be very inaccurate. The problems with it were two-fold. First, a significant amount of moisture tended to adhere to the coil and not drop down to the collection container. Second, the overnight melting period allowed for a significant amount of evaporation to occur, thus further eroding the accuracy of the measurement. These two difficulties required that another frost measurement method be pursued.

The alternate method that was selected required disconnecting the evaporator coil from the refrigeration system and removing it from the air loop. The coil was then weighed with the frost still attached on a Compax CX-6000 load cell type electronic balance which was independently verified to have an accuracy within 1% of reading. Since this entire process was performed in less than 20 minutes, evaporation was not a problem.

Chapter 6

EXPERIMENTAL RESULTS

6.1 Baseline Case

In order to obtain experimental data that is as reflective as possible of steady-state domestic refrigerator-freezer evaporator operation, a set of baseline conditions was chosen that closely match normal operating conditions assuming all return air is from the freezer compartment. The baseline conditions that were examined are given in Table 6.1.1.

Table 6.1.1 Baseline Testing Conditions

Parameter	Value
Refrigerant Inlet Temperature	-10 F (-23 C)
Evaporator Inlet Quality	0.11
Inlet Air Temperature	10 F (-12 C)
Inlet Air Relative Humidity	52%
Airflow Rate	40 cfm (18 L/s)

In addition to the conditions listed in the table, it should be noted that the evaporator was flooded during operation. This means that the refrigerant leaving the evaporator was a saturated mixture with no superheat. This was done in order to maintain a relatively constant refrigerant temperature throughout the evaporator. Since the pressure drop through the coil is relatively small (1.5 to 3.0 psid, 10 to 21 kPa), the saturation temperature of the two-phase refrigerant in the evaporator remains essentially constant (within 2 F, 1 C). Therefore, the overall UA-value of the coil may be

calculated from the log-mean-temperature-difference and the total heat load as was described in Chapter 4.

The UA-value for the baseline case is shown over a ten-hour testing period in Figure 6.1.1 for three test runs on three different days (April 6, 1990; May 17, 1990; and June 1, 1990). In the

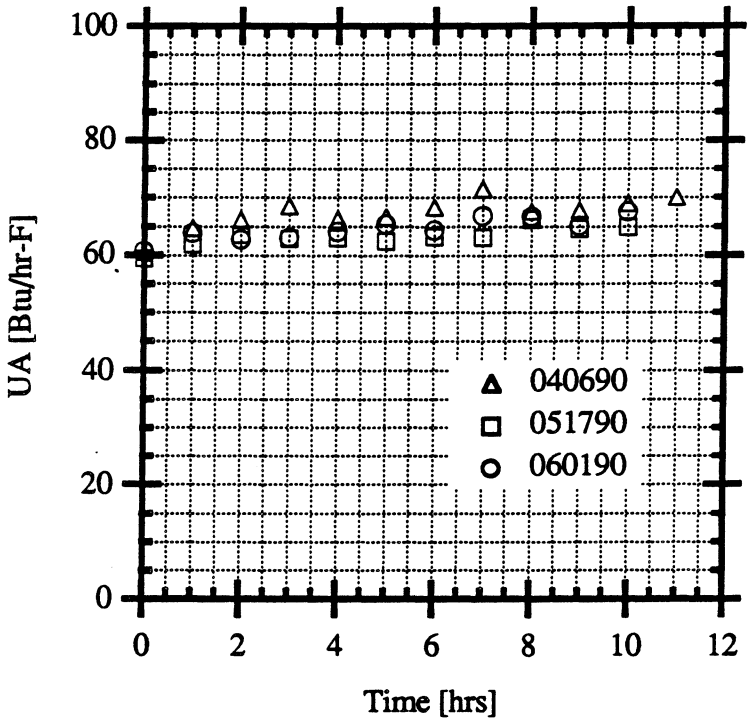

Figure 6.1.1 Evaporator UA-value Versus Time for the Baseline Conditions

figure it can be seen that there is a slight increase in UA as frost builds up on the coil. This 8% increase in UA is accompanied by a 67% increase in the air side pressure drop through the coil as frost begins to block the coil. This increase is shown in Figure 6.1.2. Since the initial pressure drop across the coil is small (~ 0.015 in. water), this increase still leaves the air side pressure drop slight.

The frost formation rate at each hour of frosting is shown in Figure 6.1.3. The frosting rate was determined by measuring the liquid level in the humidifier once an hour as described in Chapter 5 with the assumption that all of the water leaving the humidifier is deposited on the evaporator coil. The change in the level per hour was then converted to a mass change per hour by

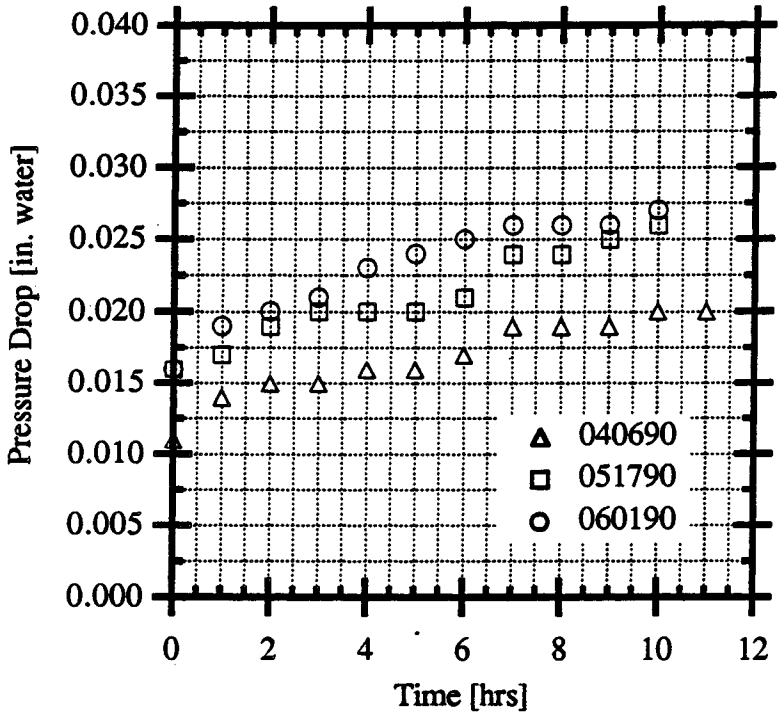

Figure 6.1.2 Evaporator Air Side Pressure Drop Versus Time for the Baseline Conditions

using the dimensions of the humidifier and the density of water. The scatter in the frosting data is due to a resolution in the liquid level measurement of only 0.02 in. (0.5 mm) which corresponds to a frosting rate resolution of 0.01 lb_m/hr. It can be seen in the figure that the frosting rate is practically constant for the duration of the test given the measurement resolution.

Figures 6.1.1 to 6.1.3 also provide information about the repeatability of the evaporator test facility and testing procedure for the baseline conditions. In Figure 6.1.1, it can be seen that all the

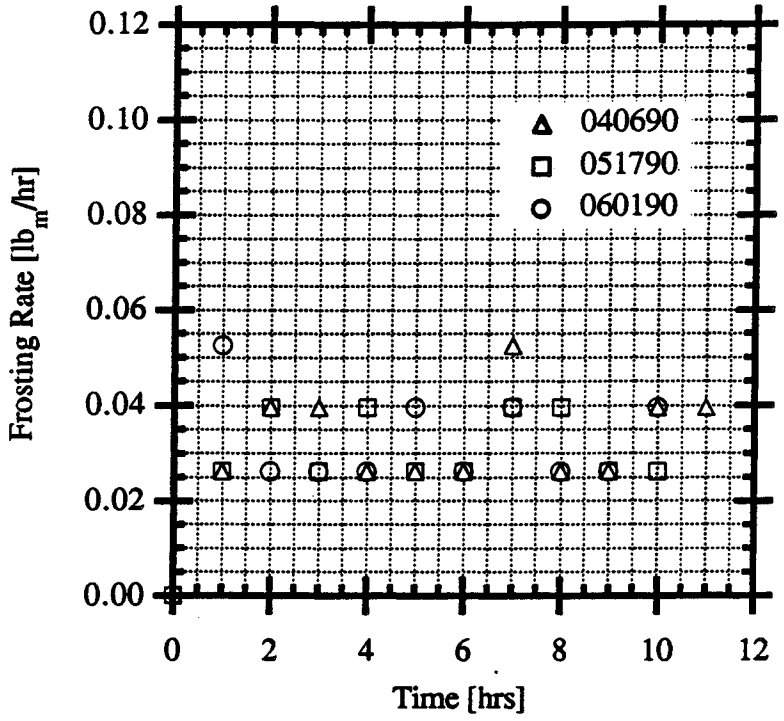

Figure 6.1.3 Evaporator Frosting Rate Versus Time for the Baseline Conditions

test data for runs 040690, 051790, and 060190 are within approximately 10% of each other. In Figure 6.1.2, the pressure drop data points are within 25% of each other. The frosting rate data in Figure 6.1.3 shows that all of the points besides the one-hour data point are within 0.015 lb_m/hr. Given the resolution of the measurement, the repeatability is acceptable. The discrepancy in the first hour is probably due to the fact that in that hour the relative humidity will usually be in a transient state since the water has just been added to the humidifier and the heater has just been activated.

There are three possible explanations for the increase in the UA-value shown in Figure 6.1.1. First, since there is only a mechanical bond between the evaporator coil tubing and the fins rather than a metallurgical one as explained in Chapter 3, when frost begins to form on the tubes of the evaporator it tends to fill in the gaps between the fin and tube. This could significantly reduce the

contact resistance between the tube and fin and, consequently, increase the overall heat transfer coefficient between the air and the refrigerant.

The second possible explanation for the UA-value increase is that the frosting on the tube and fins increases the air side convective heat transfer coefficient. There are two mechanisms by which this may happen. One mechanism is the added roughness that is provided to the surfaces of the tube and fins by the frost. This roughness will "trip" the boundary layer on the surfaces from laminar to turbulent flow more quickly than the smooth surfaces, thus providing the higher Nusselt numbers associated with turbulent flow as well as delaying boundary layer separation from the cylindrical tube surfaces. The other mechanism for increasing the air side convective heat transfer coefficient is the increased local air velocity that will occur due to the fact that the air passages are decreasing in size as the frost forms while the total airflow through the coil is maintained constant.

The third explanation for the increased UA-value is that the frost has the potential to behave as an additional extended surface. Since the frost layer may tend to be quite porous, a significant amount of microscopic surface area may be added to the tube and fins through the deposition of frost. This additional surface area would increase the heat transfer capacity of the coil.

6.2 Parametric Study Results

Once a baseline condition was established for UA-value, evaporator air side pressure drop, and frost rate, a parametric study of how each of these three quantities are affected by individually varying the relative humidity, airflow rate, air inlet temperature, and refrigerant temperature was pursued.

The first parameter that was examined was the relative humidity of the inlet airflow. The humidity was increased from the baseline value of approximately 52% to 72%. The effects of this higher humidity are given in Figures 6.2.1, 6.2.2, and 6.2.3. It is apparent in Figure 6.2.1 that the effect of frost on the UA-value is even more pronounced here than in the baseline case. Over the ten-hour testing period, UA increased approximately 48% and appears to still be headed upwards at the last measurement. This increase in UA is substantially larger than the increase for

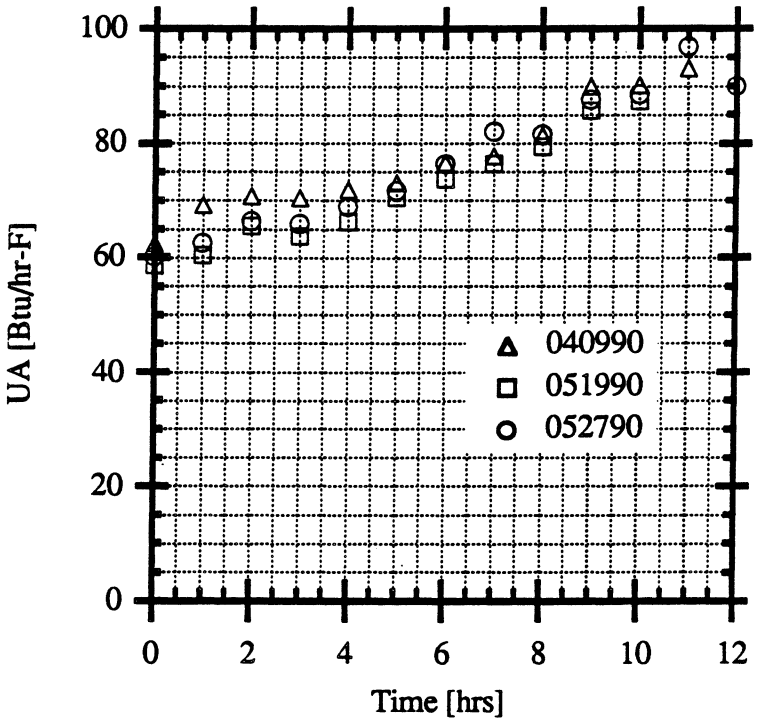

Figure 6.2.1 Evaporator UA-value Versus Time with 72% Relative Humidity

the baseline case due to the faster frosting rate. The frosting rate is more than twice as great for this case compared with the baseline case as illustrated in Figures 6.1.3 and 6.2.3. The frosting rate increases because of the larger difference that exists between the dew point of the inlet air and the surface temperature of the coil with a higher relative humidity.

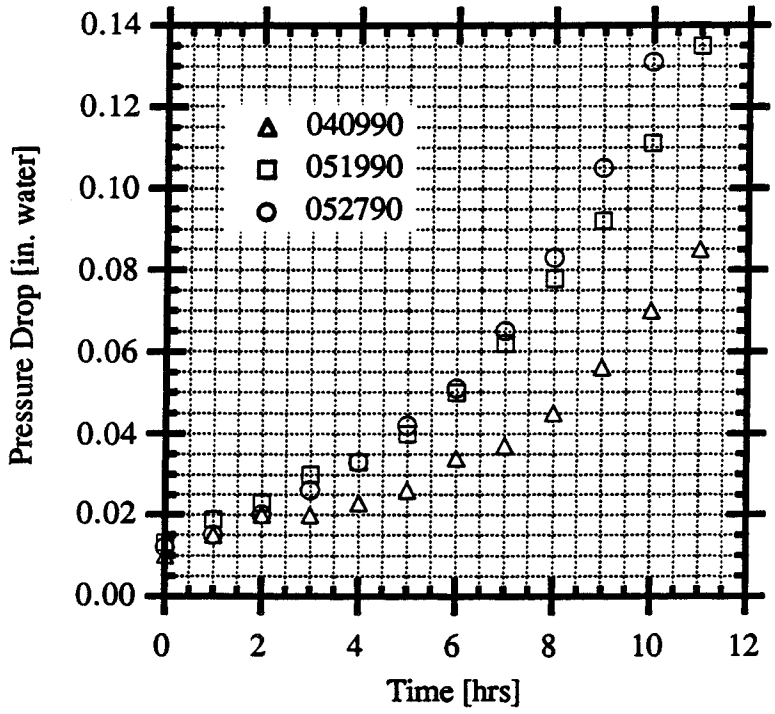

Figure 6.2.2 Evaporator Air Side Pressure Drop Versus Time with 72% Relative Humidity

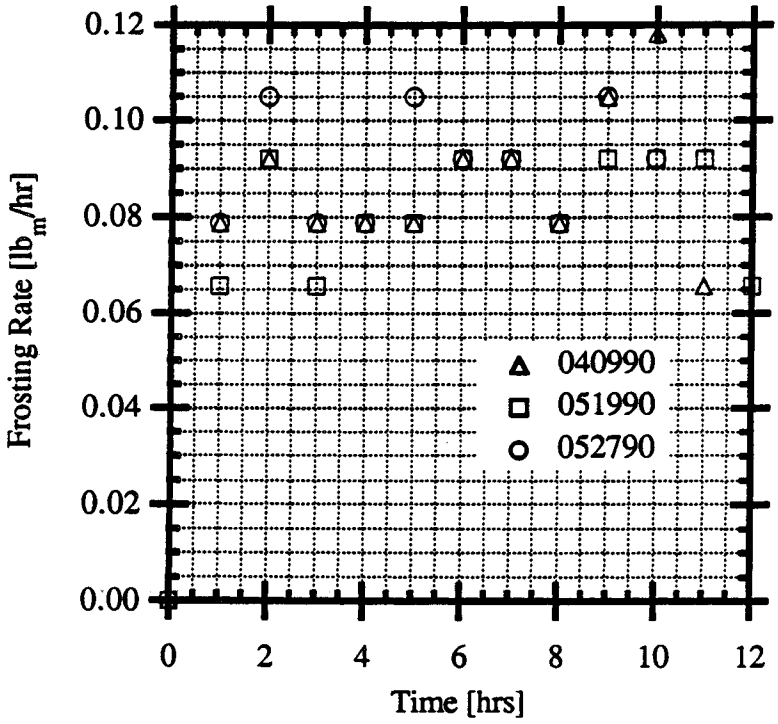

Figure 6.2.3 Evaporator Frosting Rate Versus Time with 72% Relative Humidity

Figure 6.2.2 shows that the pressure drop across the coil increases markedly just as the UA-value did. After ten hours, the pressure drop was approximately 13 times its initial value.

The repeatability of the 72% relative humidity case is as good as the baseline case for UA-value data but is significantly worse for pressure drop. In Figure 6.2.2, it can be seen that at the eleventh hour the 040990 pressure drop is almost 40% less than the corresponding 051990 pressure drop. However, the 051990 and 052790 data points are within 15% of each other at hour ten, even though there is a tendency of the two readings to diverge as the pressure drop increases. The reasons for this discrepancy are probably due to the hysteresis of the Magnehelic and a failure to zero it after every test, which was found, too late for this test, to be a requirement. The frosting rate measurements for all three case were found to agree well within 20%.

The next parameter that was varied was the airflow rate. These results are presented in Figures 6.2.4 to 6.2.9. For these cases the airflow was decreased to 25 cfm (12 L/s) (Figures 6.2.4 to 6.2.6) and increased to approximately 80 cfm (38 L/s) (Figures 6.2.7 to 6.2.9). In these figures it should be noted that the UA-value of the clean coil at 80 cfm is much higher than the UA-value of the clean coil at 40 cfm owing to the higher mass flow rate through the air loop. Likewise, the UA-value at 25 cfm is lower than it is at 40 cfm. However, like the baseline results, the UA-value does not increase very significantly from the start of testing to the completion ten hours later for either the higher-flow or lower-flow rates. Also, the frosting rates shown in Figures 6.2.6 and 6.2.9 are in the same range as the baseline frosting rates (0.02 to 0.04 lb_m/hr). These results seem to imply that air velocity has only a slight effect on the formation of frost on the coil. In the literature review in Chapter 2, it was shown that some researchers found that air velocity had little to no effect on the frosting rate while others found it to be strongly related to the frosting rate. The overall conclusion in the literature appeared to be that air velocity has a great effect at higher velocities but little effect at lower velocities. Since the velocities are relatively low

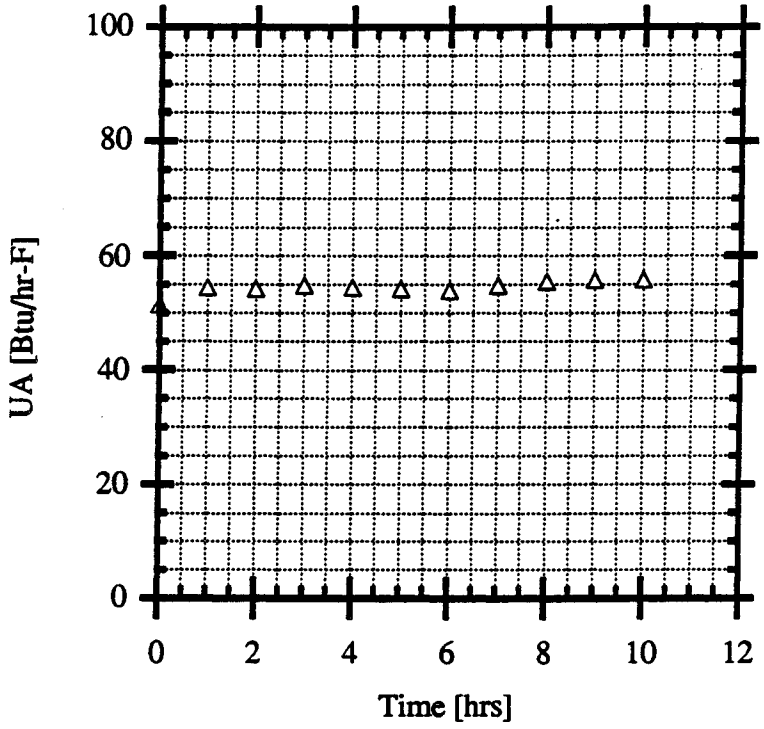

Figure 6.2.4 Evaporator UA-value Versus Time with a 25 cfm Airflow Rate

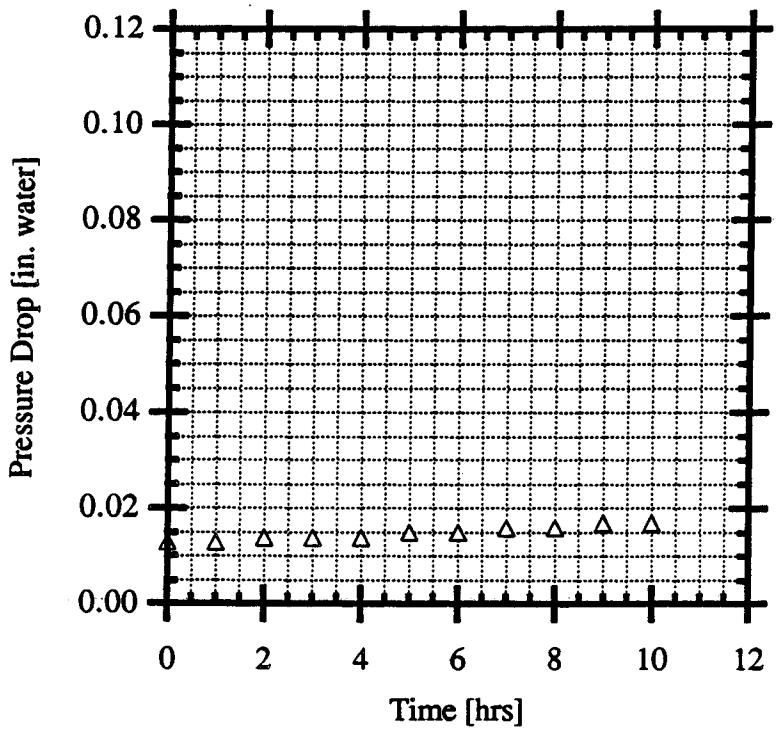

Figure 6.2.5 Evaporator Air Side Pressure Drop Versus Time with a 25 cfm Airflow Rate

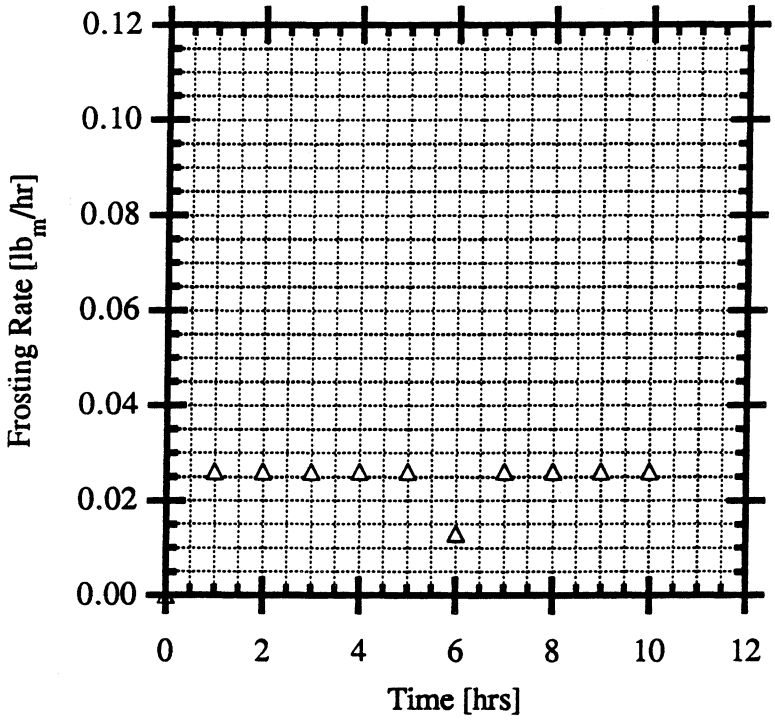

Figure 6.2.6 Evaporator Frosting Rate Versus Time with a 25 cfm Airflow Rate

in the cases illustrated here (77 to 250 ft/min, 24 to 75 m/min), these results seem to verify this conclusion. The effect of velocity on frosting rate is slight, if there is any effect at all. The reasons behind these phenomena will be discussed in Section 7.2.

In the 80 cfm plots in Figures 6.2.7 to 6.2.9, repeatability is adequate. Although worse than the previous cases presented, the UA-values are still within 15% for runs 041190 and 071090. The pressure drop measurements are within approximately 10% of each other, and the discrepancy in the frosting rate is on the same order as the previous tests.

The third parametric variation that was made was in the air temperature at the inlet to the evaporator. This temperature was raised from the baseline value of 10 F (-12 C) to 20 F (-6.7 C), thus increasing the dew point temperature of the air since the relative humidity was maintained at approximately the same value as in the baseline case. This should increase the frosting rate and

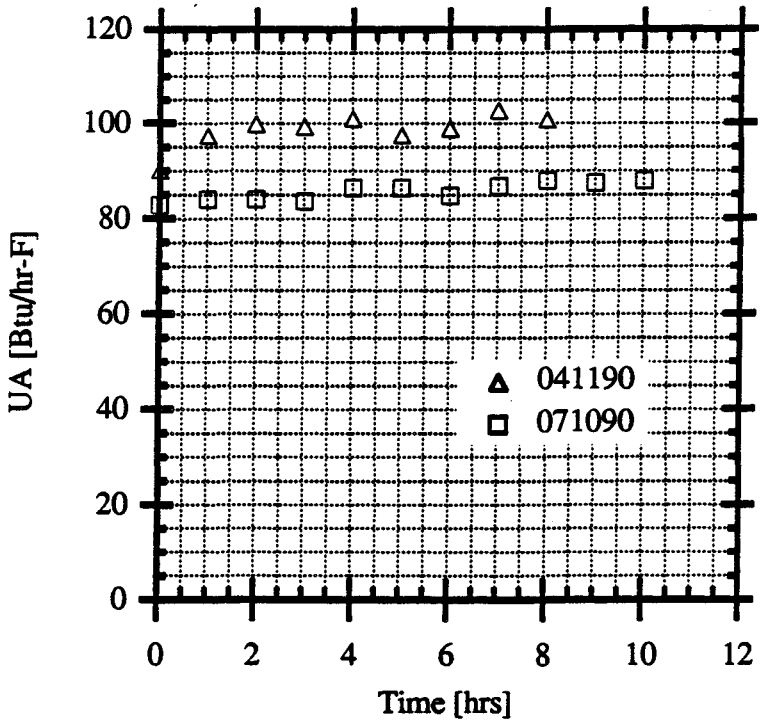

Figure 6.2.7 Evaporator UA-value Versus Time with an 80 cfm Airflow Rate

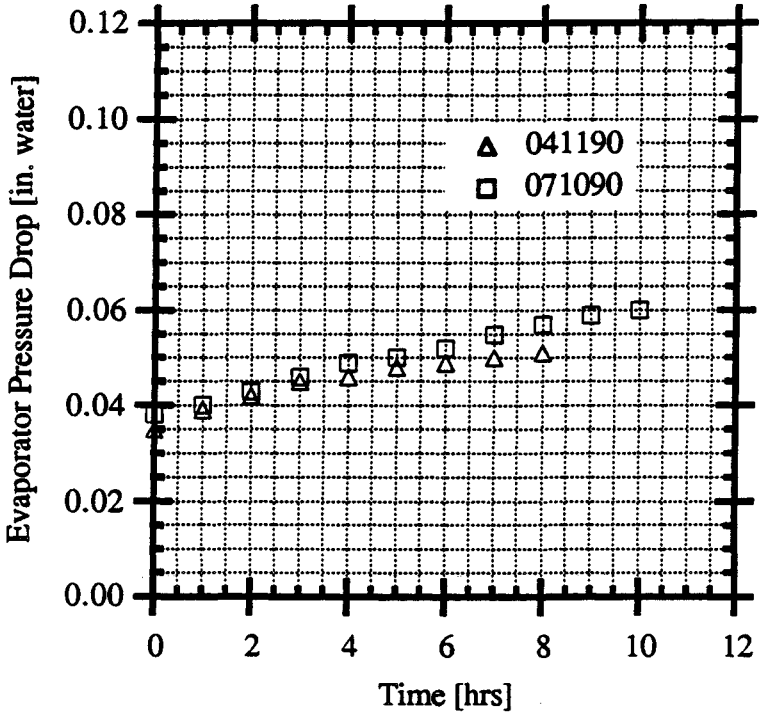

Figure 6.2.8 Evaporator Air Side Pressure Drop Versus Time with an 80 cfm Airflow Rate

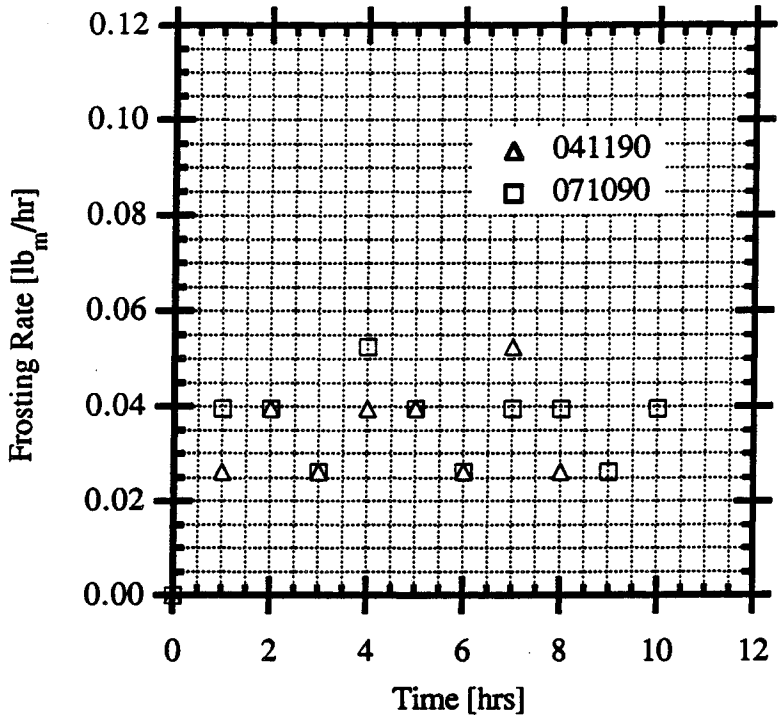

Figure 6.2.9 Evaporator Frosting Rate Versus Time with an 80 cfm Airflow Rate

UA-value just as increasing the relative humidity did in the 72% relative humidity case. Indeed, this is exactly what happens as can be seen in Figures 6.2.10 to 6.2.12. In Figure 6.2.10, the UA-value increases approximately 50% over a ten-hour period with a 20 F air inlet temperature which is comparable to the increase found in the 72% relative humidity case. The pressure drop increases 13 fold as shown in Figure 6.2.11 which is also close to the increase experienced with the high-humidity case. The frosting rates shown in Figure 6.2.12 are approximately 15% higher than the 72% relative humidity case, due to the larger difference between the dew point temperature of the air entering the evaporator and the coil surface temperature as will be further expounded upon in Section 7.2.

As far as repeatability is concerned, the UA-values for runs 041890 through 071990 are within 10%. The pressure drop results display the same tendency to diverge at higher pressure

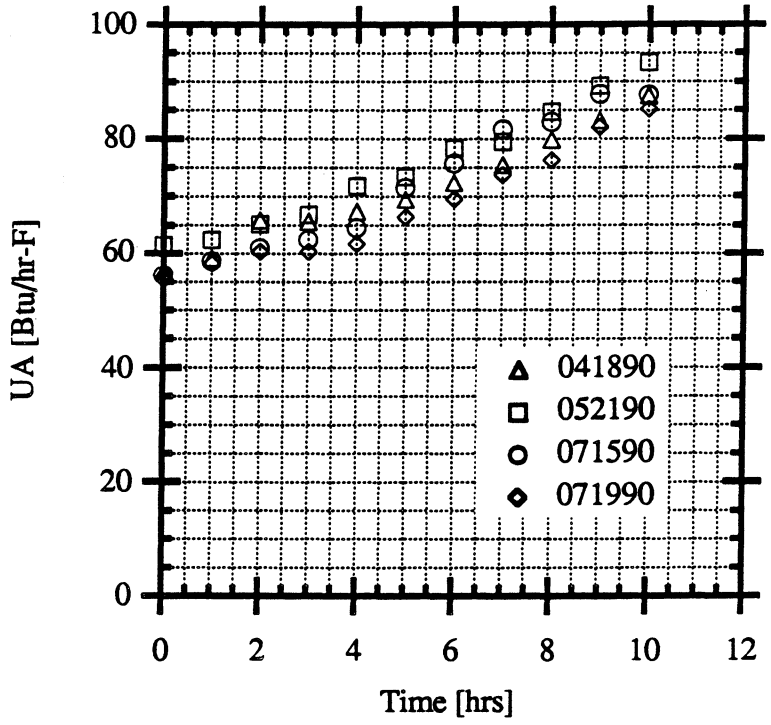

Figure 6.2.10 Evaporator UA-value Versus Time with $T_{air,\ in}$ = 20 F

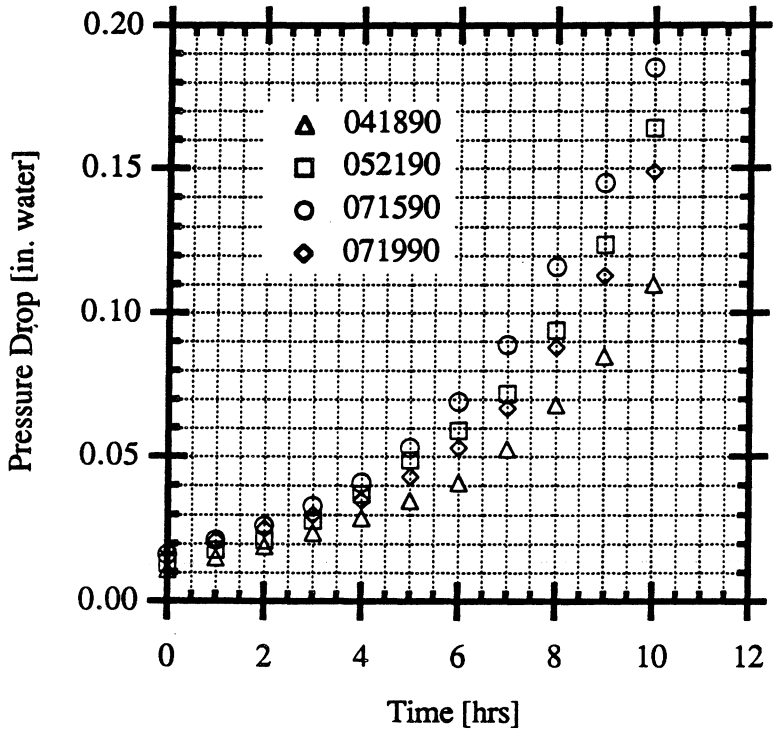

Figure 6.2.11 Evaporator Air Side Pressure Drop Versus Time with $T_{air,\ in}$ = 20 F

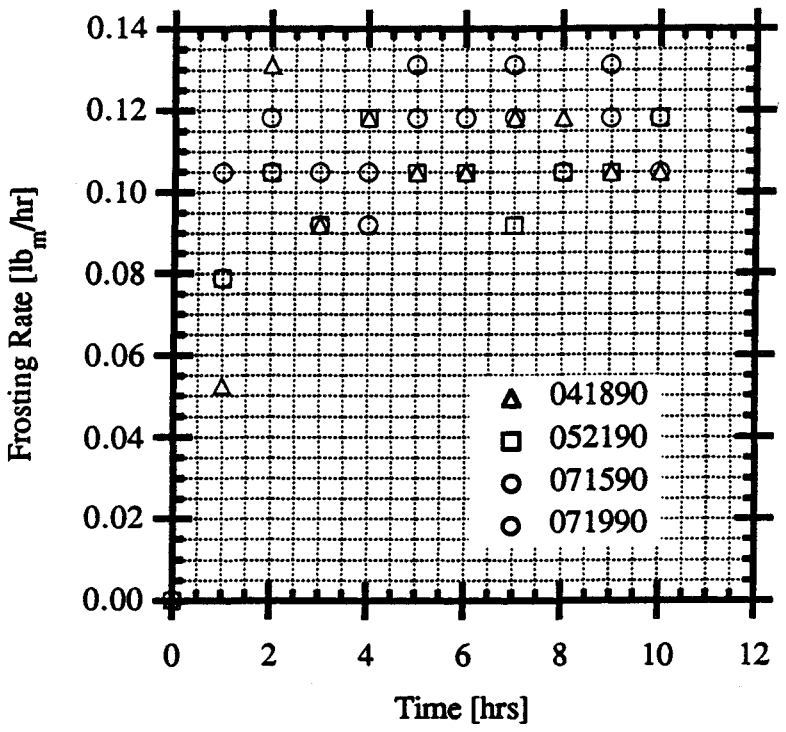

Figure 6.2.12 Evaporator Frosting Rate Versus Time with $T_{air, in}$ = 20 F

drops that was evident in the previous results. This time the discrepancy is about 30% at the tenth hour. The frosting rate repeatability is again on the order of the previous results.

The final parameter variation that was performed was on the temperature of the refrigerant entering the coil. This temperature was decreased to -20 F (-29 C). This also had a substantial effect on UA-value, pressure drop, and frosting rate during the frosting process. In Figure 6.2.13 an approximately 50% increase in UA-value is shown over the ten-hour data gathering period. The pressure drop increases eight times over its initial value as given in Figure 6.2.14. The average frosting rate in Figure 6.2.15 has increased compared with the baseline case as would be expected due once again to the larger dew point-surface temperature difference. It is, however, about 30% lower than the frosting rate for the 20 F air inlet temperature. The results shown in these three figures indicate that increasing the dry bulb temperature of the air by 10 F has more of an effect on

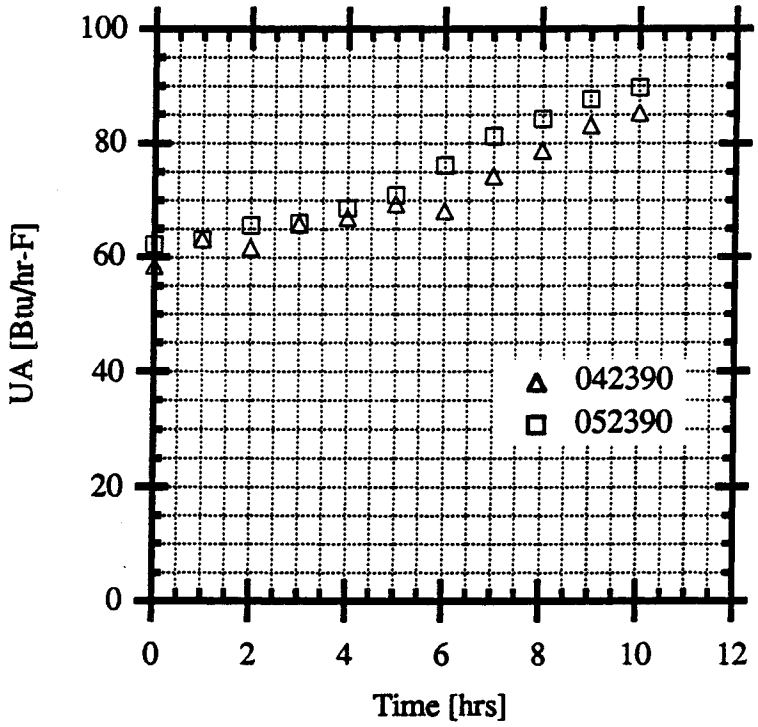

Figure 6.2.13 Evaporator UA-value Versus Time with $T_{ref, in}$ = -20 F

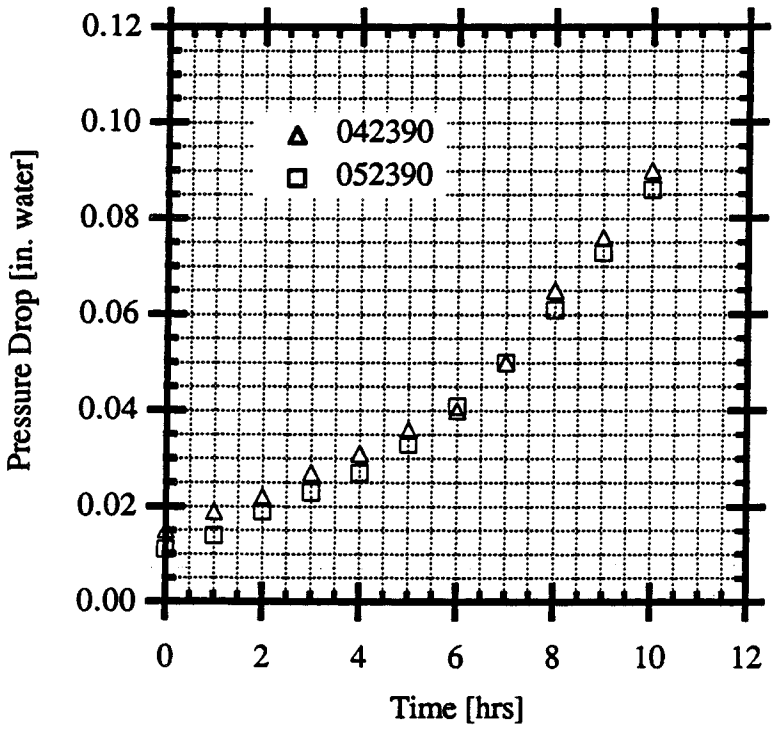

Figure 6.2.14 Evaporator Air Side Pressure Drop Versus Time with $T_{ref, in}$ = -20 F

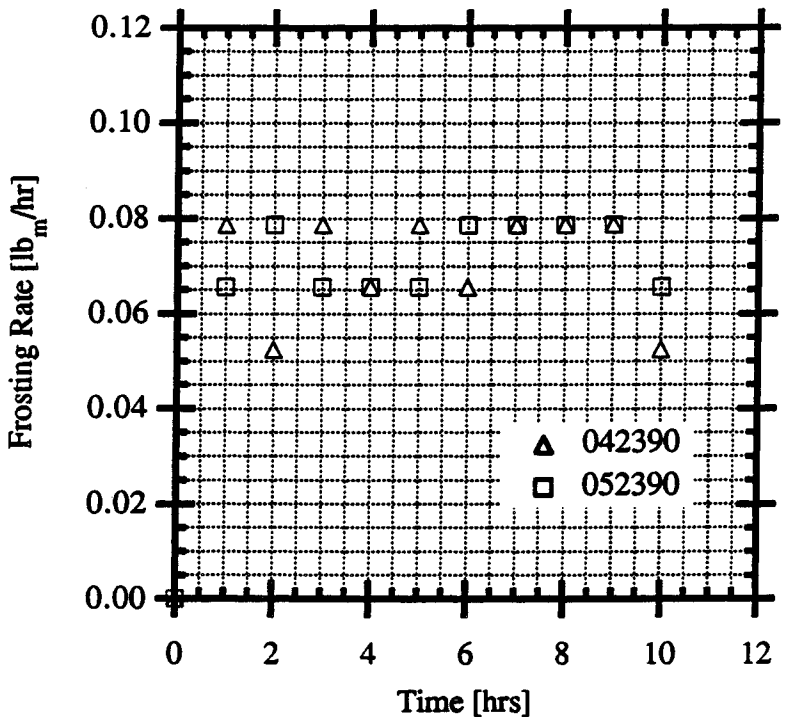

Figure 6.2.15 Evaporator Frosting Rate Versus Time with $T_{ref, in}$ = -20 F

frosting than decreasing the refrigerant temperature by 10 F. Therefore, frosting appears to be influenced more by air temperature than refrigerant temperature.

The repeatability of all three measurements in Figures 6.2.13 to 6.2.15 is within approximately 10%.

6.3 Comparison of the Baseline Case with the Parametric Studies

A useful comparison that can be made in addition to the previous comparisons of how UA-value, pressure drop, and frosting rate vary over time for different environmental conditions is to examine how the UA-value changes with accumulated frost. In Figure 6.3.1, data for 11 test

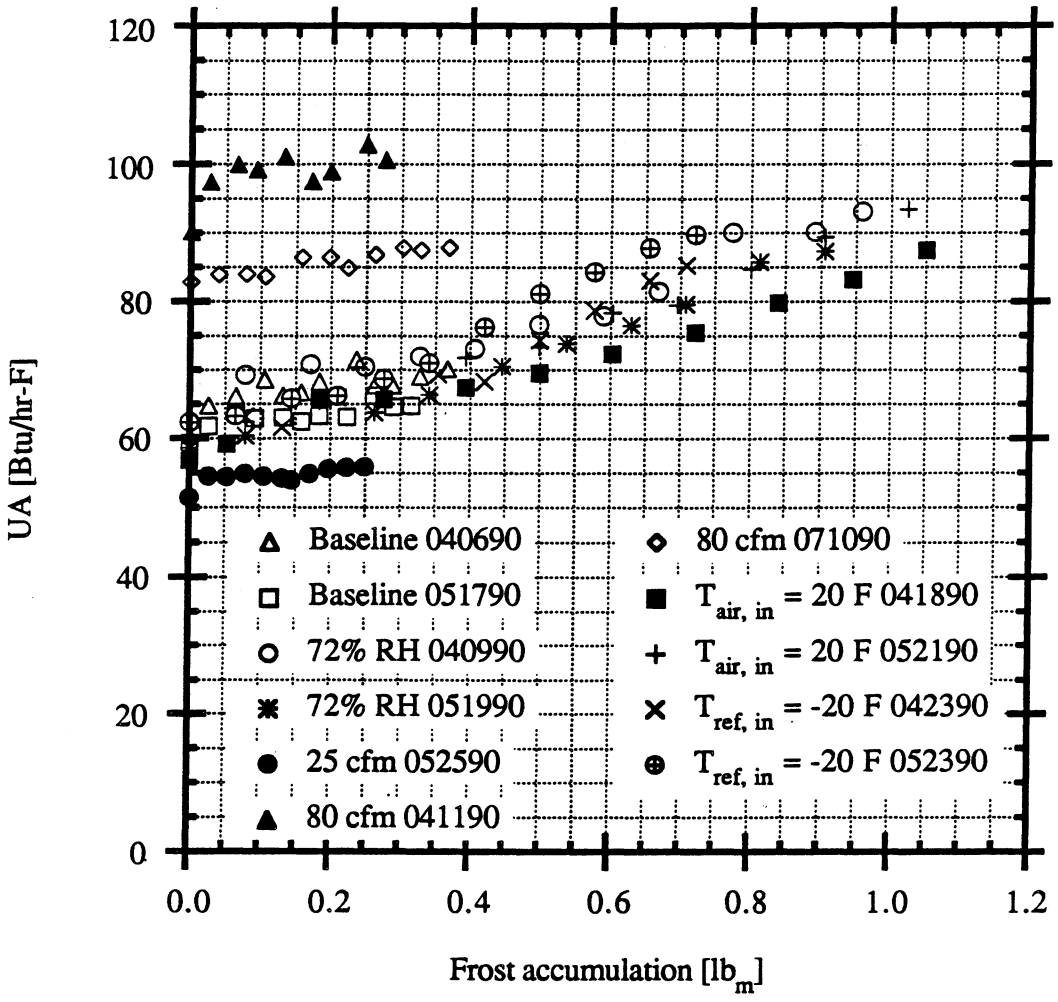

Figure 6.3.1 UA-value Versus Frost Accumulation for All Test Runs

runs have been plotted for UA-value as a function of the amount of frost accumulated on the evaporator coil. In the figure it can be seen that with less than two-tenths of a pound of frost, all of the data points except the points for the 25 cfm and 80 cfm cases fall on essentially the same line. The 25 cfm data points are significantly lower due to the lower convective heat transfer coefficients that can be expected with smaller air side velocities. Conversely, the 80 cfm data shows larger UA-values due to the larger air side velocities. As the amount of accumulated frost increases beyond two-tenths of a pound, however, the UA-value for the -20 F refrigerant temperature cases tend to increase more quickly than the 72% relative humidity and 20 F air inlet temperature cases,

which increase at essentially the same rate. Although there is sufficient scatter in the data to argue this contention, it does appear to be a valid hypothesis. One explanation for it may be that there is a change in frost structure as the surface temperature is decreased. This structure change may not occur, however, with increasing humidity or air temperature. Although the frost on the surface did appear to be the same for all three cases, it is possible that the structure of the frost with a lower surface temperature is different. This change in structure would affect the surface roughness of the frost, its density, and, consequently, its thermal conductivity. Since the UA-value for the -20 F cases are arguably higher than the UA-values for the baseline, 72% relative humidity, and 20 F air inlet cases, it would appear that this indicates that the frost has a rougher surface and/or lower density at lower surface temperatures. The rough surface increases the air side convective heat transfer coefficient, and the lower density frost increases the actual frost thickness and microscopic surface area, thus allowing for more heat transfer area. This contention is backed by the findings of Sanders, Trammell et al., and Hayashi et al. reported in Chapter 2. They also found, however, that the density should vary with humidity and air velocity as well. These findings do not seem to be evident here. One possible explanation for this is that the resultant effect of humidity and air temperature on frost surface roughness may not be as prominent as the effect of the lower surface temperature. From the results shown in Sections 6.1 and 6.2, it also appears that the thermal conductivity of the frost has little influence on the heat transfer of the evaporator. This claim is made on the basis of the fact that the insulating effect of the frost found by many previous researchers was not apparent here since the UA-value steadily increased and did not level off for the length of time that was studied.

The plot of evaporator pressure drop versus frost accumulation given in Figure 6.3.2 also shows a discrepancy among the test runs as frost builds on the coil. The 80 cfm case shows a substantially higher pressure drop than all of the other 40 cfm cases for the first two-tenths of a pound of frost accumulation as is expected because the velocity is higher. The 25 cfm data points

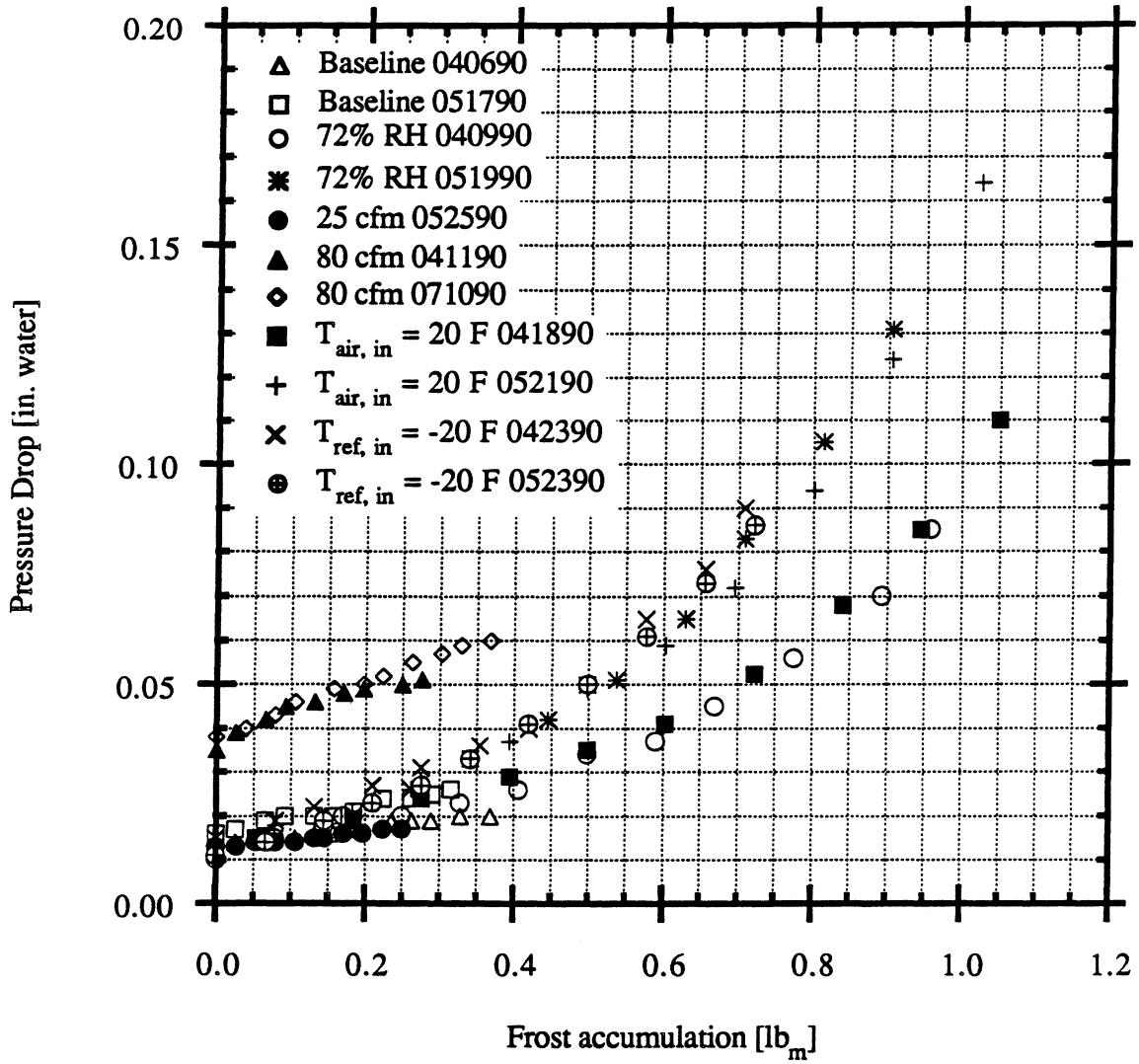

Figure 6.3.2 Evaporator Air Side Pressure Drop Versus Frost Accumulation for All Test Runs

are slightly below the 40 cfm points. Up to approximately three-tenths of a pound of frost, the pressure drops for all of the runs are bunched fairly close together. After that point, the data points tend to increase in two groups. The lower group (test runs 040990 and 041890) was also well below the other data points in Figure 6.2.2 and Figure 6.2.11, respectively. This information adds further evidence to the contention made in Section 6.2 that there are problems with the air side pressure drop measurement.

The frosting rate averaged over the first five hours of testing and the second five hours of testing for all of the test runs is shown in Table 6.3.1. It can be seen in the table that the baseline,

Table 6.3.1 Average Evaporator Frosting Rate for the First and Second Five Hours of Testing for All Test Runs

Test Run	Average Frosting Rate First Five hours [lb_m/hr]	Average Frosting Rate Second Five hours [lb_m/hr]
Baseline 040690	0.032	0.035 *
Baseline 051790	0.031	0.032
72% RH 040990	0.081	0.092 *
72% RH 051990	0.089	0.092
25 cfm 052590	0.026	0.024
80 cfm 041190	0.034	0.035 **
80 cfm 071090	0.039	0.034
$T_{air, in}$ = 20 F 041890	0.100	0.110
$T_{air, in}$ = 20 F 052190	0.100	0.100
$T_{ref, in}$ = -20 F 042390	0.071	0.071
$T_{ref, in}$ = -20 F 052390	0.068	0.076

* Averaged over six hours
** Averaged over three hours

25 cfm, and 80 cfm cases are all grouped together between 0.02 and 0.04 lb_m/hr. The 80 cfm cases, however, have slightly higher frosting rates than the baseline cases, and the baseline cases, in turn, have higher frosting rates than the 25 cfm case. Due to the resolution of the frosting rate measurement, it is not clear whether the differences among them are significant or not. This will be further addressed in Section 7.2.

The -20 F refrigerant inlet cases in the table have almost twice the average frosting rates of the three cases mentioned in the previous paragraph. The 72% relative humidity cases have approximately 29% higher frosting rates than the -20 F refrigerant inlet cases. The 20 F air inlet cases have 11% higher average frosting rates than the 72% relative humidity. This table also shows that the accumulation of frost on the coil does not significantly influence the frosting rate. As can be seen in the table, the average frosting rates for the first and the second five hours are essentially the same for all test runs as frost accumulates. This implies that the insulation effect of the frost is minimal over a ten-hour test span as was previously claimed. If the insulation effect was substantial as frost built up on the coil, the actual coil surface temperature (now the frost surface temperature) would tend to approach the air temperature and the mass transfer driving force would decrease. This would, in turn, decrease the frosting rate. Since this does not happen, it appears that the frost surface temperature is very nearly equal to the tube surface temperature, and the frost does not provide very much thermal resistance.

6.4 Extended 72% Relative Humidity Test Run

In order to determine whether or not the insulating effect discussed above will ever take effect, one test run was taken past the usual ten-hour testing period. The results of a 24-hour test for the 72% relative humidity case are shown in Figures 6.4.1 to 6.4.3. The testing was stopped after 24 hours because the airflow of 40 cfm became increasingly difficult to maintain due to the blockage of the coil. It can be seen in Figure 6.4.1 that the increase in UA-value does level off after approximately 19 hours and remains constant up to the 24-hour duration of the run. This does seem to be an indication that the frost is finally insulating the evaporator.

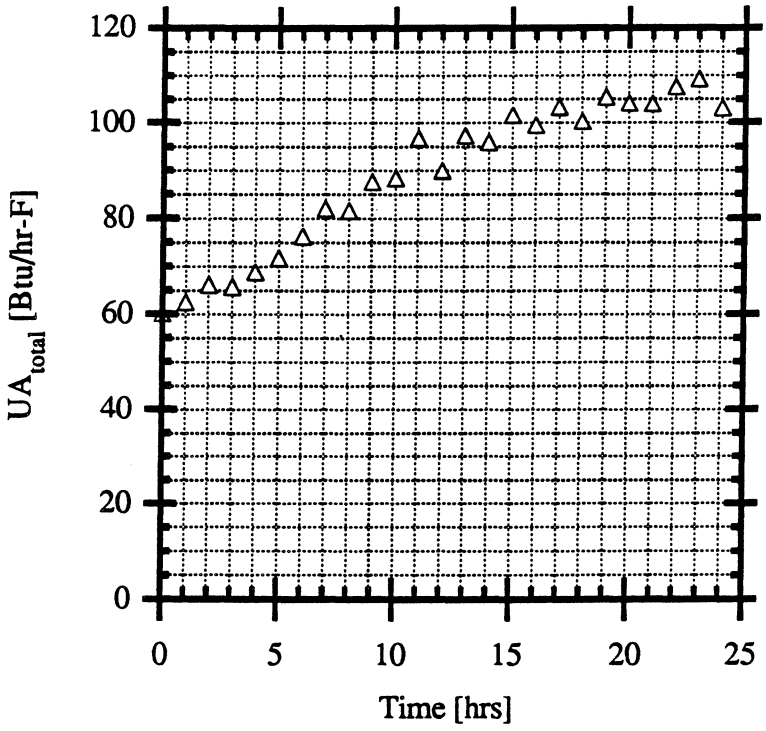

Figure 6.4.1 Evaporator UA-value Versus Time with 72% RH – 24-Hour Test Run

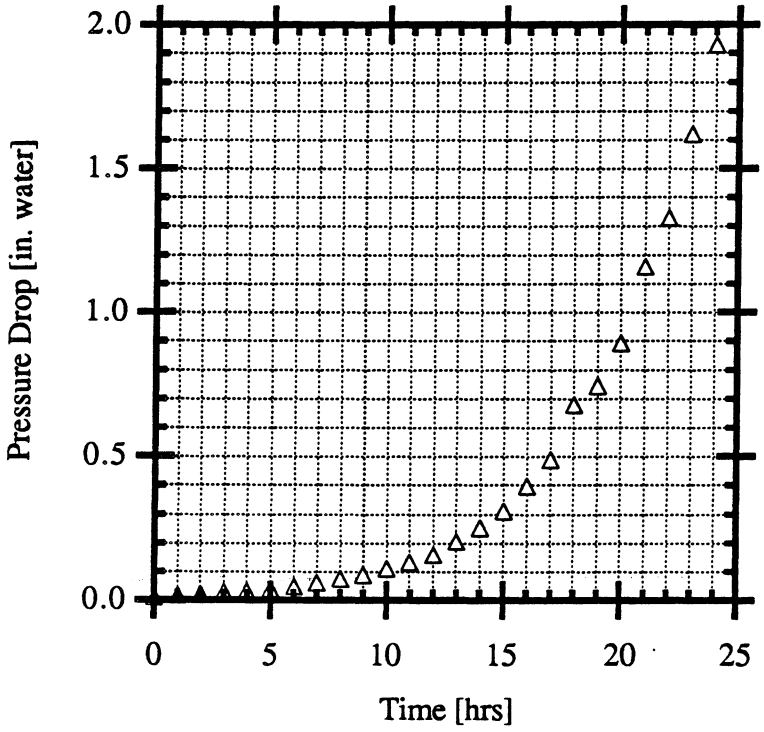

Figure 6.4.2 Evaporator Air Side Pressure Drop Versus Time with 72% RH – 24-Hour Test Run

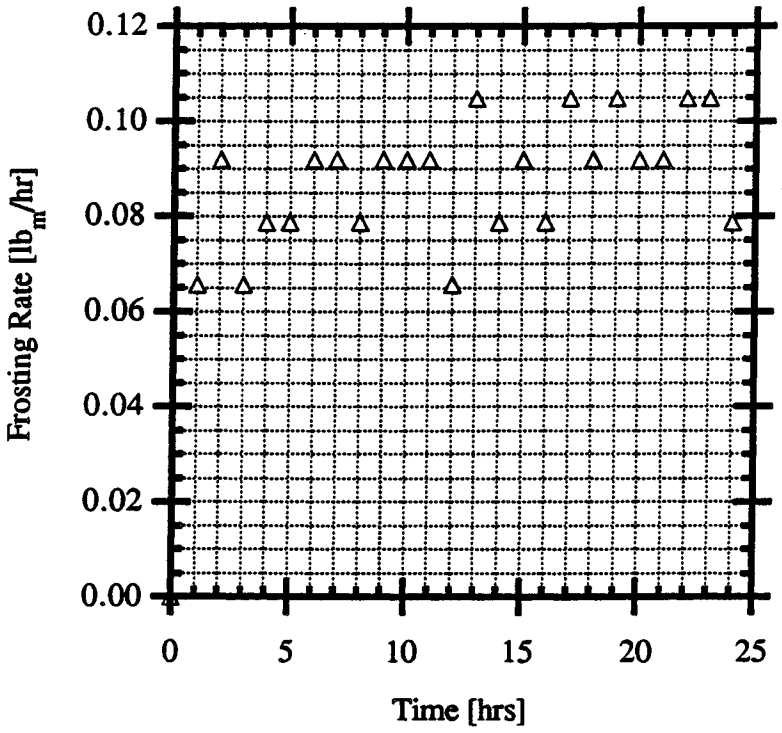

Figure 6.4.3 Evaporator Frosting Rate Versus Time with 72% RH – 24-Hour Test Run

Figure 6.4.2 shows that the air side pressure drop through the coil continually increases over the full 24 hours in an exponential manner. It should be noted that pressure drop here was measured with the 0 to 5 in. water liquid manometer rather than the Magnehelic due to the high pressure drops that are evident after ten hours.

The frosting rate is shown in Figure 6.4.3. It appears to be essentially constant for the entire duration of the test.

6.5 Qualitative Study of the Frosting Process

In addition to the quantitative results that have been provided so far, a small amount of qualitative information was also gathered. This information includes observations of the frost and photographs of the evaporator coil as the frosting process developed.

The first topic that needs to be addressed is the distribution of the frost on the entire heat exchanger. It was observed that the frosting process occurred very uniformly across the heat exchanger from left to right. Both the fin surfaces and the tube surfaces had essentially the same amount of frost. The structure of this frost also appeared to be uniform. The nonuniformity in the distribution of frost occurred in the direction of the airflow across the coil. It was observed that the bottom row of fins, which have twice the fin spacing of the other rows, had a thinner coating of frost than the six fin rows above it (a fin row will be defined as the section of fins between each of the eight tube rows, counting from the bottom of the evaporator). Above this row, both the fins and tube had essentially the same amount of frost for the next five fin rows. Over the top three rows of the coil there was a noticeable lessening of frost thickness on the tubes and fins. This was expected since the moisture content of the air decreases as it passes over the coil. This in turn reduces the frosting driving potential and reduces the frosting rate. A photograph of the entire evaporator coil at the end of the 24-hour test run discussed previously is shown in Figure 6.5.1. The long, dark, rectangular section in the bottom half of the picture is a 12-inch ruler that was affixed to the Plexiglass evaporator window.

A portion of the left side of the heat exchanger, looking into the air loop from the same perspective as shown in Figure 6.5.1, is shown in the photographs of Figures 6.5.2 to 6.5.4. The section shown includes the third, fourth, and fifth fin rows from the bottom and the fourth, fifth, and sixth tube rows from the bottom. These photographs were taken during testing with the baseline conditions. Starting from the uppermost photograph which was taken just prior to the

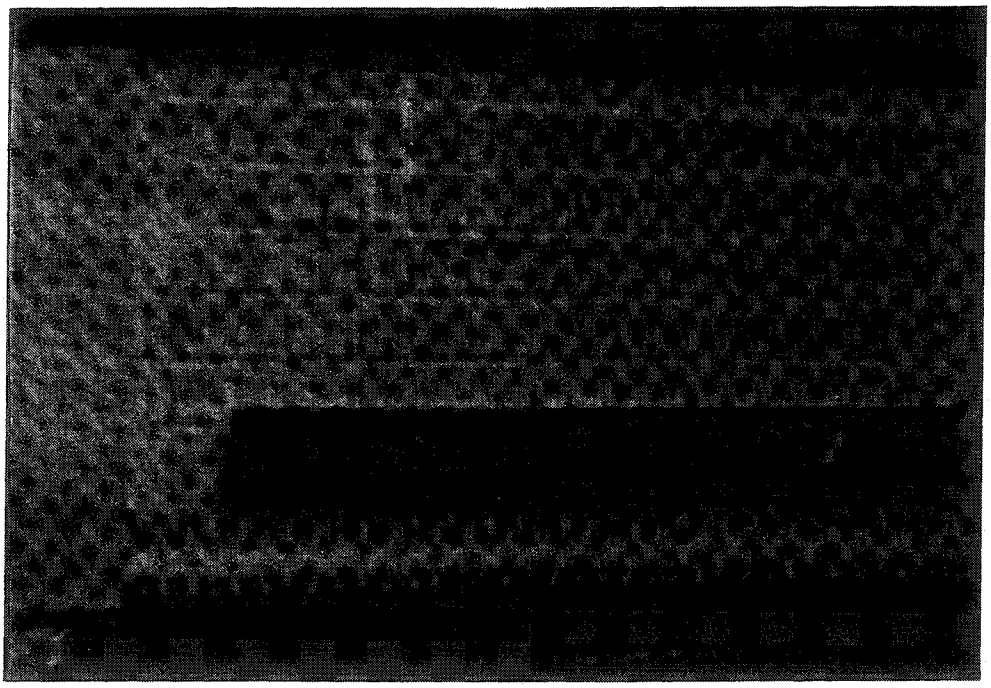

Figure 6.5.1 Photograph of Frosted Evaporator at the End of 24-Hour Test Run

start of frosting, the following ones were then made every hour for the ten-hour duration of testing.

It can be seen in the first four photos in Figure 6.5.2 that the frost began forming in blotches on the tubes. Although it cannot be seen in the photos due to the angle, the frost also tended to form on the fins in a similar manner. This seems to indicate that certain areas of the evaporator coil surfaces are more favorable to frost formation than others. This is probably a function of the surface texture of the coil. The areas with the initial frosting offer more nucleation sites than the rest of the surface, perhaps due to just the surface properties of the aluminum or possibly to some fouling of the heat exchanger that has occurred during the course of testing.

The second feature of the photos that bears closer scrutiny is how the frosting progresses on the fins. In the later photos, Figures 6.5.3 and 6.5.4, it is apparent that at the leading edge of the fin the frost is slightly thicker than it is farther up the fin. It should be remembered that the air is

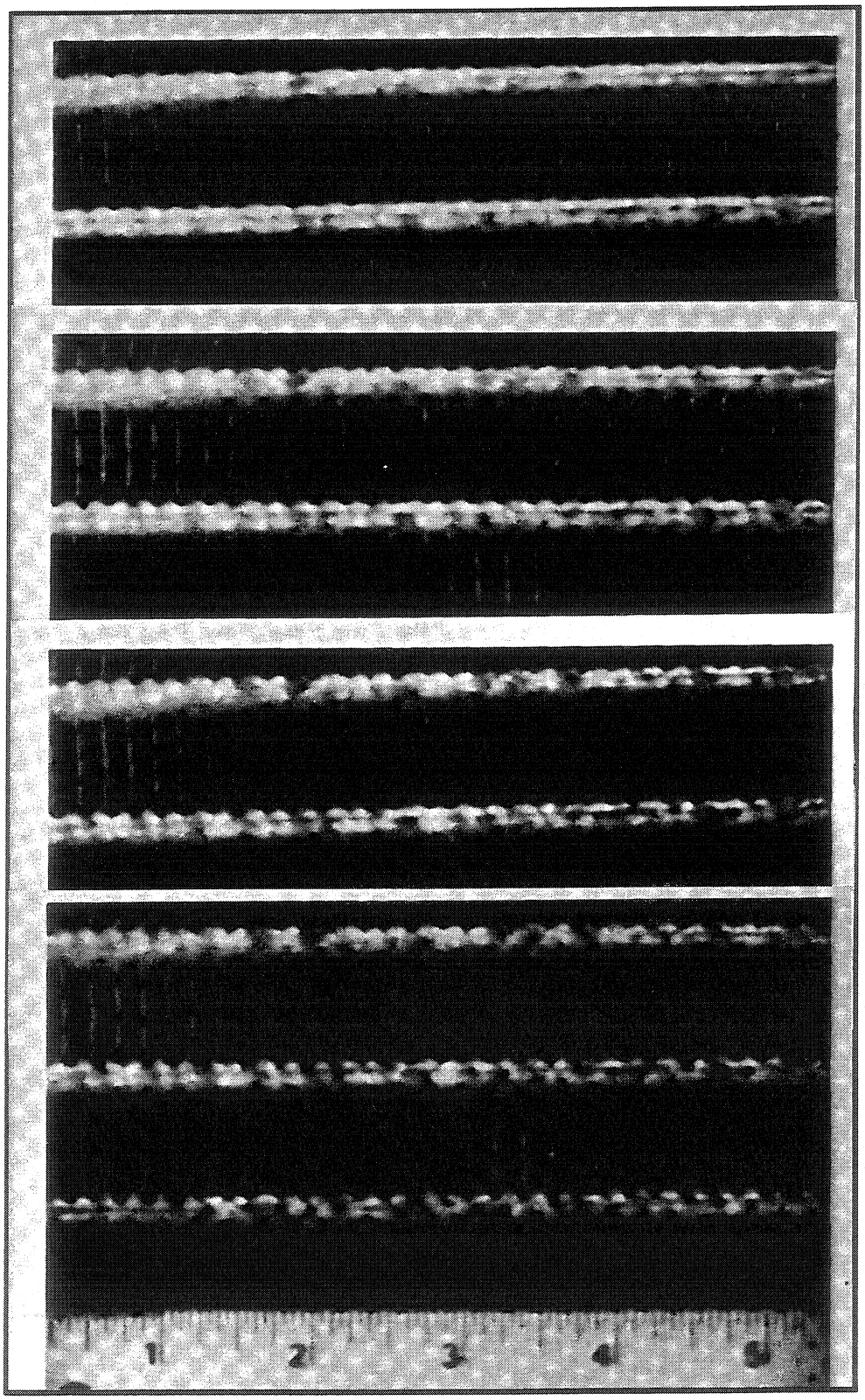

Figure 6.5.2 Frosting of a Section of the Evaporator for the Baseline Conditions – 0 to 3 Hours (Top to Bottom)

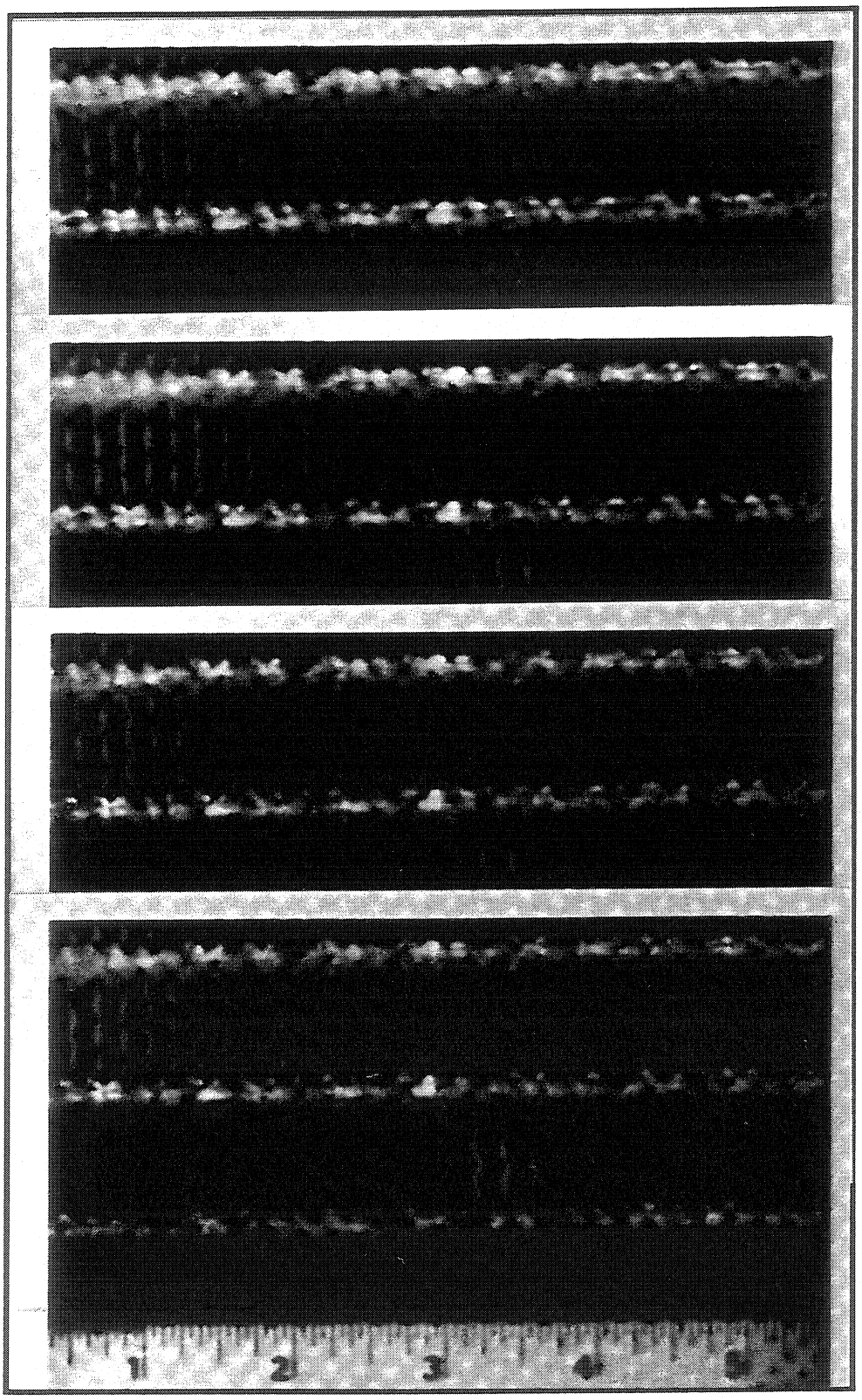

Figure 6.5.3 Frosting of a Section of the Evaporator for the Baseline Conditions – 4 to 7 Hours (Top to Bottom)

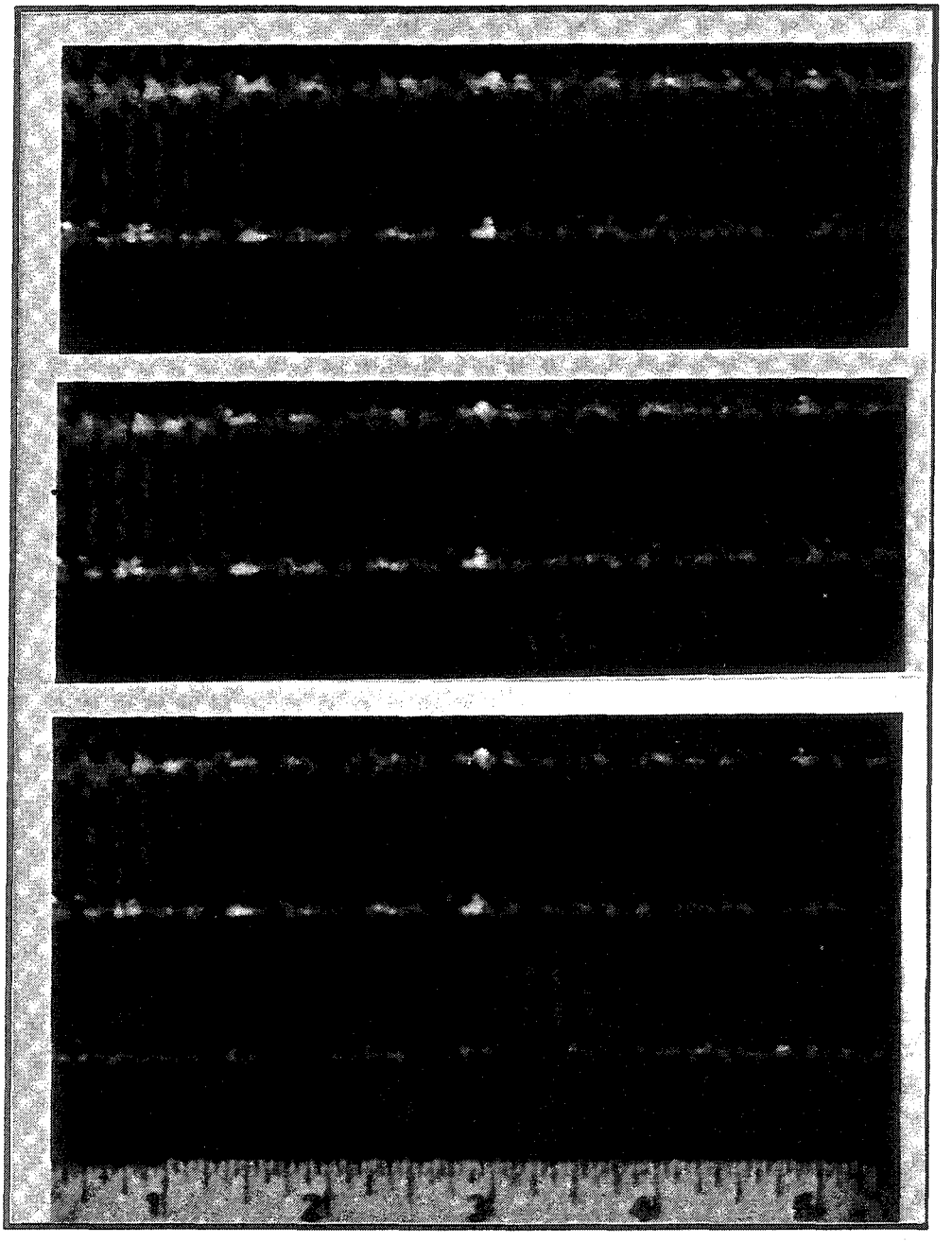

Figure 6.5.4 Frosting of a Section of the Evaporator for the Baseline Conditions – 8 to 10 Hours (Top to Bottom)

passing over the coil starting from the bottom of the photos. This pattern of frost growth is as would be expected for frost formation on a flat plate which is essentially the situation here as was shown by the researchers cited in Chapter 2. This trend of preferential frost growth on the leading

edge was not obvious, however, as far as the evaporator tubes themselves were concerned. It is possible that this is occurring, it just may not be as readily apparent as the effect on the fins.

One last feature of the frost that the photos do not completely show is the actual structure of the frost. The frost was found to have a very rough surface and the density appeared to be low for the entire length of all of the tests. The density of the frost did appear to increase, especially at the end of the 24-hour test, but it still was not even close to having ice-like density.

6.6 Comparison of Frosting Rate Measurement Methods

It was explained in Chapter 5 that four methods were used to measure the frosting rate: measuring the change in the humidifier liquid level, measuring the change in the dew point of the air as it passed through the coil, measuring the condensate that melted off of the evaporator, and weighing the evaporator with the frost still attached. Of these four methods all but the third were found to yield worthwhile results which will be discussed here.

The first comparisons are between the measurements of the frosting rates made by means of the measurement of the dew point change and the measurement of the humidifier liquid level. In the experimental data that have already been presented in Sections 6.1 to 6.5, all of the frosting information was gleaned from the liquid level measurements. Figure 6.6.1 shows a comparison of this method to the humidifier liquid level method for the baseline conditions. It can be seen in the figure that the dew point measurement is overall about 0.01 lb_m/hr lower than the humidifier liquid level measurement. This is within the resolution of the liquid level measurement.

In Figure 6.6.2, the discrepancy between the two measurements is substantially greater with 72% relative humidity. The liquid level measurement is approximately 3–4 lb_m/hr larger than the

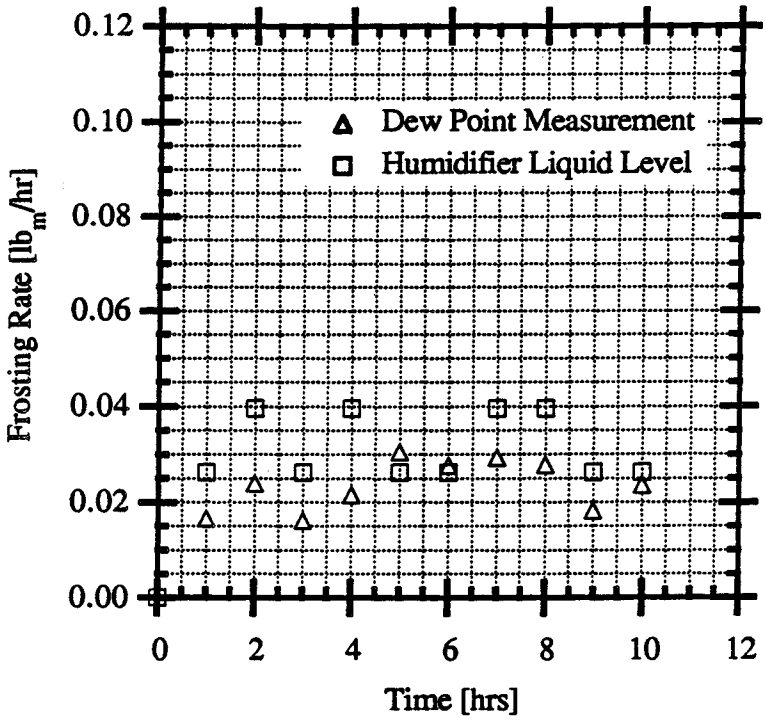

Figure 6.6.1 Comparison of Dew Point and Humidifier Liquid Level Measurement of the Evaporator Frosting Rate Versus Time for the Baseline Conditions

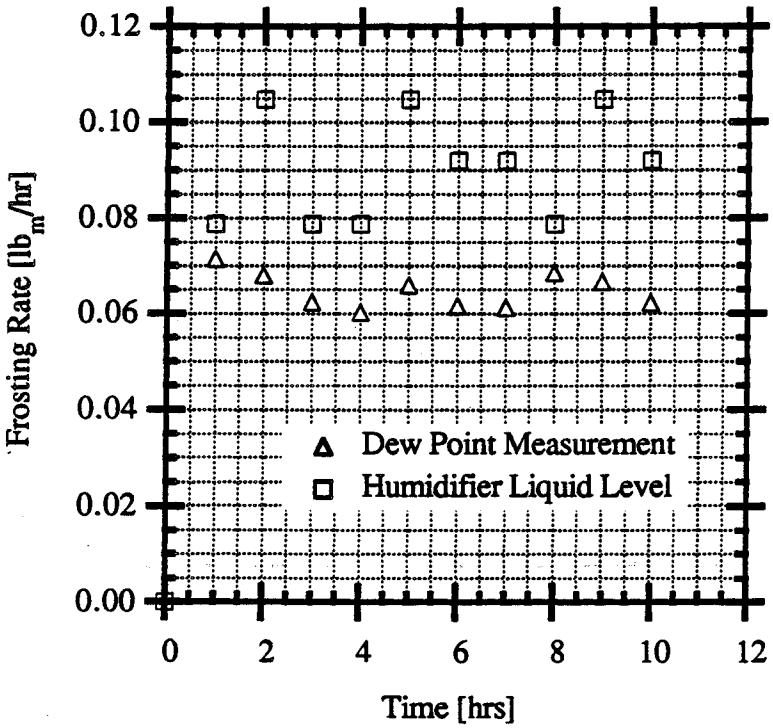

Figure 6.6.2 Comparison of Dew Point and Humidifier Liquid Level Measurement of the Evaporator Frosting Rate Versus Time with 72% Relative Humidity

dew point measurement. However, because both frosting rates are much larger than frosting rates under the baseline conditions the difference is still about 33%.

The comparison of the dew point and liquid level measurements in Figure 6.6.3 for the 25 cfm case shows that the measurements are within 20% of each other. In addition, both frosting rates are extremely uniform for the duration of the test run.

The difference between the two measurement methods increases to almost 50% in Figure 6.6.4 for the 80 cfm case. In Figure 6.6.5 for an air inlet temperature of 20 F, the humidifier liquid level measurement yields an average frosting rate approximately 19% higher than the dew point measurement. Figure 6.6.6 also shows a liquid level measurement of the frosting rate that is about 20% higher than the dew point measurement.

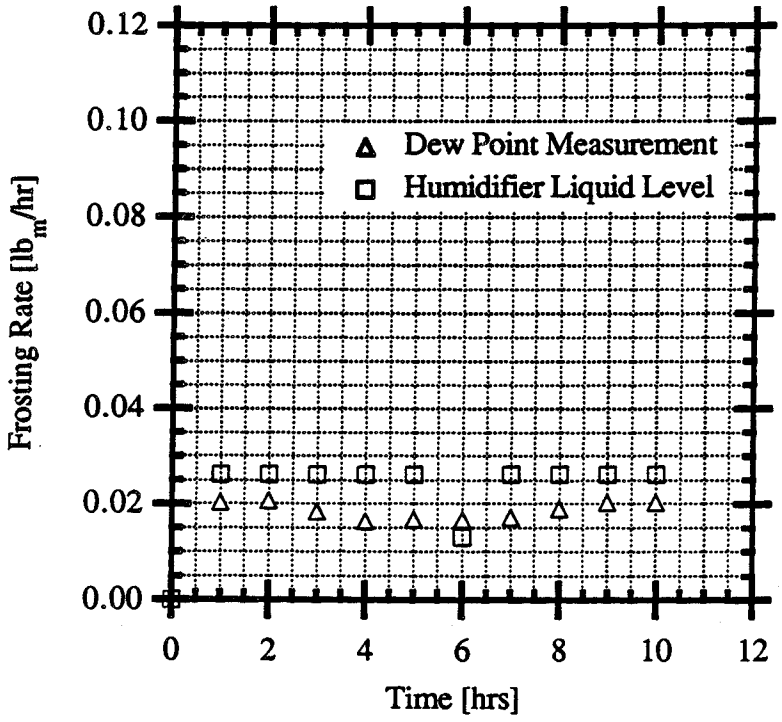

Figure 6.6.3 Comparison of Dew Point and Humidifier Liquid Level Measurement of the Evaporator Frosting Rate Versus Time with a 25 cfm Airflow Rate

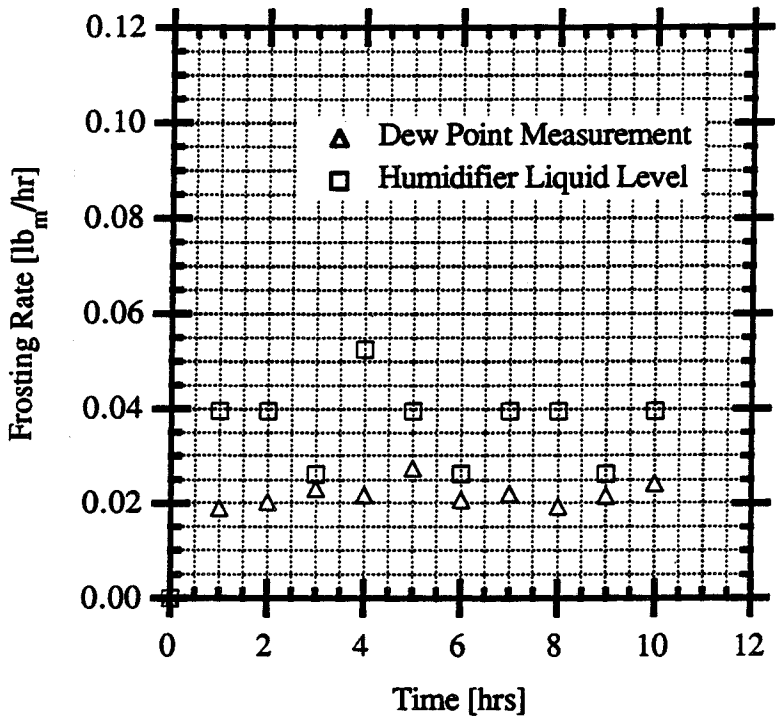

Figure 6.6.4 Comparison of Dew Point and Humidifier Liquid Level Measurement of the Evaporator Frosting Rate Versus Time with an 80 cfm Airflow Rate

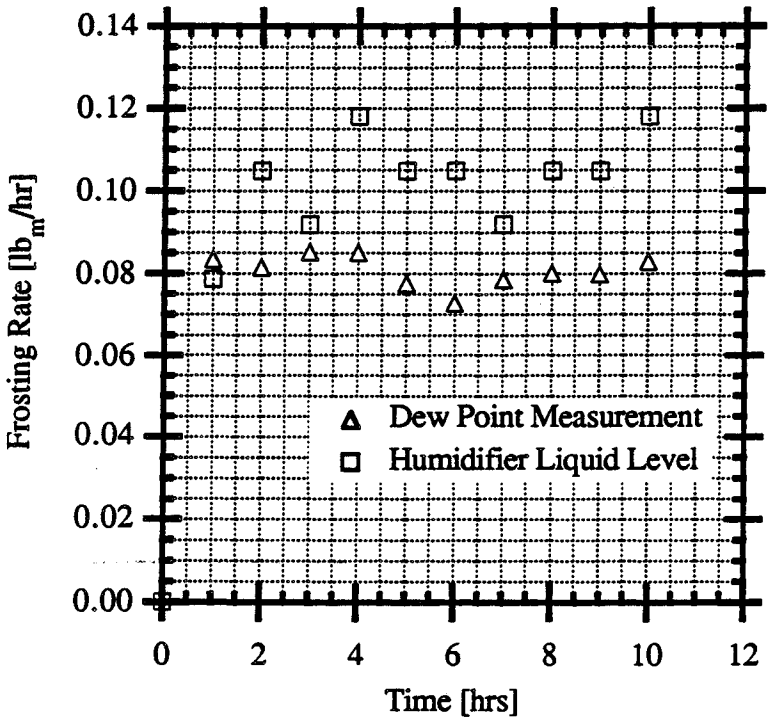

Figure 6.6.5 Comparison of Dew Point and Humidifier Liquid Level Measurement of the Evaporator Frosting Rate Versus Time with $T_{air, in}$ = 20 F

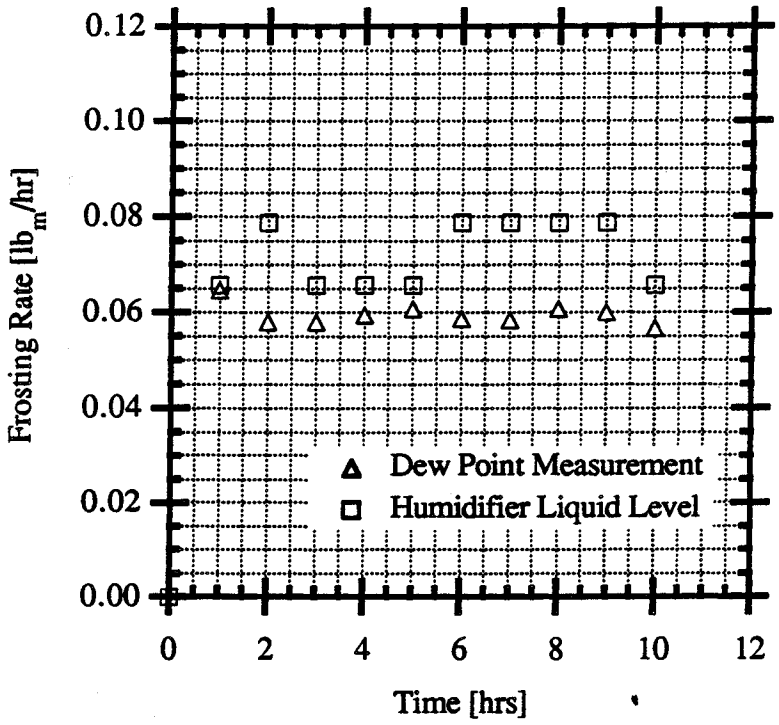

Figure 6.6.6 Comparison of Dew Point and Humidifier Liquid Level Measurement of the Evaporator Frosting Rate Versus Time with $T_{ref, in}$ = -20 F

There are several reasons for the discrepancies in the comparisons discussed above. First, for the 72% relative humidity case in Figure 6.6.2, there was significant frosting in the return duct in which the humidifier was located. This frosting was due to the supersaturated conditions that existed just above the humidifier at the water temperatures that were required to obtain a 72% relative humidity at the evaporator inlet. This causes the assumption that all of the water leaving the humidifier is deposited on the evaporator to lose its validity. Based on this difficulty, a 33% difference here is understandable. This same problem was not evident for any of the other testing conditions. However, it is possible, although great care was taken to insure the tightness of the air loop, that some of the moisture generated by the humidifier was lost from the air loop. This also would lead to a higher frosting rate being calculated by the humidifier liquid level than is actually occurring. In addition, some moisture is lost through the air sample that is drawn for the dew

point sensor. The flow rate of the sample is extremely small (~ 0.07 cfm, 0.03 L/s) but, nevertheless, there is a moisture loss because of it.

In addition to the problems with the humidifier liquid level measurement described above, an inconsistency with the dew point measurement was also evident. It was found that on the test runs with larger frost rates (i.e., the 72% relative humidity, 20 F air inlet, and -20 F refrigerant inlet cases) in the last five to six hours of the ten-hour run, the outlet dew point was higher than the measured outlet dry bulb temperature. Since this situation indicates that a nonequilibrium, supersaturated condition existed at the evaporator outlet, which is probably not feasible, a more reasonable explanation is necessary. The most plausible explanation for this incongruity is that the dew point measurement at the evaporator outlet was not given a sufficient amount of time to reach its steady-state value. This was found to be a problem. During the normal testing procedure outlined in Chapter 5, ten minutes were allowed between sample line switches from the outlet of the evaporator to the inlet. A supplementary test showed that the dew point continued to change, after the sample line was switched from the inlet to the outlet, an additional 4 to 5 F (2 to 3 C) over a one-hour period. The reason for this lengthy transient period seems to be that the copper sampling lines tend to store a significant amount of moisture. The ten-minute switch-over time was not long enough for all of the moisture that had been absorbed by the lines when evaporator inlet air was in them to be removed. This led to a higher dew point reading for the air outlet than actually existed. Although copper does not absorb much water, at the low dew points that needed to be measured here even a slight amount is significant. Stainless steel, which has more favorable hygroscopic properties than copper, should probably have been used for this installation.

A final check that was undertaken to see which measurement technique provided the most accurate assessment of the frosting rate was to weigh the frosted evaporator coil after a ten-hour test was completed. The air inlet temperature of 20 F case was selected for the comparison of the humidifier liquid level and the dew point measurements of the frost deposited on the evaporator

with the actual scale measurement of the frost weight because of its high frosting rate. The results of this comparison are shown in Table 6.6.1. The total frost accumulation was calculated for the

Table 6.6.1 Comparison of the Total Frost Accumulated on the Evaporator Measured by the Humidifier Liquid Level, the Dew Point, and the Scale with $T_{air, in} = 20$ F

	Total Frost Accumulation [lb_m] After 10 Hours		
Test Run Number	**Liquid Level**	**Dew Point**	**Scale**
041890	1.05	------	------
052190	1.02	0.807	------
071590	1.15	0.548	1.01
071990	1.06	0.504	0.99

liquid level and dew point cases by adding together the frosting rates for each hour of testing. In the table, the results of four test runs are presented. In the 041890 test run, only the humidifier liquid level measurement was made. In the 052190 test run, only the humidifier liquid level measurement and the dew point measurement were made. All three measurements were made in test runs 071590 and 071990. It can be seen in the table that all of the liquid level measurements are within 12% of each other. The dew point measurements, however, are almost 40% lower for tests 071590 and 071990 than for the 052190 test probably due to the hygroscopic problems discussed above. The two scale readings are within 3% of each other. In test 071590, the liquid level measurement is only 14% greater than the scale reading while for test 071990 the liquid level is approximately 8% higher. The agreement between the dew point and scale measurements is far worse. For the 071590 test, the dew point is 46% less than the scale reading, and for test 071990 it is 49% less. However, the dew point measurement from the 052190 case is within 20% of either the 071590 or 071990 scale measurements.

Given the results in Table 6.6.1, the humidifier liquid level measurement appears to have acceptable accuracy and, consequently, was used in all of the previous plots.

Chapter 7

ANALYSIS OF EXPERIMENTAL RESULTS

7.1 Determination of the Cause of the UA-value Increase with Frost Formation

It was shown that under all of the testing conditions that were investigated the UA-value of the evaporator increases as frost is deposited on the coil, if a constant airflow through the coil is maintained. In Section 6.1 several reasons for this behavior were presented. Among these were a reduction in the contact resistance between the fin and tube and an increase in the air side heat transfer area due to the frost layer and/or an increase in the convective heat transfer coefficient due to the increased surface roughness of the tube and fins. In order to determine which of these explanations has the most influence on heat transfer, the evaporator was instrumented with thermocouples at various locations on its surface, and the change in these temperatures was monitored as frost formed on the surface. Before this instrumentation is described in detail, the heat transfer mechanics between the air and refrigerant should be discussed.

There are two paths that the heat leaving the air and entering the refrigerant in the evaporator may take. The first path is directly from the air to the refrigerant tube. The thermal resistances encountered along this path include: a convective resistance through the air, a conductive resistance through the growing frost layer, a conductive resistance through the tube wall, and a convective resistance through the refrigerant. The second thermal path is through the fins. Along this pathway the resistances include: the air convective resistance, the frost conductive resistance, the fin conductive resistance, the contact resistance between tube and fin, the resistance of the frost on the tube, the tube conductive resistance, and the refrigerant convective resistance. A thermal resistance network schematic of this situation is shown in Figure 7.1.1. In the figure, a cross-sectional cut of an evaporator tube and part of its adjoining fin is shown. The resistance path from

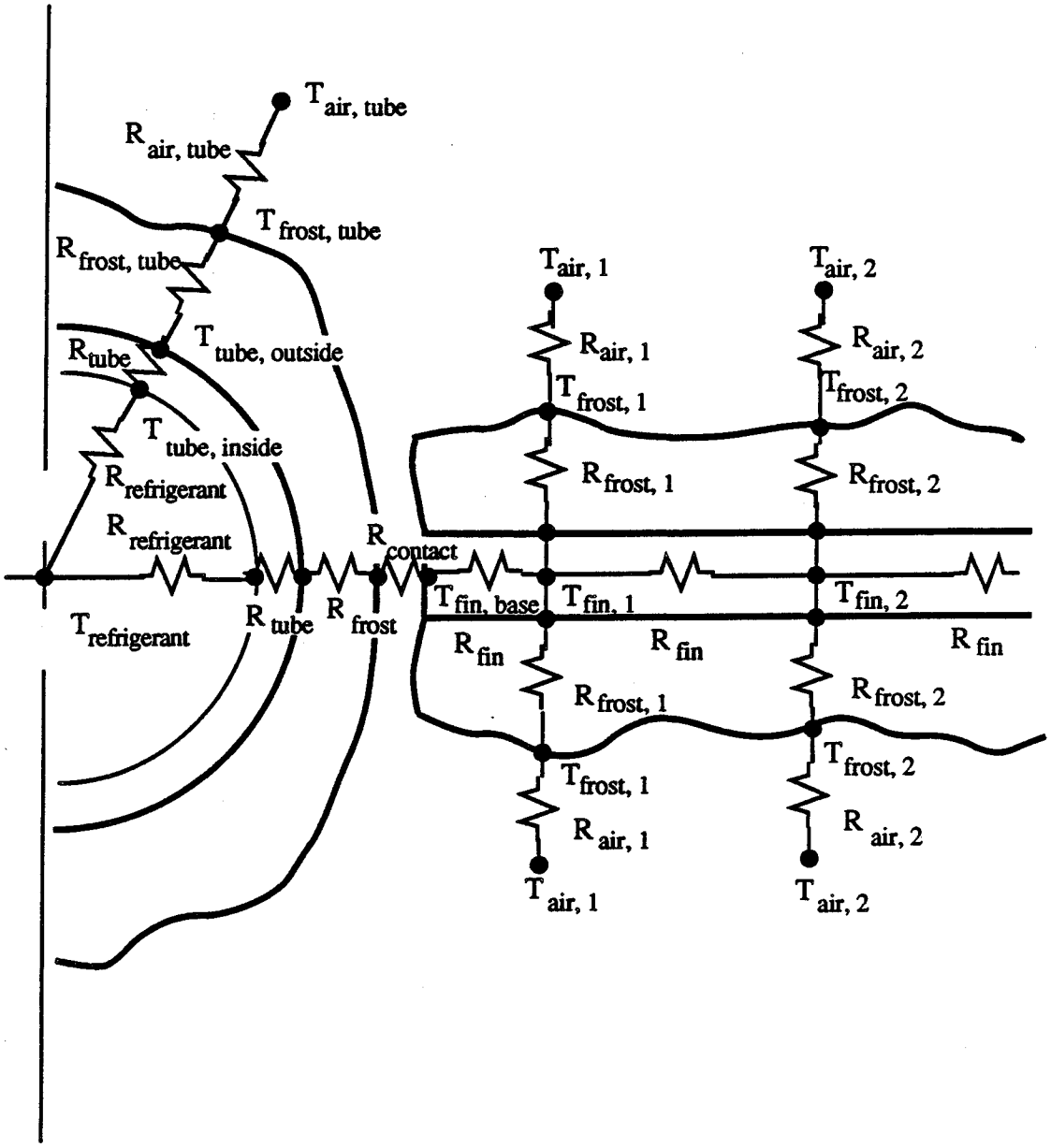

7.1.1 Thermal Resistance Network Schematic of Air to Tube Heat Transfer Paths

the air through the tube surface to the refrigerant that is illustrated is quite straightforward. The path through the fin, however, requires some explanation. This path is shown broken into a series of steps (only two steps are shown due to space considerations). The steps represent the fact that as heat is conducted down from the midpoint of the fin to its base, the fin continues to pick up heat

along the way due to convective heat transfer from the air. Since the fin has a high thermal conductivity (k ≈ 128 Btu/hr-ft-F, 221 W/m-K) compared with ice (1.4 Btu/hr-ft-F, 2.4 W/m-K), the vast majority of the conductive heat transfer along the fin will occur through the aluminum and not through the frost layer, so only the conductive path through the fin stock is illustrated. Also, the contact resistance between fin and tube is shown in series with the conductive resistance of the tube frost. Most likely the relationship between these resistances is both a parallel and a series relationship as was alluded to in Section 6.1. Unfortunately, space does not allow for representing it completely.

Several simplifications must be made to the thermal resistance network in Figure 7.1.1 in order to make an analytical solution feasible. First, due to the high thermal conductivity and thinness of the evaporator tube wall (t_w = 0.028 in., 0.71 mm), it can be assumed that the tube wall resistance is negligible. If the air convective resistance and frost conductive resistance are lumped into an equivalent resistance, $R_{surface}$, and a mean fin temperature is defined at which all of the convective heat transfer to the fin from the air occurs, the thermal resistance network may be simplified to the form shown in Figure 7.1.2. In the figure $R_{tube,\ surface}$ is defined as

$$R_{tube,\ surface} = \frac{1}{h_{air\ tube} A_{tube}} + \frac{t_{frost}}{k_{frost} A_{tube}} \qquad (7.1.1)$$

and

$$R_{fin,\ surface} = \frac{1}{h_{air\ fin} A_{fin}} + \frac{t_{frost}}{k_{frost} A_{fin}} \qquad (7.1.2)$$

where,

$h_{air\ tube}$ = the air side convective heat transfer coefficient at the tube surface,

$h_{air\ fin}$ = the air side convective heat transfer coefficient at the fin surface,

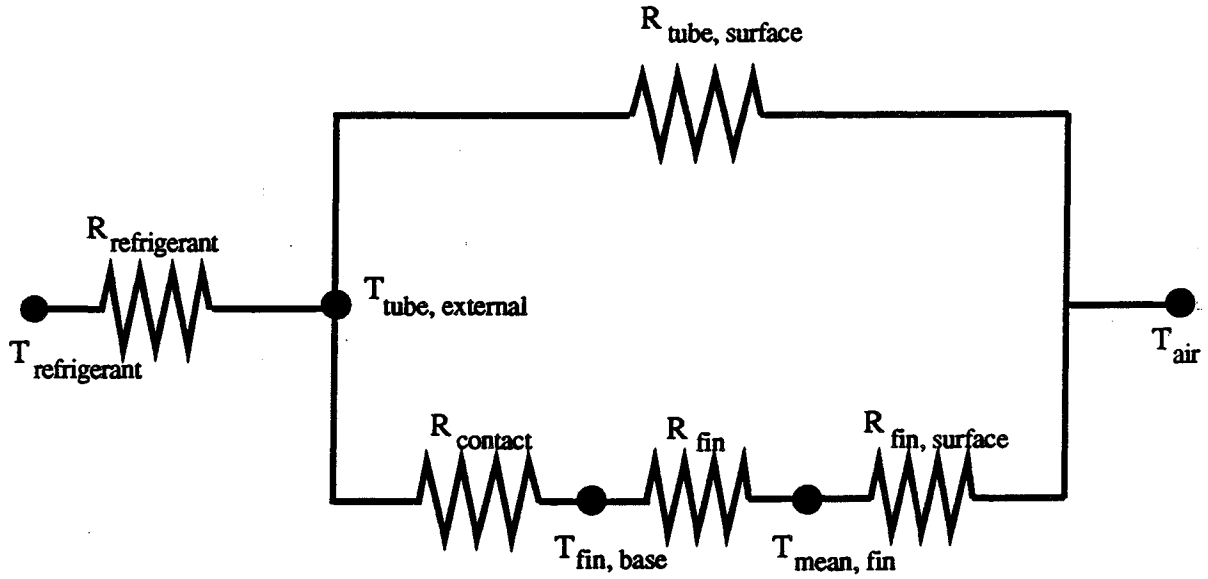

Figure 7.1.2 Simplified Thermal Resistance Network of Air to Tube Heat Transfer Paths – Intermediate Version

A_{tube} = the surface area of the frost surrounding the tube,

t_{frost} = the thickness of frost layer,

k_{frost} = the thermal conductivity of frost,

and

A_{fin} = the surface area of the frost surrounding the fin.

The conductive resistance of the fin, R_{fin}, is represented by

$$R_{fin} = \frac{L_{fin}}{k_{fin} A_c} \tag{7.1.3}$$

where,

L_{fin} = the length of the fin to the mean temperature location,

k_{fin} = the thermal conductivity of the fin,

and

A_c = the cross-sectional area of the fin.

The refrigerant resistance may be defined as

$$R_{refrigerant} = \frac{1}{h_{refrigerant} A_{tube\ inside}} \tag{7.1.4}$$

where,

$h_{refrigerant}$ = the refrigerant side convective heat transfer coefficient

and

$A_{tube\ inside}$ = the inner tube surface area.

Since there is no information available about the thickness of the frost layer or its thermal conductivity at this time, additional simplifications of the thermal resistance network in Figure 7.1.2 are required. One of the additional simplifications that will be made is that the outer surface areas of the tube and fins are constant throughout the duration of testing. The area added to both surfaces by the frost layer will be neglected. A second simplification that will be made is the elimination of the conductive resistance of the frost from the network. Lastly, the mean fin temperature defined in Figure 7.1.2 is also unknown, so, in order to take into account the temperature gradient that exists through the length of the fin, the heat transfer to the fin will be defined in terms of a fin efficiency. The fin efficiency is defined as

$$\eta_f = \frac{\dot{Q}}{\dot{Q}_{max}} \tag{7.1.5}$$

where

$$\dot{Q} = h_{air,\ fin} A_{fin} (T_{air} - T_{mean,\ fin}) \tag{7.1.6}$$

and

$$\dot{Q}_{max} = h_{air,\,fin}\, A_{fin}\, (T_{air} - T_{fin,\,base}). \qquad (7.1.7)$$

With these modifications the thermal resistance network may then be configured as shown in Figure 7.1.3.

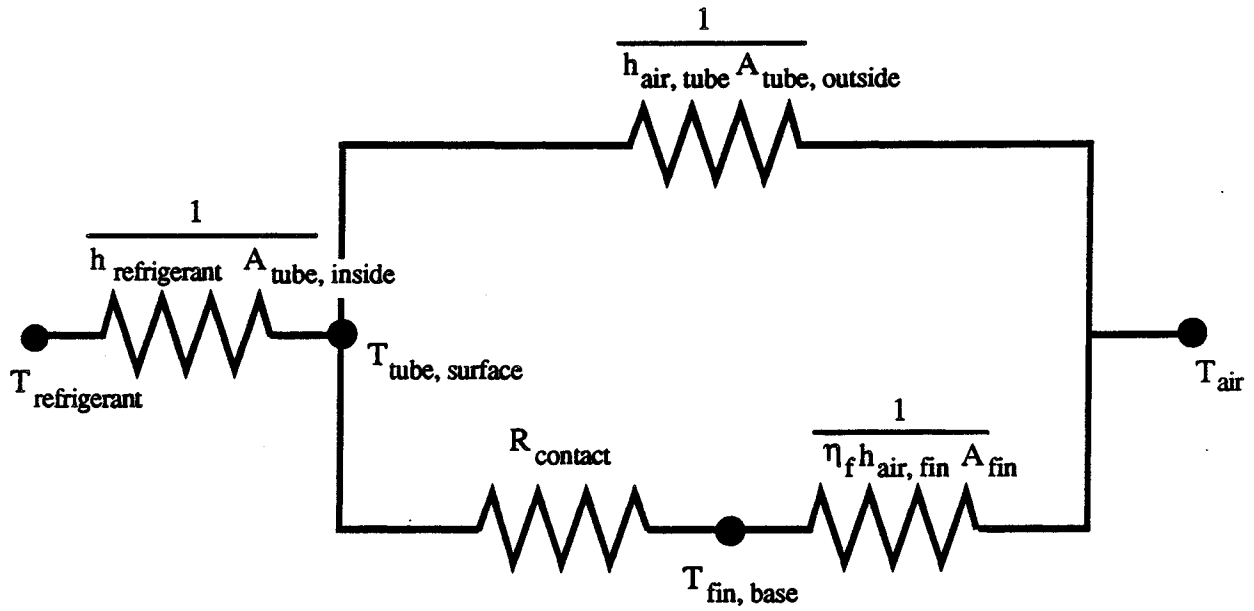

Figure 7.1.3 Simplified Thermal Resistance Network of Air to Tube Heat Transfer Paths – Final Version

In order to measure the temperatures shown in Figure 7.1.3, a set of thermocouples was placed at the bottom of the evaporator where the air enters the coil. A fin at approximately the center of the evaporator was selected for the thermocouple arrangement shown in Figure 7.1.4. The thermocouple configuration consists of two differential temperature Type-T thermocouples and one absolute temperature Type-T thermocouple. Differential temperatures were measured between the evaporator tube surface and the base of the fin and the fin base and the middle of the fin. An absolute temperature measurement was made at the middle of the fin. The thermocouples are attached to the fin and tube surfaces with Delta Bond 152 thermally conductive epoxy. The

temperatures were recorded at the beginning of frosting and at the end of the ten-hour test run. The 20 F air inlet test condition was chosen for these experiments on account of its rapid frosting rate.

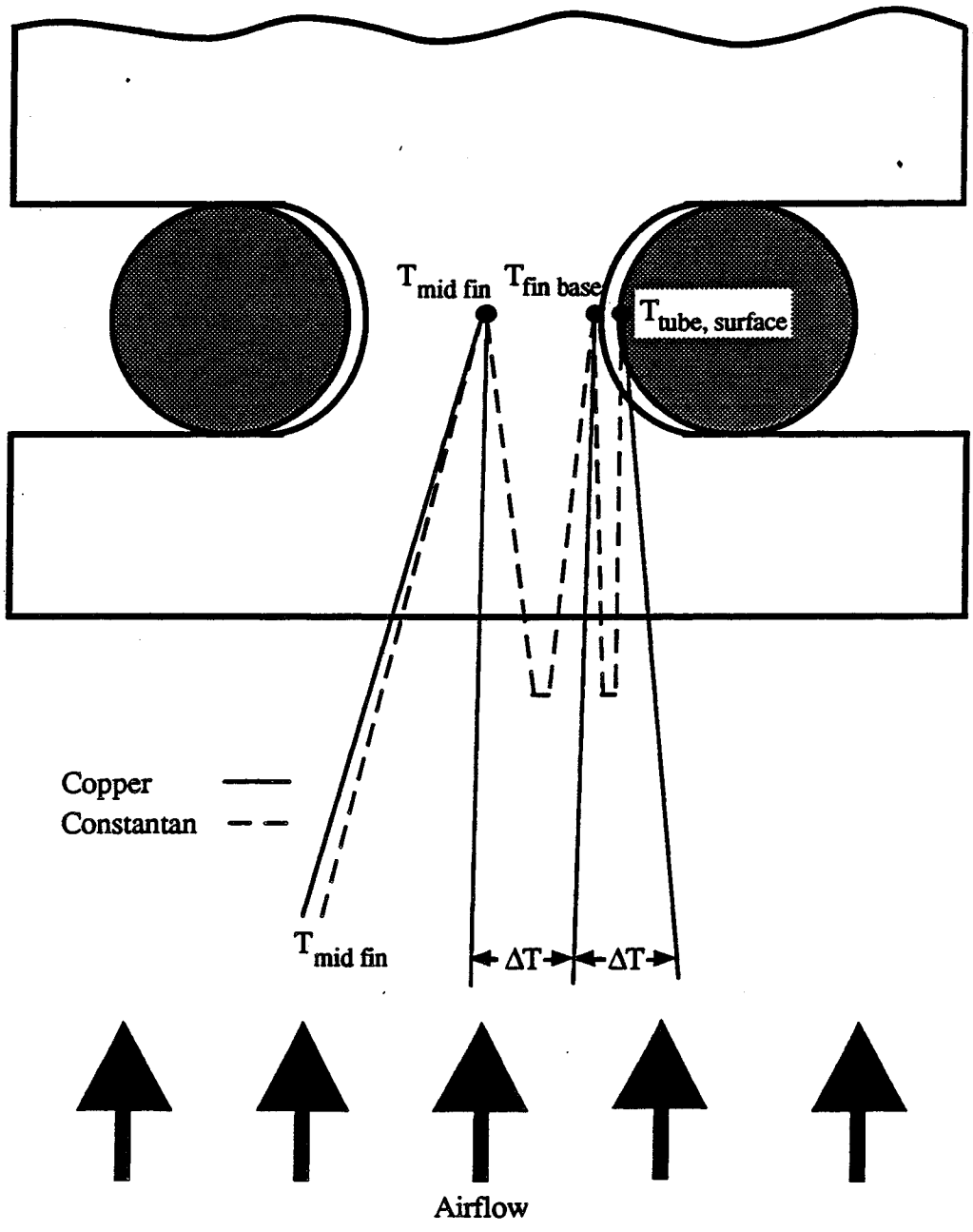

Figure 7.1.4 Evaporator Thermocouple Configuration

The temperatures that were recorded are shown in Table 7.1.1. The $T_{air,\ in}$ temperature is the average air inlet temperature that was measured with the three 6 inch probes discussed in Chapter 3.

Table 7.1.1 Fin and Tube Differential Temperatures for $T_{air,\ in}$ = 20 F

Testing Hour	$T_{air,\ in} - T_{mid\ fin}$	$\Delta T_{mid\ fin\ -\ fin\ base}$	$\Delta T_{fin\ base\ -\ tube}$
0	14.0 F	3.6 F	6.1 F
10	15.8 F	4.6 F	7.7 F

Once the temperatures are recorded, a method must be devised to calculate the fin efficiency. It was decided to utilize the equivalent annulus method outlined by Rohsenow, Hartnett, and Ganic (1985) and Kern and Kraus (1972). This method entails approximating the fin surrounding each tube as an annular fin with an adiabatic edge. Since the refrigerant in the evaporator tube is two-phase, the temperature of the refrigerant will be essentially the same throughout the length of the tube. Also, the fin that is dealt with here is at the air inlet, so the air should have a uniform temperature. These two factors combined with the thinness of the fin should make the assumption of an adiabatic edge acceptable. Figure 7.1.5 shows an end view of the fin and tube. In the figure it can be seen that the fin can be divided into squares surrounding each tube. These squares are then approximated as circles having equivalent areas. The radius chosen is as shown in the figure.

The fin efficiency of an annular fin can be determined by finding the temperature gradient through the fin. A first law of thermodynamics analysis of the annular fin geometry yields a conduction equation of the form:

$$\frac{d^2\Theta}{dr^2} + \frac{1}{r}\frac{d\Theta}{dr} - \frac{2\ h_{air\ fin}}{t_{fin}\ k_{fin}}\ \Theta = 0 \qquad (7.1.8)$$

where,

$$\Theta = T_{air} - T,$$

and

r = the radius of the fin.

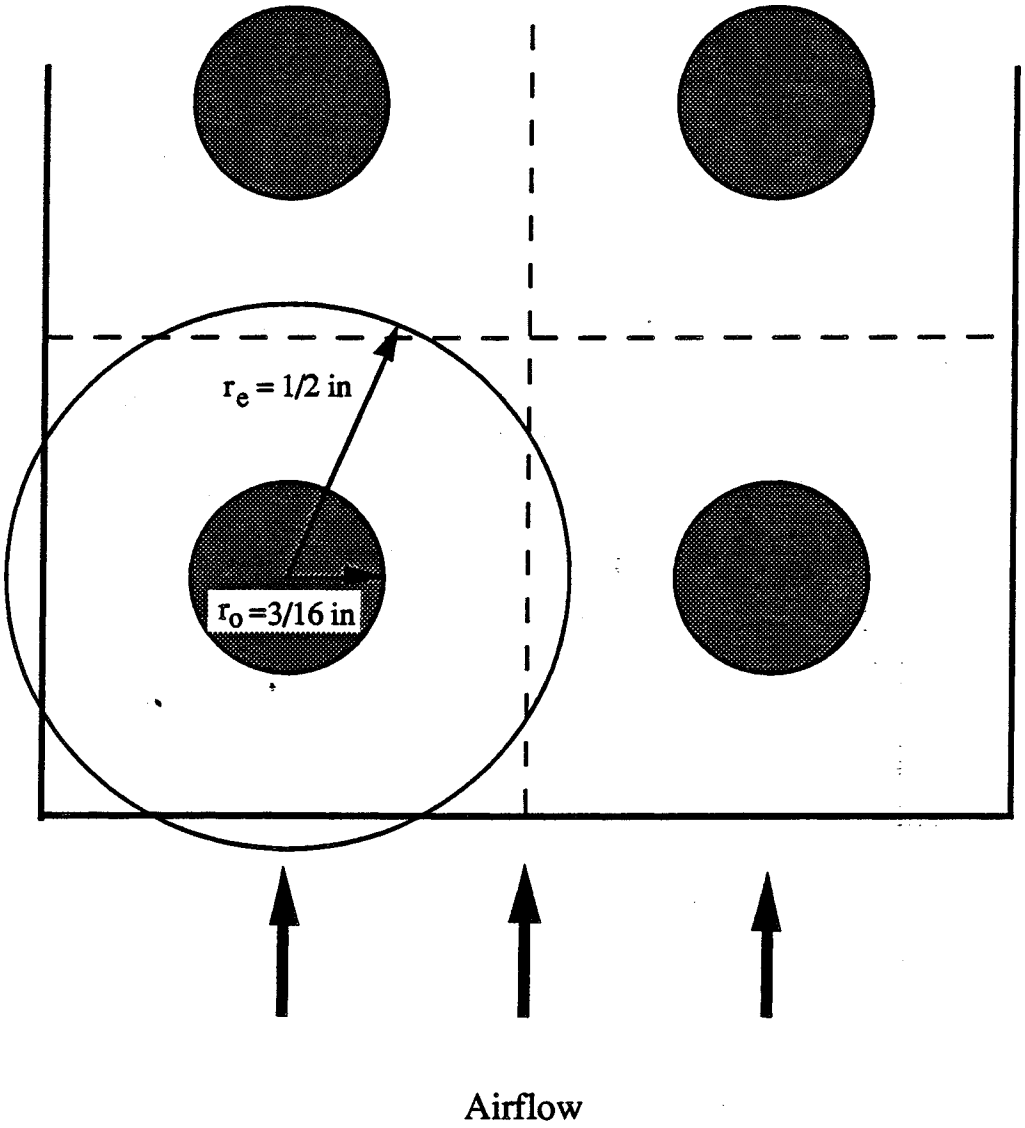

Figure 7.1.5 Schematic of the Implementation of the Equivalent Annulus Method on the Evaporator

The boundary conditions for this differential equation are

$$\text{at} \quad r = r_o: \qquad \Theta = T_{air} - T_{fin\ base} = \Theta_b \tag{7.1.9}$$

and

$$\text{at} \quad r = r_e: \qquad \frac{d\Theta}{dr} = 0. \tag{7.1.10}$$

Since the air side convective coefficient is not known, an additional equation is required in order to solve equation 7.1.8. The temperature at radius r_e of the fin has been measured so that will provide the additional equation:

$$\text{at} \quad r = r_e: \qquad \Theta = T_{air} - T_{r_e} = \Theta_{r_e}. \tag{7.1.11}$$

The solution of this second-order, ordinary differential equation involves a modified Bessel function of the first and second kind, I_0 and K_0, and may be written as

$$\Theta(r) = C_1 I_0 \{(\frac{2\, h_{air\ fin}}{t_{fin}\, k_{fin}})^{\frac{1}{2}} r\} + C_2 K_0 \{(\frac{2\, h_{air\ fin}}{t_{fin}\, k_{fin}})^{\frac{1}{2}} r\} \tag{7.1.12}$$

where C_1 and C_2 are constants. These two constants plus the unknown $h_{air\ fin}$ are determined by applying the three boundary conditions. Doing this results in the following three equations with three unknowns:

$$\Theta_b = C_1 I_0 \{(\frac{2\, h_{air\ fin}}{t_{fin}\, k_{fin}})^{\frac{1}{2}} r_o\} + C_2 K_0 \{(\frac{2\, h_{air\ fin}}{t_{fin}\, k_{fin}})^{\frac{1}{2}} r_o\} \tag{7.1.13}$$

$$0 = C_1 I_1 \{(\frac{2\, h_{air\ fin}}{t_{fin}\, k_{fin}})^{\frac{1}{2}} r_e\} + C_2 K_1 \{(\frac{2\, h_{air\ fin}}{t_{fin}\, k_{fin}})^{\frac{1}{2}} r_e\} \tag{7.1.14}$$

and

$$\Theta_{r_e} = C_1 I_0 \{(\frac{2\, h_{air\ fin}}{t_{fin}\, k_{fin}})^{\frac{1}{2}} r_e\} + C_2 K_0 \{(\frac{2\, h_{air\ fin}}{t_{fin}\, k_{fin}})^{\frac{1}{2}} r_e\}. \qquad (7.1.15)$$

These equations may be solved iteratively to obtain $h_{air\ fin}$, then η_f is determined from equation 7.1.5 and the fact that $\dot{Q}$ is equal to

$$\dot{Q} = k_{fin} A_c \frac{d\Theta}{dr} \qquad (7.1.16)$$

evaluated at the base of the fin.

From the temperatures in Table 7.1.1 and the equations listed above, the results shown in Table 7.1.2 were determined. The contact resistance shown in the table was calculated by dividing $\Delta T_{fin\ base\ -\ tube}$ by the heat transfer rate, $\dot{Q}$, such that

$$R_{contact} = \frac{\Delta T_{fin\ base\ -\ tube}}{\dot{Q}}. \qquad (7.1.17)$$

Table 7.1.2 Results of Equivalent Annulus Method Analysis of Evaporator with $T_{air,\ in}$ = 20 F

Parameter	Hour: 0	Hour: 10	Percent Change
h [Btu/hr-ft^2-F]	20.73	23.55	13.6
Q [Btu/hr]	2.87	3.71	29.3
Q_{max} [Btu/hr]	3.41	4.50	32.0
Fin Efficiency	0.84	0.82	-2.1
$R_{contact}$ [hr-F/Btu]	2.14	2.08	-2.4
$R_{surface}$ [hr-F/Btu]	6.12	5.50	-10.1

In Table 7.1.2, it can be seen that the surface resistance decreases by over 10% during the ten-hour test run, while the contact resistance only decreases approximately 2.4%. This indicates that the increases in the UA-value which have been observed are due mainly to an increase in the surface heat transfer capability and not a decrease in the contact resistance. From this analysis it cannot be determined whether the increase is due to an increase in $h_{air\ fin}$ because of surface roughening or whether it is due to an increase in the macroscopic and microscopic surface areas of the fins. In order to determine this the frost thickness and thermal conductivity would have to be determined. However, it is clear that the filling of the gaps between the fin and the tube by the frost have only marginal influence on the UA-value of the heat exchanger.

The findings presented above suggest it may be advisable to add some sort of artificial surface roughening such as a porous coating to boost the heat transfer capacity of an evaporator. If a coating can be found that results in UA-value increases on the order of 50%, as was evident in the higher frosting rate cases discussed here, it would be a potentially cost effective way to boost the effectiveness of an evaporator provided that the pressure drop increase is not prohibitive.

7.2 Frosting Rate Versus Driving Potential

A last analysis of the data that was done looked at the average frosting rate per unit area of evaporator surface to see how it changes as the frosting driving potential changes. One way in which the average driving potential may be approximated is by examining the difference between the average dew point of the air passing through the evaporator and the average of the refrigerant temperatures entering and leaving the evaporator. Assuming that the thermal resistance between the refrigerant and the outer tube surface is negligible due to the high heat transfer coefficients associated with two-phase flow (the validity of this assumption will be addressed a little later) and the high thermal conductivity of the aluminum evaporator tube, the bulk refrigerant temperature

may be taken as the surface temperature. Although the surface which participates in the mass and heat transfer on the air side of the evaporator is continually changing as frost is deposited on the coil, its temperature will be assumed to be adequately represented by the refrigerant temperature for the moment. Finally, because the frosting rate was found to be basically constant with respect to time for all the test conditions as shown in Sections 6.1, 6.2, and 6.3, an average of the data for each ten-hour test may be taken with confidence.

Figure 7.2.1 shows the plot of the average frosting rate per unit evaporator surface area (or frosting rate flux) as a function of the driving potential defined above for the six test conditions. The evaporator surface area consists of 2.6 ft^2 (0.24 m^2) of primary tube area and 17.8 ft^2 (1.65 m^2) of secondary fin area. The velocities shown in parenthesis under the test label are face velocities based on an evaporator face area of 0.324 ft^2 (0.0301 m^2). In the figure, it can be seen that a fairly convincing straight line may be fit to three out of the six data point sets. The -20 F refrigerant inlet data points, 20 F air inlet, and 72% relative humidity data points, however, are well off of this line.

The -20 F refrigerant inlet cases have frosting rate fluxes that are less than the frosting rate that would be predicted by the straight line for that driving potential, and the 20 F air inlet cases have frosting rate fluxes that are more than the frosting rate flux that would be predicted by the straight line for that potential. One reason for this discrepancy may be the nonlinearity of the relationship between the dew point and the humidity ratio. From *ASHRAE Handbook – Fundamentals* (1981), it can be seen that at -20 F for a 1 F (0.5 C) change in dew point there is a 0.0000150 $lb_{m\ water}/lb_{m\ air}$ change in humidity ratio. At 20 F, a 1 F change in dew point corresponds with a 0.000104 $lb_{m\ water}/lb_{m\ air}$ change almost seven times greater in humidity ratio. Since humidity ratio is a more quantitative measure of the humidity concentration than dew point, this change in slope of the dew point versus humidity ratio curve could result in a poor correlation of frosting rate flux to driving potential.

The 72% relative humidity cases are probably off the line due to the frosting in the return duct that was mentioned in Section 6.6. This problem would tend to make the evaporator frosting rate

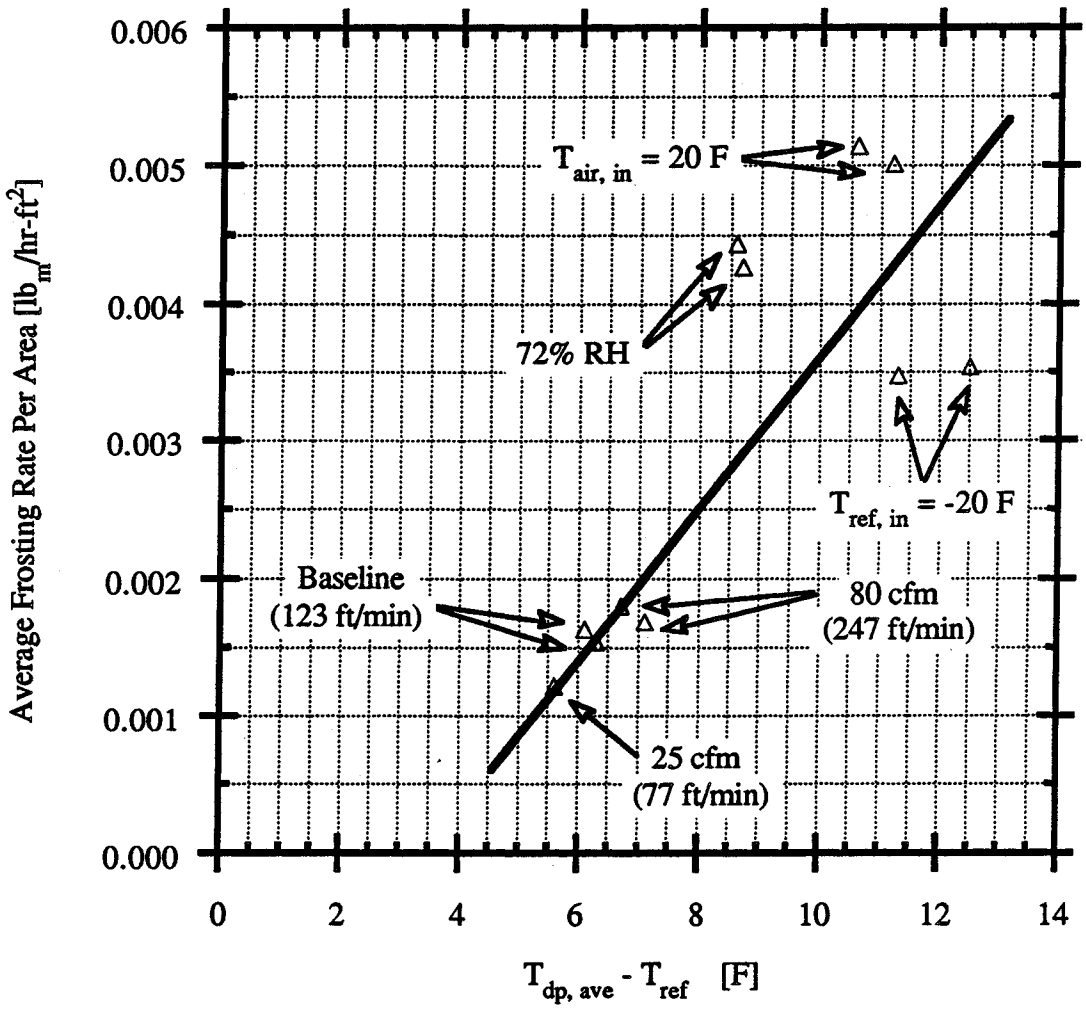

Figure 7.2.1 Average Evaporator Frosting Rate Per Unit Area of Evaporator Surface Versus $T_{dp, ave} - T_{ref}$ for All Test Runs

less than what was measured with the humidifier liquid level and cause the actual frosting rate to be very close to the straight line for the given driving potential.

One last comment that needs to be made about Figure 7.2.1 is the fact that the 25 cfm and 80 cfm cases fall on the linear curve-fit quite nicely with the baseline cases. This would seem to

contradict the assertion that was made earlier that the frosting rate is a function of the airflow rate for the air velocity range provided. To see if this is the case or if the given driving potential is prejudicing the results, a more accurate representation of the driving potential is required.

A more accurate driving potential may be defined as the average of the differences between the dew point of the air passing through the evaporator and temperature of the tube surface without any frost at the evaporator air inlet and air outlet. The inlet and outlet tube surface temperatures were calculated by means of the differential and absolute temperatures that were measured for the material in Section 7.1. Although using the tube surface temperature is not completely accurate since the temperatures of the fin surfaces are different from the tube surface temperatures and the frost layer does provide some finite thermal resistance, it should provide a more accurate assessment of the driving potential than the refrigerant temperature.

In order to determine the tube surface temperature for all of the testing conditions, the convective resistance of the refrigerant, $R_{refrigerant}$, was first determined. Looking at a location of the evaporator near the air inlet, this resistance can be represented as

$$R_{refrigerant} = \frac{T_{surface\ in} - T_{refrigerant}}{UA\ (T_{air,\ in} - T_{refrigerant})} \qquad (7.2.1)$$

where,

$T_{surface,\ in}$ = the temperature of the tube surface at the air inlet of the evaporator

and

$T_{air,\ in}$ = the average temperature of the air entering the evaporator.

The temperature at the middle of a fin was measured for a 20 F air inlet case as described in Figure 7.1.4. The corresponding tube surface temperature was obtained from the differential temperatures

listed in Table 7.1.1. The refrigerant temperature, air inlet temperature, and UA-value are known in every case.

Based on the UA-value, air inlet temperature, refrigerant temperature, and surface temperature of the tube at the air inlet for a 20 F air inlet case, it was found that $R_{refrigerant}$ is equal to 0.003216 hr-F/Btu (0.006097 K/W) which is approximately 18% of the total thermal resistance of the evaporator before any frost is accumulated. This is a significant portion of the total resistance and belies the common belief stated in the opening paragraph of this section that for all evaporators the refrigerant side convective resistance is negligible compared with the air side convective resistance.

The convective resistance of the refrigerant was assumed to be the same for all of the test cases and throughout the evaporator tube. The surface temperature at the air inlet was then determined for each case using equation 7.2.1.

Similarly, the surface temperature at the air outlet was determined by using an equation of the same form:

$$R_{refrigerant} = \frac{T_{surface\ out} - T_{refrigerant}}{UA\ (T_{air,\ out} - T_{refrigerant})} \qquad (7.2.2)$$

where,

$T_{surface,\ out}$ = the temperature of the tube surface at the air outlet of the evaporator

and

$T_{air,\ out}$ = the temperature of the air leaving the evaporator.

The surface temperature at the air inlet was then subtracted from the dew point measured at the inlet, and the surface temperature at the air outlet was subtracted from the dew point at the outlet

which was calculated from the frosting rate as described in Chapter 4. The average of these two differences is the abscissa in Figure 7.2.2.

In Figure 7.2.2, the average frosting rate flux is plotted as a function of the new driving potential. A straight line has once again been fitted to the data as was done in Figure 7.2.1. How-

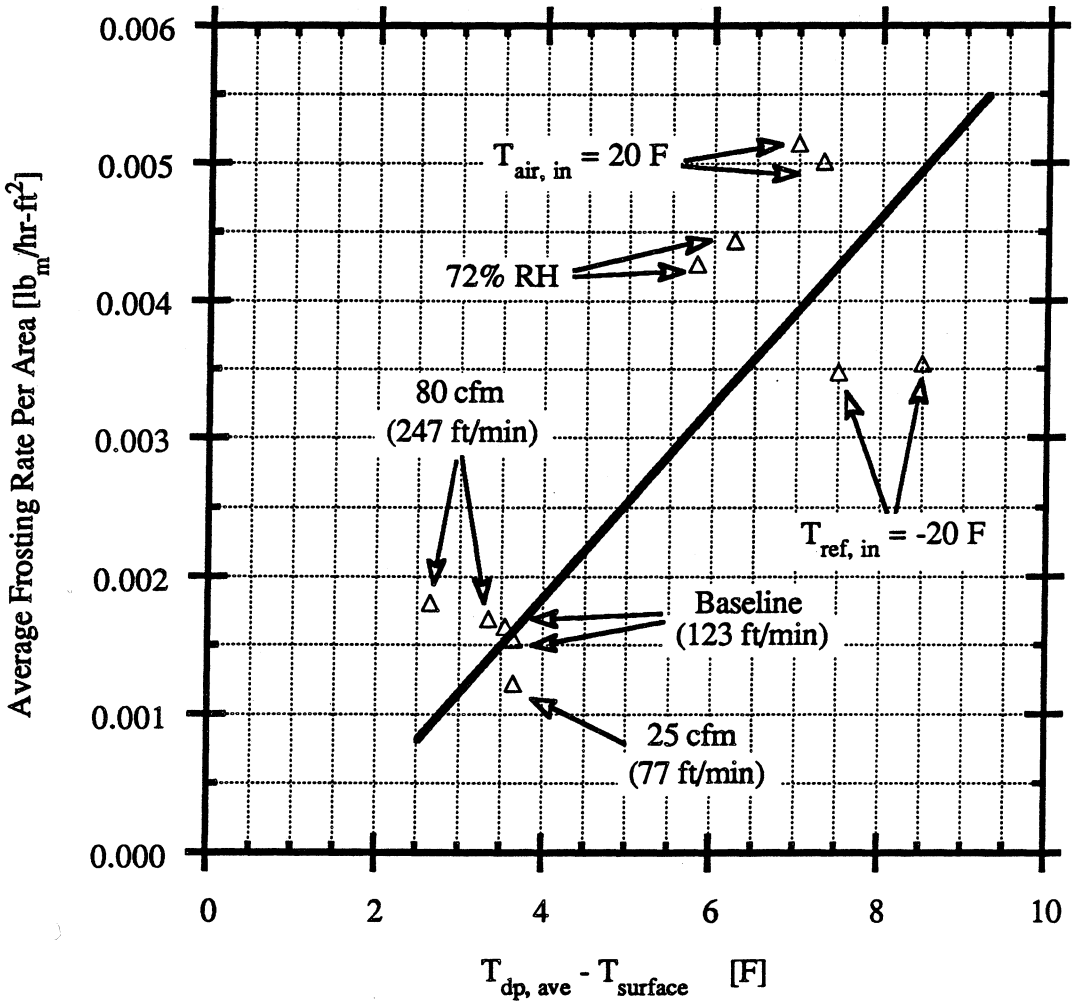

Figure 7.2.2 Average Evaporator Frosting Rate Per Unit Area of Evaporator Surface Versus $T_{dp,ave} - T_{surface}$ for All Test Runs

ever, this time only the baseline data points fall on the line. The 72% relative humidity data points and the 20 F air inlet temperature data points are above the line and the -20 F refrigerant inlet

temperature data points are below the line as they were in Figure 7.2.1. The important difference is that the 80 cfm and 25 cfm points are now off the line. The two 80 cfm points are both above the line and the 25 cfm point is below the line. This indicates that airflow rate does influence the frosting rate to some extent. Given the same driving potential, the frosting rate will increase if airflow rate or velocity is increased. Likewise, the frosting rate will decrease as the airflow rate is decreased, if the driving potential is maintained at a constant value. This effect was masked in Figure 7.2.1 due to the fact that the effect of airflow rate on the UA-value and, consequently, the surface temperature was not taken into account when the refrigerant temperature was used.

Before the conclusion outlined above is accepted, it should be kept in mind that the difference in the average frosting rates among all three cases may not be of a significant magnitude given the resolution of the frosting rate measurement to justify doing so.

Since there are still several discrepancies in the results presented in Figures 7.2.1 and 7.2.2, a third method for defining the mass transfer driving potential was pursued. This method involves the humidity ratio. First, using a heat transfer-mass transfer analogy, the rate of frost deposition per unit area, may be expressed as

$$\dot{m}_v'' = h_m (W_{air} - W_{surface}) \qquad (7.2.3)$$

where,

$\dot{m}_v''$ = the frosting rate $[\frac{lb_{m\ water}}{hr\text{-}ft^2}]$,

h_m = a convective mass transfer coefficient $[\frac{lb_{m\ air}}{hr\text{-}ft^2}]$,

W_{air} = the humidity ratio of the air passing through the evaporator at the bulk dew point $[\frac{lb_{m\ water}}{lb_{m\ air}}]$ averaged over the duration of frosting,

and

$W_{surface}$ = the humidity ratio of the the air at the surface of the evaporator tube $[\frac{lb_{m\ water}}{lb_{m\ air}}]$ averaged over the duration of frosting.

This then defines the mass transfer driving potential as the difference between the humidity ratio of the air away from the surface of the evaporator and the humidity ratio at the surface of the evaporator. The values of W_{air} and $W_{surface}$ were evaluated at the the air inlet and outlet of the evaporator by means of the dew points and surface temperatures, respectively. The average of these differences was then computed and used as the abscissa in the plot in Figure 7.2.3. This average value, ΔW_{ave}, is defined as

$$\Delta W_{ave} = \frac{(W_{air\ in} - W_{surface\ in}) + (W_{air\ out} - W_{surface\ out})}{2} \qquad (7.2.4)$$

It can be seen in Figure 7.2.3 that once again a straight line may be fit to the data points from the six test conditions. There is, however, a better correlation between this line and the data points for the 20 F air inlet and -20 F refrigerant inlet cases than there was in Figures 7.2.1 and 7.2.2. This indicates that these points were above and below the line, respectively, in those two figures due to the reason given previously: the nonlinearity of the dew point-humidity ratio relationship.

The 72% relative humidity case points are still above the line as they were in Figures 7.2.1 and 7.2.2. This was expected since changing the abscissa to humidity ratio difference from dew point difference will not change the fact that there was frosting in the return duct of the air loop, and, consequently, the measured frosting rate will be higher than the actual frosting rate.

The last point that needs to be mentioned about Figure 7.2.3 concerns the airflow rate and its effect on the frosting rate. In the figure, the 25 cfm data point is below the curve-fit line while one

of the 80 cfm points is well above the line and the other is only slightly above. This is similar to the results shown in Figure 7.2.2. These results are the consequence of the relationship between frosting rate and airflow rate. This relationship involves three forces: the mass transfer coefficient, the evaporator surface temperature, and the moisture capacity.

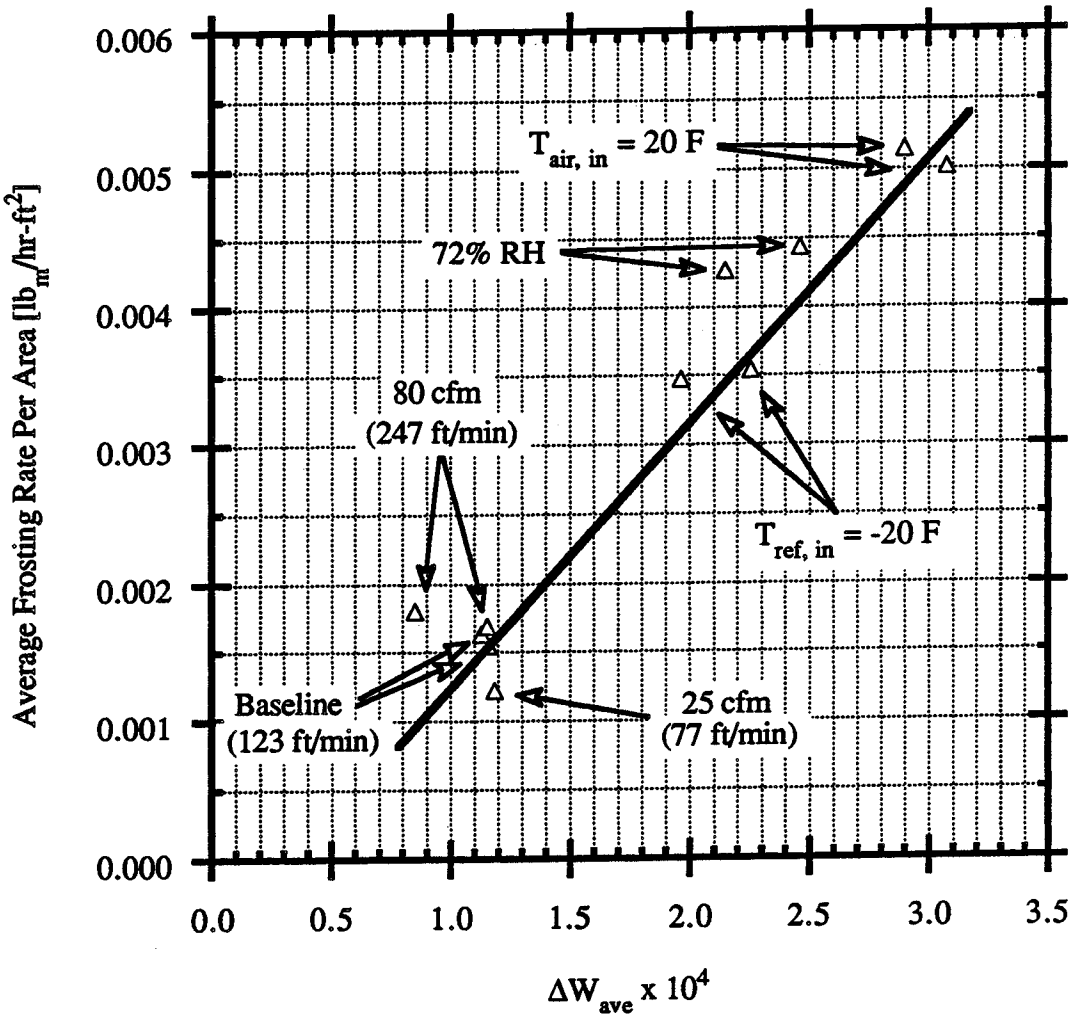

Figure 7.2.3 Average Evaporator Frosting Rate Per Unit Area of Evaporator Surface Versus ΔW_{ave} for All Test Runs

Referring back to equation 7.2.3, the frosting rate per unit area was given as the product of a convective mass transfer coefficient and the humidity ratio driving potential. It is apparent that as the airflow rate increases the mass transfer coefficient will tend to increase just as the heat transfer

coefficient tends to increase, drawing an analogy between mass and heat transfer. An increase in airflow rate has the opposite net effect on the driving potential. The quantity, ΔW_{ave}, was observed to decrease as the airflow rate was increased. This is shown in Table 7.2.1. In the table, the average humidity ratios at the bulk air conditions and at the surface conditions for the air inlet and outlet as well as ΔW_{ave} are given for each test run at each of the six testing conditions. The av-

Table 7.2.1 Average Inlet and Outlet Air and Surface Humidity Ratios Over the Duration of the Frosting Tests for All Conditions

Case	Date	$W_{air,\ in}$	$W_{air,\ out}$	$W_{surf,\ in}$	$W_{surf,\ out}$	ΔW_{ave}
Baseline	040690	0.000720	0.000572	0.000572	0.000495	0.000113
	051790	0.000725	0.000570	0.000573	0.000490	0.000116
	Average	0.000722	0.000571	0.000573	0.000492	0.000114
72% RH	040990	0.000935	0.000525	0.000554	0.000476	0.000215
	051990	0.001020	0.000549	0.000580	0.000501	0.000246
	Average	0.000979	0.000537	0.000567	0.000488	0.000231
25 cfm	052590	0.000735	0.000545	0.000563	0.000481	0.000118
	Average	0.000735	0.000545	0.000563	0.000481	0.000118
80 cfm	041190	0.000746	0.000667	0.000650	0.000533	0.000115
	071090	0.000704	0.000616	0.000626	0.000524	0.000085
	Average	0.000725	0.000642	0.000638	0.000529	0.000100
$T_{air,\ in}$ = **20 F**	041890	0.001130	0.000564	0.000617	0.000498	0.000290
	052190	0.001160	0.000600	0.000640	0.000505	0.000308
	Average	0.001150	0.000582	0.000629	0.000501	0.000299
$T_{ref,\ in}$ = **-20 F**	042390	0.000710	0.000340	0.000366	0.000292	0.000196
	052390	0.000744	0.000369	0.000373	0.000288	0.000226
	Average	0.000727	0.000355	0.000369	0.000290	0.000211

erage of all the test runs at each of the six testing conditions is also provided. It can be seen that the average driving potential is slightly less for the 25 cfm case compared with the baseline case, and the baseline case is slightly less than 80 cfm case. There are two causes for this effect: the change in the surface temperature as the airflow rate is varied and the change in the moisture capacity with airflow rate variation.

The air side convective heat transfer coefficient tends to increase as the airflow rate is increased. This causes the surface temperature of the evaporator to move closer to the temperature of the air stream. Both of these effects are shown in Table 7.2.2. In the table, an average UA-value, averaged over the duration of each test run, is shown for each testing case. The corresponding air, surface, and refrigerant temperatures averaged in the same manner are also pro-

Table 7.2.2 Average UA-values and Air, Surface, and Refrigerant Temperatures Over the Duration of the Frosting Tests for All Conditions

Case	Date	UA [Btu/hr-F]	$T_{ref,\ ave}$ [F]	$T_{air,\ in}$ [F]	$T_{air,\ out}$ [F]	$T_{surf,in}$ [F]	$T_{surf,out}$ [F]
Baseline	040690	67.3	-10.2	10.9	-4.0	-6.3	-9.0
	051790	63.2	-10.8	10.0	-4.8	-6.7	-9.6
	Average	65.3	-10.5	10.5	-4.4	-6.5	-9.3
72% RH	040990	77.3	-11.2	9.6	-5.6	-6.9	-9.7
	051990	71.7	-10.2	10.8	-4.6	-6.5	-9.2
	Average	74.5	-10.7	10.2	-5.1	-6.7	-9.5
25 cfm	052590	54.5	-10.4	10.6	-6.4	-7.0	-9.9
	Average	54.5	-10.4	10.6	-6.4	-7.0	-9.9
80 cfm	041190	98.6	-9.8	9.7	-1.8	-4.2	-7.9
	071090	85.7	-10.6	10.2	-1.8	-4.9	-8.2
	Average	92.2	-10.2	10.0	-1.8	-4.6	-8.1
$T_{air,\ in}$ = **20 F**	041890	71.2	-10.5	20.2	-2.6	-4.9	-8.9
	052190	75.2	-10.7	20.0	-3.4	-4.6	-9.0
	Average	73.2	-10.6	20.1	-3.0	-4.8	-9.0
$T_{ref,\ in}$ = **-20 F**	042390	70.5	-20.6	10.2	-12.3	-14.8	-18.8
	052390	74.2	-20.7	10.8	-12.4	-14.4	-19.0
	Average	72.4	-20.7	10.5	-12.4	-14.6	-18.9

vided. The average UA-value is shown to be higher for the 80 cfm case than for the baseline case. The baseline case, in turn, has a higher average UA-value than the 25 cfm case. This causes the surface temperatures to behave as shown in the table and more clearly in Figure 7.2.4.

In Figure 7.2.4, the average temperature of the refrigerant, the surface, and the air as the air passes from the inlet to the outlet is shown for the baseline case, the 25 cfm case, and the 80 cfm case. Linear temperature profiles have been selected for the purposes of this discussion. It can be seen that due to the higher UA-value of the 80 cfm case compared with the baseline case, the line representing the surface temperature for the 80 cfm case has shifted above the baseline case, toward the air temperature line. Conversely the surface temperature line has shifted below the baseline case, away from the air temperature line. These shifts in the surface temperatures result in

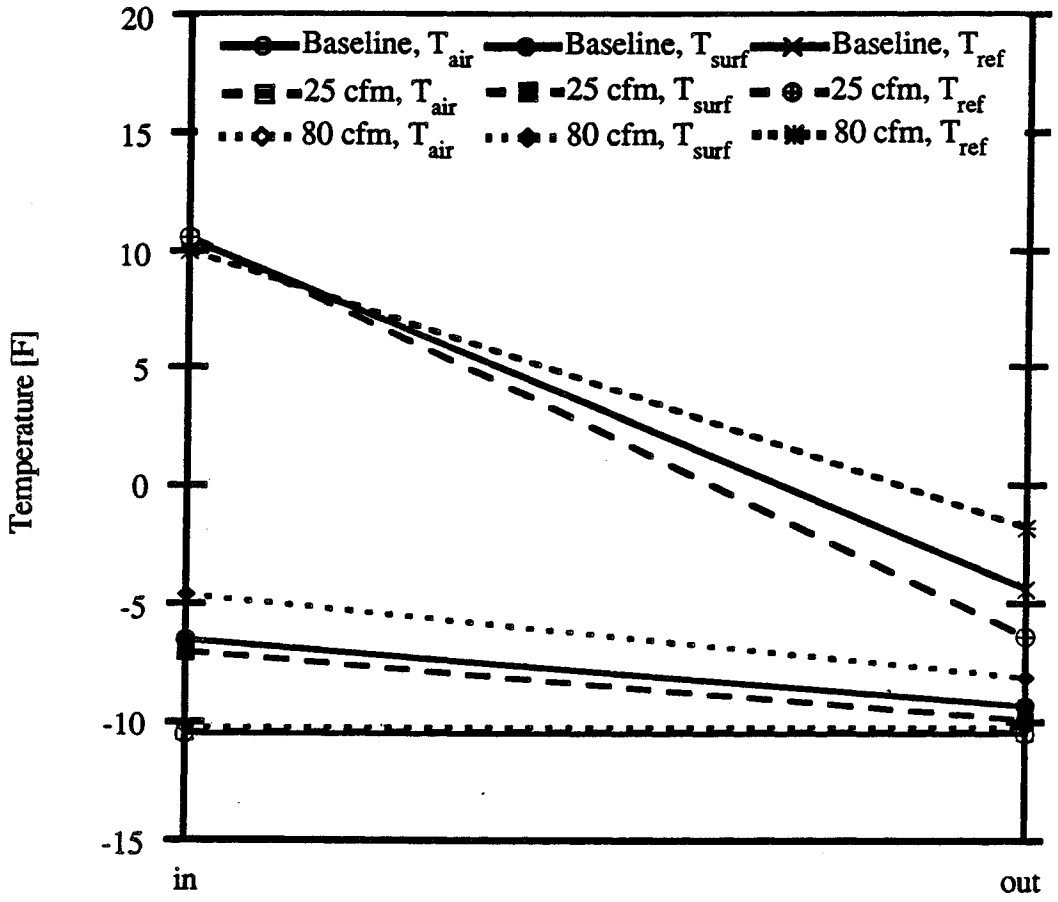

Figure 7.2.4 Average Air, Surface, and Refrigerant Temperatures Versus Evaporator Air Side Location for the Baseline, 25 cfm, and 80 cfm Cases

similar shifts in the humidity ratios at the surface as shown in Figure 7.2.5. In this figure, the average humidity ratios at the bulk air conditions and at the surface conditions as the air proceeds

from inlet to outlet are plotted. Again, since only the inlet and outlet conditions are known, linear profiles have been assumed. It is evident that the line representing surface humidity ratio has shifted upward from the baseline case with an airflow rate of 80 cfm

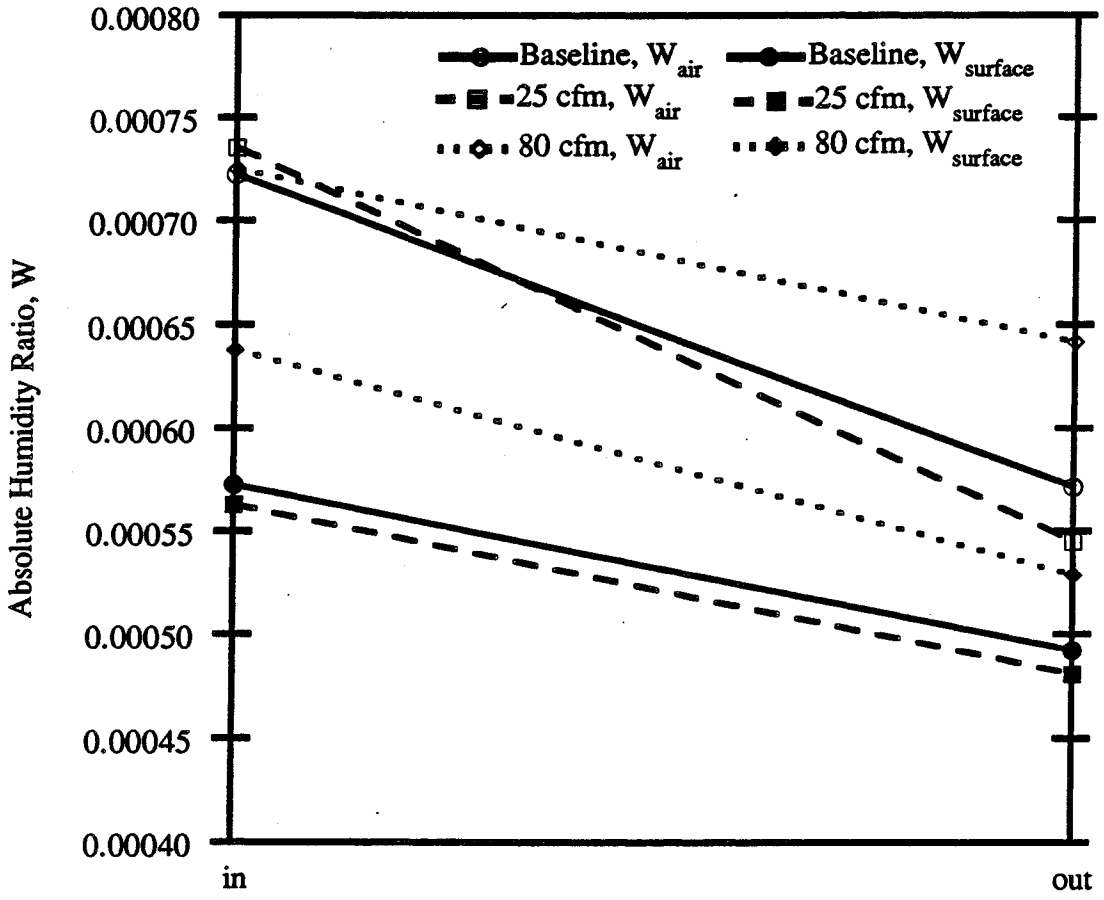

Figure 7.2.5 Average Air and Surface Humidity Ratios Versus Evaporator Air Side Location for the Baseline, 25 cfm, and 80 cfm Cases

and downward from the baseline case with an airflow rate of 25 cfm. The end result of this behavior is a decrease in the driving potential as the airflow rate is increased, and an increase in the driving potential as the airflow rate is decreased.

While the activities described above are occurring, the moisture capacity which will be defined here as the mass flow rate of the moist air as it passes through the evaporator is also influencing ΔW_{ave}. It was shown in Chapter 4 that the frosting rate, $\dot{m}_v$, can be represented as

$$\dot{m}_v = \dot{m}_{air} (W_{air\ in} - W_{air\ out}) \qquad (7.2.5)$$

where,

$\dot{m}_{air}$ = the mass flow rate of air [$lb_{m\ air}$/hr].

It is apparent in Figure 7.2.5 that as $\dot{m}_{air}$ is increased, $W_{air\ in} - W_{air\ out}$ decreases. Conversely, as $\dot{m}_{air}$ is decreased, $W_{air\ in} - W_{air\ out}$ increases. This then results in airflow rate having the opposite effect on the driving potential that it had in relation to surface temperature. Namely, a higher airflow rate tends to result in a higher driving potential, while a lower airflow rate tends to result in a lower driving potential.

The net effect of airflow rate on frosting rate is determined by how well the forces described above (mass transfer coefficient, surface temperature, and mass transfer capacity) balance one another. If an increase in the mass transfer coefficient and the mass transfer capacity is equally matched by an increase in the surface temperature, the frosting rate will be the same for all airflow rates. If the first two factors are able to overpower the last factor, then the frosting rate will increase as the airflow rate is increased. If the opposite is true, then the frosting rate will decrease as the airflow rate is increased. This behavior may account for the conflicting results concerning air velocity and frosting rate that were cited in Chapter 2.

Finally, one last method of defining a driving potential was pursued in order to see if any further insights could be gleaned from the experimental data. Since the heat transfer performance of the evaporator can be analyzed in terms of a log-mean-temperature-difference as described in

Chapter 4, it follows that the mass transfer performance may also be analyzed in terms of some log-mean difference. It was decided to define a log-mean driving potential in terms of the humidity ratios described above. The log-mean-humidity ratio-difference (LMWD) is defined as

$$LMWD = \frac{\Delta W_1 - \Delta W_2}{\ln(\Delta W_1 / \Delta W_2)} \tag{7.2.6}$$

where

$$\Delta W_1 = W_{air,\,in} - W_{surface,\,in} \tag{7.2.7}$$

and

$$\Delta W_2 = W_{air,\,out} - W_{surface,\,out}. \tag{7.2.8}$$

Using this definition, the plot of average frosting rate flux versus LMWD shown in Figure 7.2.6 was generated. Unfortunately, it can be seen in the figure that no new information is provided by using the log-mean. The data points for all of the cases fall in essentially the same locations that they did in the arithmetic-mean plot in Figure 7.2.3. One reason for this may be the fact that the true surface temperatures are not being used here. If these temperatures could be determined more accurately, a better relationship between the data points and the straight-line fit might be possible.

7.3 Comparison of the Results to Previous Results in the Literature

In order to see whether the results shown for the driving potential approximated as the average of the difference between the humidity ratio away from the evaporator surface and at the surface can be verified by the results of previous researchers, the references cited in Chapter 2 were examined again. Unfortunately, due to a lack of information in all of the heat exchanger frosting papers concerning the precise surface area of the heat exchangers that were studied, it was impossi-

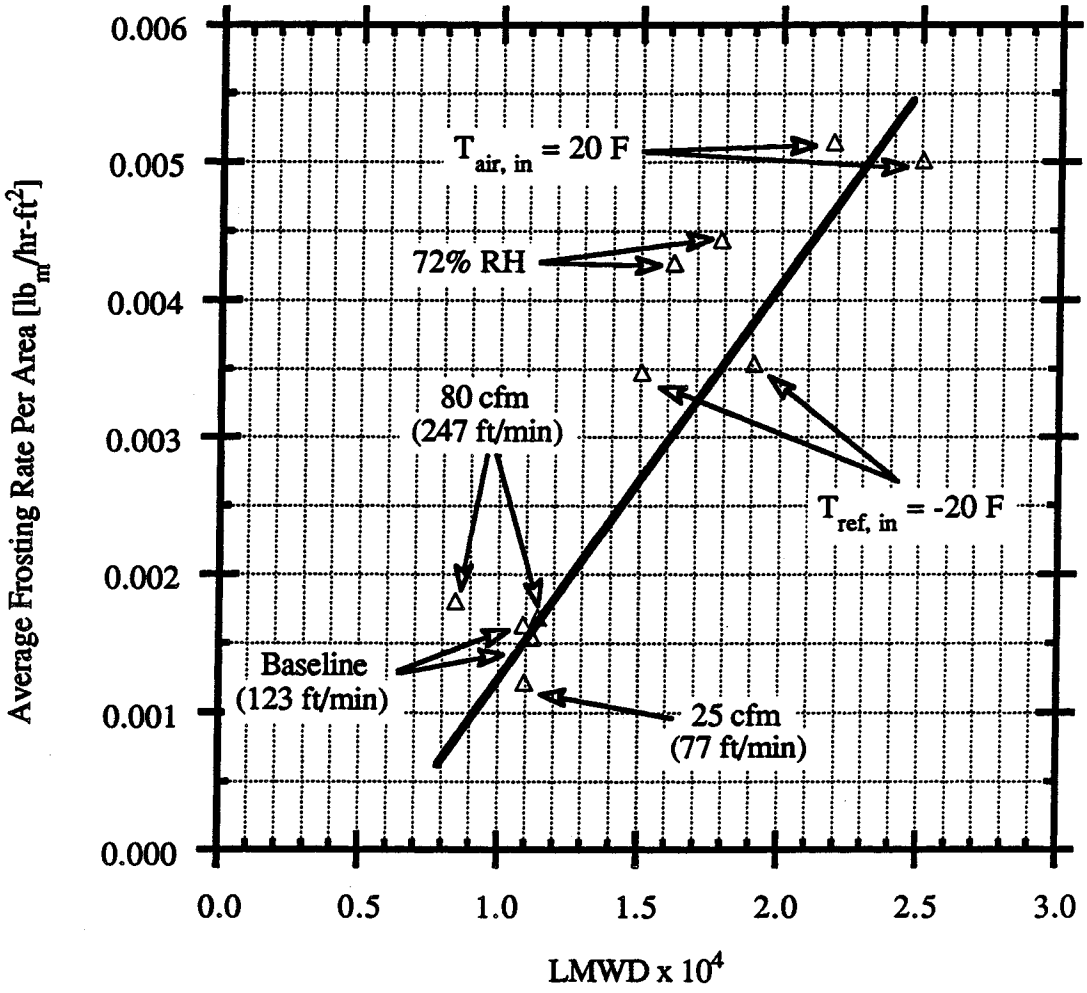

Figure 7.2.6 Average Evaporator Frosting Rate Per Unit Area of Evaporator Surface Versus the Log-Mean-Humidity Ratio-Difference (LMWD) for All Test Runs

ble to calculate a frosting rate flux as defined earlier. This renders any comparison between that data and the data presented here useless, since the frosting rate is greatly affected by the available surface area. Having made this discovery, it was decided instead to attempt a comparison with some of the simple surface geometry work that was listed in the first paragraph of Chapter 2. It was not possible, however, to find anywhere in the literature simple geometry work that involved driving potentials in the same range that was dealt with here. One flat plate frost study and one cylinder frost study were found to be amenable to comparison with the data here even though their

driving potentials were relatively high. These studies are by O'Neal and Tree (1984) and Chung and Algren (1958), respectively.

The O'Neal and Tree result that was cited involved an air temperature of 44 F (6.7 C), a surface temperature of 23 F (-5 C), an air humidity ratio of 0.00395 $lb_{m\ water}/lb_{m\ air}$, and a Reynolds number based on length of 15900. For a 25 in. (0.69 m) long plate, this Reynolds number translates into a velocity of 69 ft/min (21 m/min). The frosting rate flux was determined by dividing the average increase in the frosting thickness per hour by the frost density. For the test cited, the frost density was given as 17.7 lb_m/ft^3 (284 kg/m^3).

The Chung and Algren study involved frosting on a 1 in. (25.4 mm) diameter cylinder with a testing length of 1.0 ft (0.3 m). The test result that was cited for comparison with the data here involved an air temperature of 60 F (16 C), a surface temperature of 0.0 F (-18 C), an air humidity ratio of 0.00427 $lb_{m\ water}/lb_{m\ air}$, a Reynolds number based on diameter of 9965, and a corresponding velocity of 1134 ft/min (345.6 m/min). The frosting rate flux in this case was determined by dividing the measured rate of frost mass deposition on the cylinder per hour by the surface area of the cylinder.

Figure 7.3.1 shows the comparison of the O'Neal and Tree and Chung and Algren data described above to the data that was generated in this study. The present data points shown are the same ones that were presented in Figure 7.2.3, however, the scale on the abscissa in this plot has been expanded to allow for the relatively large driving potentials of the literature data. The straight line that was fitted to the data points in Figure 7.2.3 has been extended in this figure to allow for a comparison with the two data points from the literature. It can be seen that the O'Neal and Tree data point and the Chung and Algren data point are below the frosting rate fluxes predicted by the extrapolated line for the given driving potentials. One possible explanation for these results is the fact that with a heat exchanger there should be better mixing of the air stream as it passes over the

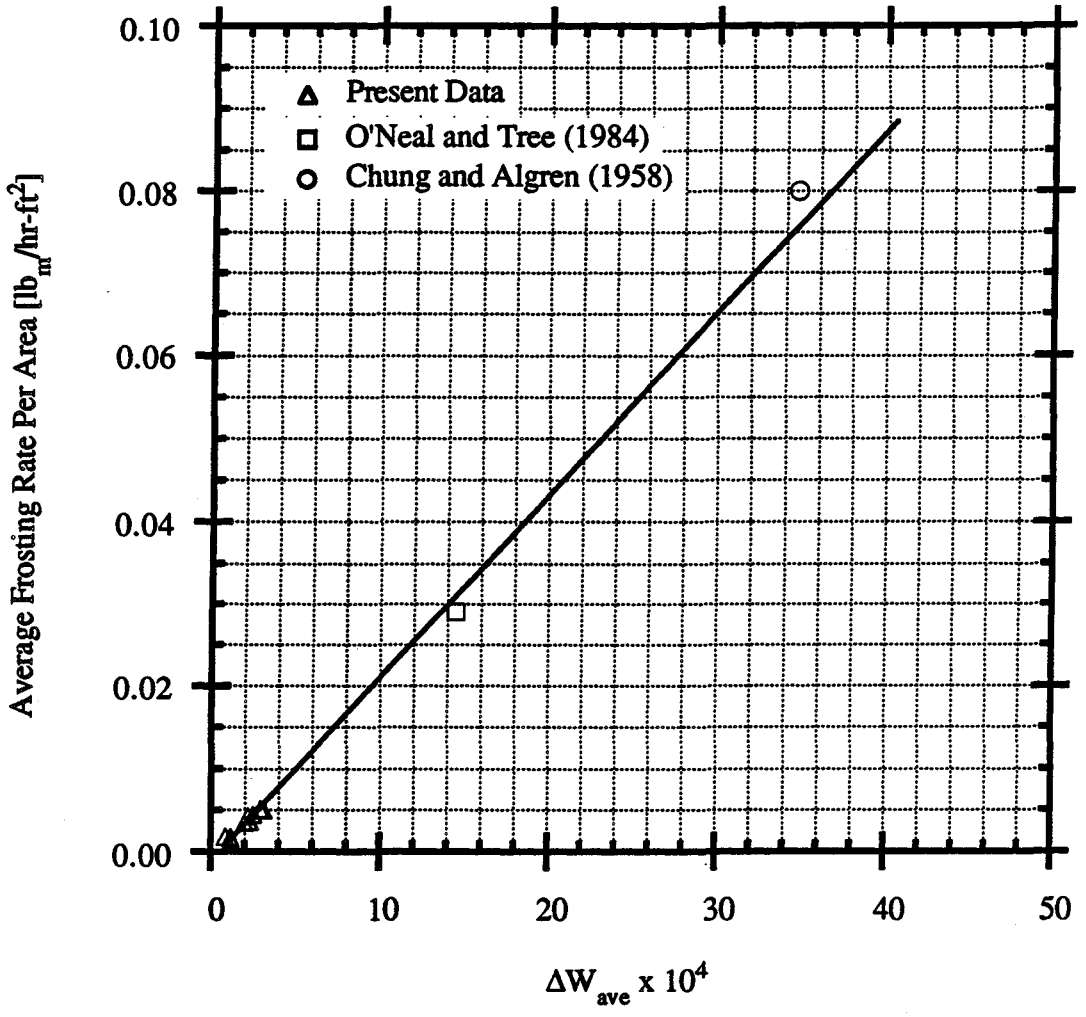

Figure 7.3.1 Average Evaporator Frosting Rate Per Unit Area of Evaporator Surface Versus ΔW_{ave} for the Present Data Compared with Data from Previous Researchers

flat fin surfaces and cylindrical tube surfaces than if these two geometries are studied separately in an isolated environment. This better mixing should result in higher mass transfer coefficients and, consequently, higher frosting rate fluxes as is shown in Figure 7.3.1.

Chapter 8

CONCLUSION

8.1 Summary

The extensive number of test runs that were performed with the 5 fpi Peerless refrigerator-freezer evaporator coil under frosting conditions yielded a number of important results. The following is a summary of the results:

a. The frosting rates for all of the test conditions examined were found to be constant with respect to time over a ten-hour test period.

b. The frosting rates for the 25 cfm, 80 cfm, and baseline cases were all relatively close to each other, having average rates between 0.02 and 0.04 lb_m/hr. There was evidence, however, of a relationship between airflow rate and frosting rate. As the airflow rate was increased, the frosting rate increased slightly. Likewise, as the airflow rate was decreased the frosting rate decreased slightly.

c. The airflow rate affected the frosting rate as described above due to its influence on three parameters: the mass transfer coefficient, the evaporator surface temperature, and the moisture capacity of the air stream. If the frosting rate per unit area is defined as the product of the mass transfer coefficient and a mass transfer driving potential, the effect of airflow rate on frosting rate can be shown by its effect on the two components in this product. First, it is known that the mass transfer coefficient increases as the airflow rate is increased. This then implies that the frosting rate should increase as the airflow rate is increased. However, the evaporator surface temperature and

the moisture capacity of the air have opposing effects on the mass transfer driving potential. The surface temperature, which increases as the airflow rate is increased, decreases the driving potential as it is increased, while the moisture capacity, which also increases as the airflow rate is increased, increases the driving potential as it is increased. For this study, the net result of these two parameters on the mass transfer driving potential was to decrease it as the airflow rate was increased. This decrease was overcome by the mass transfer coefficient increase such that the frosting rate was slightly greater for the higher-airflow rate cases. This will probably not always be the case. The amount that each of the parameters listed above changes with respect to each other as airflow rate is changed determines the magnitude and direction of the effect of airflow rate on frosting rate.

d. The -20 F refrigerant inlet cases had average frosting rates approximately double the 25 cfm, 80 cfm, and baseline cases. The 72% relative humidity cases had average frosting rates 29% higher than this. The 20 F air inlet cases had average frosting rates approximately 11% higher than the 72% relative humidity cases.

e. While a constant airflow was maintained through the evaporator coil, the UA-value of the evaporator was found to increase significantly as frost was deposited on the coil. The percent increases in the UA-value and corresponding percent increases in the air side pressure drop for the six different test conditions that were investigated are shown in Table 8.1.1. The increases occurred over a ten-hour period.

f. There are three potential reasons for the increase in the UA-value of the evaporator as frost formed: a decrease in the contact resistance between fins and tube as the gap filled with frost, an increase in the air side convective heat transfer coefficient due to a greater surface roughness, and an increase in the surface area of the tube and fins as the frost built up.

Table 8.1.1 Summary of the Effect of Frost on the UA-value and Air Side Pressure Drop of the Evaporator Over Ten Hours

Test Conditions	Increase in UA-value [%]	Increase in ΔP [%]
Baseline	13	80
72% RH	48	1300
25 cfm	8	40
80 cfm	10	60
$T_{air, in}$ = 20 F	50	1300
$T_{ref, in}$ = -20 F	50	800

g. In order to determine which of the reasons listed above was most responsible for the UA-value increase, a section of tube and fins was instrumented with thermocouples. It was found that over a ten-hour testing period with a 20 F air inlet temperature the contact resistance between the fin and the tube only decreased 2.5% while the resistance between the fin surface and the air decreased over 10%. This indicates that the effect of frost on the convective heat transfer coefficient and the external surface area is more important than its effect on the contact resistance.

h. Based on the findings in f, it may be advisable to artificially roughen the surface of the tubes and fins in order to take advantage of the improved convective heat transfer coefficient and extended surface area that the frost provides. This may be done by applying some sort of coating or perhaps by roughening the outer surfaces of the evaporator through mechanical means. However, the penalty of increased air side pressure drop through the evaporator should be taken into account.

i. It was determined that the convective thermal resistance of the refrigerant in the evaporator accounted for approximately 18% of the total resistance of the evaporator. Clearly, the refrigerant side resistance is much more important than previously believed.

8.2 Recommendations

There are several modifications in the evaporator test facility that are recommended in order to improve and expand upon the data that have been presented here. These improvements include:

- Full implementation of an automatic control system for the main expansion valve, the bypass valve, and the subcooler 2 valve on the refrigeration system and on the damper in the air loop using a separate controller for each function,

- Reconstruction of the air loop to reduce all air leaks and to facilitate an intensive visual analysis of the frosted evaporator coil,

- Development of either a new method to introduce moisture into the air loop, possibly a water injection system, or a better mixing method for the present evaporative pan humidifier so that higher inlet relative humidities may be achieved,

- Installation of better instrumentation for measuring the air side pressure drop through the evaporator and the humidifier liquid level such as a capacitance-type level gauge,

- Replacement of the present copper, dew point sampling lines with stainless steel lines.

It is also recommended that the present hand valves on the dew point sampling lines be replaced with remotely actuated solenoid valves so that they may be switched between inlet and outlet automatically during testing. This would eliminate the need to have an operator present throughout testing.

In addition to the physical changes recommended above, there are also some additions that should be made to the testing procedure and analysis. First of all, another parameter that could be studied to see how it influences the effect of frosting on UA-value, pressure drop, and frosting rate is evaporator configuration. Evaporators made by different manufacturers could be tested to see how design affects frosting. It would also be informative to examine the effect of different fin spacing on frosting.

A second area that should be further pursued is the determination of frost thickness on the evaporator fins and tube. In the work presented here, there was no facility for determining the frost thickness. Some photographs were presented in Chapter 6 from which a rough estimate of frost thickness at one section of the evaporator could be obtained, but this information cannot be extrapolated to the entire evaporator with any degree of accuracy. A photographic procedure may be pursued if a high resolution imaging system was applied to the problem. This imaging system could produce hourly, digitized images of the evaporator as frost forms on it. These images could then be analyzed on the computer to determine frost thicknesses. By using this imaging system on the entire evaporator, an accurate measurement of total frost on the coil could be obtained. This would provide another method for measuring the frost accumulation. This frost thickness information would also provide the information needed to more precisely evaluate the thermal resistances that were approximated in Section 7.1.

Based on the effect of the frost on the UA-value of the evaporator which was discussed in Chapters 6 and 7 and summarized in this chapter in Section 8.1, it appears that some future work

on coatings for evaporators may be warranted. Although this does not directly relate to frosting, research into various surface coatings to boost heat transfer (keeping in mind the inherent increase in pressure drop) could be accomplished with the evaporator test facility.

The final recommendation for future work is that the information about frosting gathered here be used for the purpose for which it was intended, the determination of optimum defrosting criteria. Although some of the equipment used in this study does not even remotely resemble actual refrigerator-freezer hardware (e.g., the fan and the damper), and the airflow rate is not maintained at a constant level in a refrigerator-freezer, the information gathered here can be used to aid the development of defrosting schemes. It should be possible to determine the optimum trade-off between pressure drop and UA-value so that the augmented heat transfer that the frost seems to provide may be utilized without creating an untenably large pressure drop.

BIBLIOGRAPHY

Air Movement and Control Association, Inc. 1985. *ANSI/AMCA Standard 210-85, Laboratory Methods of Testing Fans for Rating*. pp. 12-13.

ASHRAE. 1981. 1981 ASHRAE Handbook -- Fundamentals, American Society of Heating, Refrigerating and Air-Conditioning Engineers, Inc.

Barron, R. F. and Han, L. S. 1965. Heat and mass transfer to a cryosurface in free convection. Journal of Heat Transfer, November 1965, pp. 493-506.

Barrow, Henry. 1985. A note on frosting of heat pump evaporator surfaces. Heat Recovery Systems, Vol. 5, No. 3, 1985, pp. 195-201.

Beatty, K. O., Finch, E. B., and Schoenborn, E. M. 1951. Heat transfer from humid air to metal under frosting conditions. Refrigerating Engineering, December 1951, pp. 1203-1207.

Bong, Tet-Yin. 1965. An Experimental Investigation of the Operating Characteristics of a Frosted Evaporator Coil. Master of Science Thesis. University of Kentucky.

Chen, M. M. and Rohsenow, W. 1964. Heat, mass, and momentum transfer inside frosted tubes – experiment and theory. Journal of Heat Transfer, August 1964, pp. 334-340.

Chung, P. M. and Algren, A. B. 1958. Frost formation and heat transfer on a cylinder surface in humid air cross flow (Part 1). Heating, Piping, and Air Conditioning, Volume 30, Number 9, September 1958, pp. 171-178.

Chung, P. M. and Algren, A. B. 1958. Frost formation and heat transfer on a cylinder surface in humid air cross flow (Part 2). Heating, Piping, and Air Conditioning, Volume 30, Number 10, October 1958, pp. 115-122.

Gatchilov, T. S., Ivanova, V. S., and Kaltchev, K. I. 1979. Some aspects of construction and exploitation of extended surface air coolers operating under frosting conditions. Proceedings of the XVth International Congress of Refrigeration, Volume II, 1979, pp. 991-995.

Gatchilov, T. S. and Ivanova, V. S. 1979. Characteristics of the frost formed on the surface of the finned air coolers. Proceedings of the XVth International Congress of Refrigeration, Volume II, 1979, pp. 997-1003.

Gates, R. R., Sepsy, C. F., and Huffman, G. D. 1967. Heat transfer and pressure loss in extended surface heat exchangers operating under frosting conditions, part I: literature survey, test apparatus, and preliminary results. ASHRAE Transactions, Volume 73, Part 2, pp. I.2.1-I.2.13.

Hayashi, Yeujiro, Aoki, Kazuoi, and Yuhara, Hiroshi. 1977. Study of frost formation based on a theoretical model of the frost layer. Heat Transfer - Japanese Research, Volume 6, Number 3, 1977, pp. 79-94.

Hayashi, Y., Aoki, A., Adachi, S., and Hori, K. 1977. Study of frost properties correlating with frost formation types. Journal of Heat Transfer, Volume 99, May 1977, pp. 239-245.

Heflin, Christopher. 1989. Design and Fabrication of a Low Airflow Frosted Evaporator Test Facility. Master of Science Thesis. University of Illinois.

Huffman, G. D. and Sepsy, C. F. 1967. Heat transfer and pressure loss in extended surface heat exchangers operating under frosting conditions, part II: data analysis and correlation. ASHRAE Transactions, Volume 73, Part 2, pp. I.3.1-I.3.16.

Incropera, Frank P. and DeWitt, David P. 1981. Fundamentals of Heat Transfer.

Jones, B. W. and Parker, J. D. 1975. Frost formation with varying environmental parameters. Journal of Heat Transfer, Volume 97, May 1975, pp. 255-259.

Kamei, S., Mizushina, T., Kifune, S., and Koto, T. 1952. Research on the frost formation in a low temperature cooler. The Japan Science Review, Volume 2, Number 3, 1952, pp. 317-326.

Kern, Donald Q. and Kraus, Allan D. 1972. Extended Surface Heat Transfer.

Kondepudi, S. N. and O'Neal, D. L. 1987. The effects of frost growth on extended surface heat exchanger performance: a review. ASHRAE Transactions, Volume 93, Part 2, pp. 258-277.

Kondepudi, S. N. and O'Neal, D. L. 1989. Effect of frost growth on the performance of louvered finned heat exchangers. International Journal of Refrigeration, Volume 12, May 1989, pp. 151-158.

Kondepudi, S. N. and O'Neal, D. L. 1990. The effects of different fin configurations on the performance of finned-tube heat exchangers under frosting conditions. ASHRAE Transactions, Volume 96, Part 2, (preprint).

Lotz, H. 1967. Heat and mass transfer and pressure drop in frosting finned coils. Progress in Refrigeration Science and Technology, Volume II, Proceedings of the XII International Congress of Refrigeration, pp. 499-505.

Marinyuk, B. T. 1980. Heat and mass transfer under frosting conditions. International Journal of Refrigeration, Volume 3, Number 6, November 1980, pp. 366-368.

Niederer, Ronald H. 1986. Frosting and defrosting effects on coil heat transfer. ASHRAE Transactions, Volume 92, Part 1, pp. 467-473.

O'Neal, D. L. and Tree, D. R. 1984. Measurement of frost growth and density in a parallel plate geometry. ASHRAE Transactions, Volume 90, Part 2, pp. 278-290.

O'Neill, Patrick J. 1988. Thermal Performance Analysis of Finned-Tube Heat Exchangers at Low Temperatures and Airflow Rates. Master of Science Thesis, University of Illinois.

Oskarsson, S. P., Krakow, K. I., and Lin, S. 1990. Evaporator models for operation with dry, wet, and frosted finned surfaces, part I: heat transfer and fluid flow theory. ASHRAE Transactions, Volume 96, Part 1 (preprint).

Oskarsson, S. P., Krakow, K. I., and Lin, S. 1990. Evaporator models for operation with dry, wet, and frosted finned surfaces, part II: evaporator models and verification. ASHRAE Transactions, Volume 96, Part 1 (preprint).

Parish, H. C. and Sepsy, C. F. 1972. A numerical analysis of frost formation under forced convection. ASHRAE Transactions,Volume 78, Part 1, pp. 236-251.

Rohsenow, W. M., Hartnett, J. P., and Ganic, E. N. 1985. Handbook of Heat Transfer Applications.

Sami, S. M. and Duong, T. 1989. Mass and heat transfer during frost growth. ASHRAE Transactions, Volume 95, Part 2 (preprint).

Sanders, C. Th. 1975. Frost Formation: The Influence of Frost Formation and Defrosting on the Performance of Air Coolers. Ph. D. Thesis. Technische Hogeschool. Schulte, D. W. and Howell, R. H. 1982. The effect of air turbulence on the rate of frost growth on a horizontal flat plate. ASHRAE Transactions, Volume 88, Part 2, pp. 201-217.

Schneider, H. W. 1978. Equation of the growth rate of frost forming on cooled surfaces. International Journal of Heat and Mass Transfer, Volume 21, 1978, pp. 1019-1024.

Schulte, D. W. and Howell, R. H. 1982. The effect of air turbulence on the rate of frost growth on a horizontal flat plate. ASHRAE Transactions, Volume 88, Part 2, pp. 201-217.

Senshu, T.; Yasuda, H.; Oguni, K.; and Ishibani, K. 1990. Heat pump performance under frosting conditions: part I - heat and mass transfer on cross-finned tube heat exchangers under frosting conditions. ASHRAE Transactions, Volume 96, Part 1 (preprint).

Stoecker, W. F. 1957. How frost formation on coils affects refrigeration systems. Refrigerating Engineering, February 1957, pp. 42-46.

Stoecker, W. F. 1960. Frost formation on refrigeration coils. ASHRAE Transactions, Volume 66, pp. 91-103.

Tantakitti, C. and Howell, R. H. 1986. Air-to-air heat pumps operating under frosting conditions on the outdoor coil. ASHRAE Transactions, Volume 92, Part 1, pp. 827-842.

Trammell, G. J., Little, D. C., and Killgore, E. M. 1968. A study of frost formed on a flat plate held at sub-freezing temperatures. ASHRAE Journal, July 1968, pp. 42-47.

Wagner, Walter Berry. 1963. Frost Formation on an Extended Surface Heat Exchanger in Crossflow of Humid Air. Master of Science Thesis. Ohio State University.

Yamakawa, Norio; Takahashi, Nobuyuki; and Ohtani, Shigemori. Forced convection heat and mass transfer under frost conditions. Heat Transfer – Japanese Research, Volume 1, Number 2, April-June 1972, pp. 1-10.

Yasuda, H.; Senshu, T.; Kuroda, S.; Atsumi, A.; and Oguni. K. Heat pump performance under frosting conditions: part II – simulation of heat pump cycle characteristics under frosting conditions. ASHRAE Transactions, Volume 96, Part 1 (preprint).

APPENDIX A. Air Volumetric Flow Calculation

In determining the volumetric airflow rate, a simplified version of Bernoulli's equation was used. The basic Bernoulli equation may be expressed as

$$\frac{V_1^2}{2} + \frac{p_1}{\rho} = \frac{V_2^2}{2} + \frac{p_2}{\rho} \qquad (A.1)$$

where,

V = the velocity of the air,

p = the pressure of the air,

and

ρ = the density of the air.

The subscripts 1 and 2 represent the two separate chambers through which the fluid, air, is flowing. Location 1 is situated in the plenum after the evaporator. Location 2 is at the throat of the nozzle as shown in Figure A.1. L is the nozzle length and D is the nozzle throat diameter.

The density is determined by the ideal gas law for dry air:

$$\rho = \frac{P}{R\,T} \qquad (A.2)$$

where,

R = the ideal gas constant for air= 53.35 $[\frac{\text{ft-lb}_f}{\text{lb}_m\text{-R}}]$

and

T = the air temperature [R].

The moisture content was not included in the density calculation because at the low dry bulb temperatures which were dealt with here, even at the highest humidities encountered, the absolute water content of the air is negligible and does not significantly affect the density calculation.

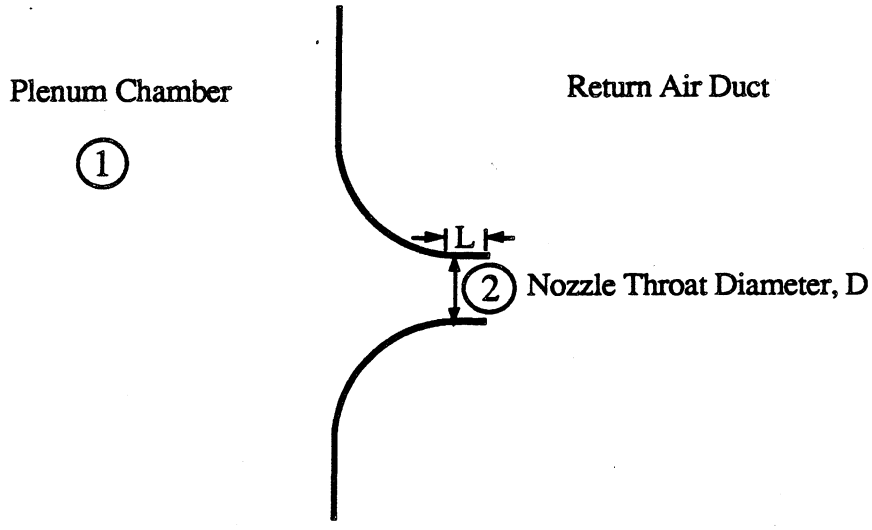

Figure A.1 Sketch of Air Loop Nozzle Configuration

Assuming that the velocity at location 1 is approximately zero, Equation A.1 may be simplified to:

$$\frac{p_1}{\rho} = \frac{V_2^2}{2} + \frac{p_2}{\rho} \quad . \tag{A.3}$$

This may be rewritten as

$$V_2 = \left(\frac{2\Delta p}{\rho}\right)^{\frac{1}{2}} \tag{A.4}$$

where,

Δp = the pressure drop between the two chambers.

The volumetric airflow rate, Q, may then be expressed as

$$Q = A_2 V_2 \qquad (A.5)$$

where,

A_2 = the nozzle throat area.

"Laboratory Methods of Testing Fans for Rating" (1985) suggests for nozzle flow that Q be expressed as a function of expansion factor, Y, the pressure drop, Δp [in. water], density, ρ [$\frac{lb_m}{ft^3}$], discharge coefficient, C, and nozzle exit area, A [ft^2] in the following manner:

$$Q = 1096\, Y \left(\frac{\Delta p}{\rho}\right)^{\frac{1}{2}} CA \qquad (A.5)$$

where,

$$C = 0.9986 - \frac{6.688}{Re^{\frac{1}{2}}} + \frac{131.5}{Re} \quad \text{for} \quad \frac{L}{D} = 0.5 \text{ and } Re > 12{,}000, \qquad (A.6)$$

$$Y = 1 - 0.548\,(1 - a) \quad \text{for} \quad b \approx 0, \qquad (A.7)$$

Re = Reynolds number $\left(\frac{\rho VD}{\mu}\right)$,

a = alpha ratio (ratio of absolute nozzle exit pressure to absolute approach pressure), and

b = beta ratio (ratio of nozzle exit diameter to the approach duct diameter).

An approximate Re is also given for $b \approx 0$, $C = 0.95$, $Y = 0.96$, and $\mu = 1.222 \times 10^{-5} \frac{lb_m}{ft\text{-}s}$ at a temperature of 68 F (20 C). It has the form:

$$Re = 1.363 \times 10^6 D \left(\frac{\Delta p}{\rho}\right)^{\frac{1}{2}}. \qquad (A.8)$$

An approximate expression for a is given as

$$a = 1 - 5.187 \frac{\Delta p}{\rho R T} . \qquad (A.9)$$

When more than one nozzle was used, the total volumetric airflow rate was determined by summing the individual volumetric airflow rates for each nozzle.

APPENDIX B. Experimental Data

In the data below, the first line of numbers at each hour consists of the date in terms of month, day, and year (e.g., the number 040690 represents April 6, 1990) and the average value for each of the 14 parameters listed below for 10 readings taken over a one-minute time span. The second line of data shows the standard deviation of each of the parameters over that same one-minute interval.

Definition of Abbreviations

RH: Relative Humidity [%]
TRI: Refrigerant Inlet Temperature [F]
TRO: Refrigerant Outlet Temperature [F]
DPI: Measured Inlet Dew Point [F]
DPO: Measured Outlet Dew Point [F]
TAI: Inlet Air Temperature [F]
ΔT: Air Side Temperature Drop [F]
CFM: Air Flow Rate [cfm]
RMF: Refrigerant Mass Flow [lb_m/min]
ΔP: Air Side Pressure Drop [in. water]
LL: Humidifier Liquid Level [cm]
PAM: Ambient Pressure [Psia]
X: Inlet Refrigerant Quality
---: Not Available

Baseline Case

Date	Hour	RH	TRI	TRO	DPI	DPO	TAI	ΔT	CFM	RMF	ΔP	LL	PAM	X
040690	0	54.5	-10.0	-10.9	-1.7	-----	10.0	14.1	40.2	0.34	0.011	6.40	14.7	0.12
Std Dev.		0.10	0.57	0.74	0.01	-----	0.07	0.26	1.03	0.00	-----	-----	-----	0.00
	1	51.7	-9.7	-10.7	-2.2	-----	10.6	14.5	40.5	0.34	0.014	6.30	-----	0.11
Std. Dev.		0.24	0.34	0.41	0.07	-----	0.05	0.17	0.77	0.00	-----	-----	-----	0.00
	2	52.5	-9.7	-10.7	-1.8	-----	10.7	14.7	40.0	0.34	0.015	6.15	-----	0.12
Std. Dev.		0.26	0.34	0.40	0.09	-----	0.06	0.15	0.95	0.00	-----	-----	-----	0.00
	3	52.9	-9.0	-10.1	-1.5	-----	11.0	14.5	40.6	0.34	0.015	6.00	-----	0.12
Std. Dev.		0.22	0.20	0.22	0.08	-----	0.06	0.09	0.64	0.00	-----	-----	-----	0.00
	4	52.3	-9.4	-10.4	-1.7	-----	10.9	14.8	39.7	0.35	0.016	5.90	-----	0.11
Std. Dev.		0.21	0.39	0.43	0.07	-----	0.06	0.19	0.60	0.00	-----	-----	-----	0.00
	5	52.3	-9.3	-10.2	-1.7	-----	10.9	14.7	40.0	0.34	0.016	5.80	-----	0.11
Std. Dev.		0.15	0.35	0.31	0.05	-----	0.05	0.21	0.58	0.00	-----	-----	-----	0.00
	6	51.0	-9.6	-10.7	-2.4	-----	10.7	14.7	41.6	0.34	0.017	5.70	-----	0.11
Std. Dev.		0.69	0.32	0.31	0.25	-----	0.06	0.15	0.65	0.00	-----	-----	-----	0.00
	7	52.2	-9.7	-10.6	-1.7	-----	10.9	15.0	41.7	0.34	0.019	5.50	-----	0.11
Std. Dev.		0.07	0.53	0.61	0.00	-----	0.07	0.26	0.96	0.00	-----	-----	-----	0.00

	8	52.2	-9.9	-11.0	-1.7	-----	10.9	15.0	41.4	0.34	0.019	5.40	-----	0.11
Std. Dev.		0.06	0.29	0.27	0.06	-----	0.06	0.14	0.55	0.00	-----	-----	-----	0.00
	9	52.5	-10.1	-11.3	-1.6	-----	11.0	15.3	41.5	0.34	0.019	5.30	-----	0.11
Std. Dev.		0.42	0.22	0.22	0.16	-----	0.06	0.16	0.56	0.00	-----	-----	-----	0.00
	10	52.0	-10.1	-11.2	-1.7	-----	11.0	15.3	41.5	0.34	0.020	5.15	-----	0.11
Std. Dev.		0.09	0.30	0.28	0.00	-----	0.06	0.19	0.79	0.00	-----	-----	-----	0.00
	11	52.0	-9.7	-10.8	-1.7	-----	11.0	15.1	41.4	0.34	0.020	5.00	-----	0.12
Std. Dev.		0.22	0.22	0.19	0.07	-----	0.06	0.16	0.78	0.00	-----	-----	-----	0.00

Date	Hour	RH	TRI	TRO	DPI	DPO	TAI	ΔT	CFM	RMF	ΔP	LL	PAM	X
051790	0	35.0	-10.5	-11.4	-9.5	-----	10.6	15.2	40.1	0.33	0.016	5.50	14.3	0.11
Std Dev.		0.29	0.31	0.30	0.15	-----	0.03	0.17	0.19	0.00	-----	-----	-----	0.00
	1	53.9	-9.8	-10.7	-2.3	-4.7	9.7	14.1	40.0	0.35	0.017	5.40	-----	0.11
Std. Dev.		0.40	0.32	0.33	0.14	0.07	0.03	0.21	0.20	0.00	-----	-----	-----	0.01
	2	53.6	-10.2	-11.1	-2.5	-6.1	9.6	14.4	40.0	0.35	0.019	5.25	-----	0.11
Std. Dev.		0.20	0.09	0.16	0.08	0.06	0.04	0.03	0.31	0.00	-----	-----	-----	0.00
	3	52.6	-9.3	-10.2	-3.0	-5.4	9.5	14.5	40.2	0.35	0.020	5.15	-----	0.08
Std. Dev.		0.06	0.09	0.06	0.00	0.00	0.03	0.03	0.36	0.00	-----	-----	-----	0.01
	4	51.2	-11.2	-12.2	-3.1	-6.4	9.8	15.2	40.1	0.34	0.020	5.00	-----	0.12
Std. Dev.		0.06	0.17	0.20	0.00	0.07	0.03	0.12	0.24	0.00	-----	-----	-----	0.00
	5	54.2	-10.7	-11.7	-1.8	-6.3	10.1	15.1	40.1	0.34	0.020	4.90	-----	0.12
Std. Dev.		0.19	0.15	0.23	-1.8	0.05	0.03	0.07	0.22	0.00	-----	-----	-----	0.00
	6	53.5	-10.3	-11.2	-2.0	-6.1	10.2	15.0	40.2	0.34	0.021	4.80	-----	0.11
Std. Dev.		0.27	0.25	0.25	0.10	0.00	0.03	0.13	0.20	0.00	-----	-----	-----	0.00
	7	54.1	-11.0	-12.1	-1.7	-6.0	10.2	15.4	40.0	0.34	0.024	4.65	-----	0.11
Std. Dev.		0.07	0.20	0.27	0.00	0.08	0.03	0.10	0.20	0.00	-----	-----	-----	0.00
	8	54.5	-9.4	-10.3	-1.4	-5.4	10.4	14.7	40.0	0.34	0.024	4.50	-----	0.12
Std. Dev.		0.19	0.34	0.36	0.05	0.05	0.03	0.21	0.28	0.00	-----	-----	-----	0.00
	9	51.3	-10.0	-10.9	-2.7	-5.4	10.3	15.0	40.1	0.35	0.025	4.40	-----	0.11
Std. Dev.		0.22	0.27	0.26	0.08	0.00	0.03	0.14	0.23	0.00	-----	-----	-----	0.00
	10	52.0	-10.5	-11.4	-2.4	-5.9	10.3	15.4	40.1	0.35	0.026	4.30	-----	0.10
Std. Dev.		0.16	0.36	0.46	0.05	0.00	0.03	0.20	0.27	0.00	-----	-----	-----	0.00

Date	Hour	RH	TRI	TRO	DPI	DPO	TAI	ΔT	CFM	RMF	ΔP	LL	PAM	X
060190	0	34.8	-10.2	-11.1	-10.1	-----	10.1	14.7	40.4	0.34	0.016	5.70	14.4	0.10
Std. Dev.		0.15	0.36	0.36	0.09	-----	0.04	0.22	0.19	0.00	-----	-----	-----	0.01
	1	57.5	-9.8	-10.8	-0.7	-4.3	10.1	14.4	40.3	0.34	0.019	5.50	-----	0.10
Std. Dev.		0.17	0.57	0.56	0.05	0.08	0.04	0.27	0.20	0.00	-----	-----	-----	0.00
	2	56.2	-9.8	-10.8	-1.3	-4.5	9.9	14.3	40.1	0.34	0.020	5.40	-----	0.10
Std. Dev.		0.23	0.43	0.52	0.09	0.10	0.04	0.24	0.22	0.00	-----	-----	-----	0.00

	3	54.0	-9.8	-10.9	-2.1	-4.9	9.9	14.4	40.0	0.34	0.021	5.30	-----	0.10
Std. Dev.		0.16	0.33	0.35	0.06	0.00	0.04	0.20	0.19	0.00	-----	-----	-----	0.00
	4	52.8	-9.6	-10.7	-2.5	-4.8	9.9	14.3	40.3	0.34	0.023	5.20	-----	0.11
Std. Dev.		0.25	0.52	0.59	0.08	0.09	0.05	0.22	0.31	0.00	-----	-----	-----	0.00
	5	52.3	-9.5	-10.5	-2.6	-5.1	10.0	14.2	40.4	0.34	0.024	5.05	-----	0.11
Std. Dev.		0.04	0.42	0.39	0.04	0.05	0.04	0.25	0.23	0.00	-----	-----	-----	0.00
	6	51.5	-9.7	-10.7	-2.9	-5.4	9.9	14.4	40.3	0.34	0.025	4.95	-----	0.11
Std. Dev.		0.07	0.46	0.43	0.07	0.00	0.05	0.26	0.20	0.00	-----	-----	-----	0.00
	7	51.8	-9.6	-10.5	-2.9	-5.2	9.9	14.4	40.4	0.34	0.026	4.80	-----	0.11
Std. Dev.		0.25	0.44	0.47	0.08	0.00	0.05	0.22	0.13	0.00	-----	-----	-----	0.00
	8	51.8	-9.2	-10.2	-2.7	-5.1	10.1	14.4	40.4	0.34	0.026	4.70	-----	0.11
Std. Dev.		0.24	0.29	0.28	0.09	0.00	0.04	0.18	0.17	0.00	-----	------	-----	0.00
	9	51.7	-9.7	-10.6	-2.4	-4.9	10.4	14.8	40.3	0.34	0.026	4.60	-----	0.14
Std. Dev.		0.06	0.61	0.68	-2.4	0.00	0.05	0.25	0.20	0.00	-----	------	-----	0.00
	10	51.5	-9.3	-10.3	-2.5	-4.7	10.4	14.6	40.4	0.34	0.027	4.45	-----	0.13
Std. Dev.		0.39	0.38	0.46	0.14	0.00	0.04	0.16	0.17	0.00	-----	-----	-----	0.00

72% Relative Humidity

Date	Hour	RH	TRI	TRO	DPI	DPO	TAI	ΔT	CFM	RMF	ΔP	LL	PAM	X
040990	0	33.2	-10.1	-10.9	-11.0	-----	10.0	14.2	41.0	0.34	0.010	4.75	14.7	0.12
Std Dev.		0.15	0.54	0.59	0.07	-----	0.08	0.27	0.86	0.00	-----	-----	-----	0.00
	1	73.2	-10.2	-11.2	3.5	-----	9.6	14.0	40.3	0.34	0.015	4.45	-----	0.11
Std. Dev.		0.33	0.27	0.30	0.09	-----	0.05	0.13	1.30	0.00	-----	-----	-----	-----
	2	69.2	-9.5	-10.5	3.4	-----	10.6	14.1	42.0	0.33	0.020	4.10	-----	0.11
Std. Dev.		0.26	0.26	0.24	0.08	-----	0.07	0.06	1.27	0.00	-----	-----	-----	0.00
	3	71.8	-9.8	-10.9	3.0	-----	9.5	13.9	39.8	0.33	0.020	3.80	-----	0.11
Std. Dev.		0.22	0.24	0.27	0.05	-----	0.05	0.07	0.74	0.22	-----	-----	-----	0.00
	4	72.6	-9.8	-10.9	3.1	-----	9.5	14.2	40.1	0.34	0.023	3.50	-----	0.12
Std. Dev.		0.47	0.51	0.51	0.11	-----	0.03	0.30	0.73	0.00	-----	-----	-----	0.00
	5	70.6	-10.7	-11.9	2.2	-----	9.0	14.5	40.3	0.33	0.026	3.20	-----	0.13
Std. Dev.		0.37	0.14	0.16	0.09	-----	0.03	14.5	1.02	0.00	-----	-----	-----	0.00
	6	70.3	-11.3	-12.4	2.6	-----	9.5	15.0	43.2	0.34	0.034	2.85	-----	0.08
Std. Dev.		0.40	0.18	0.16	0.09	-----	0.04	0.12	0.76	0.00	-----	-----	-----	0.00
	7	71.0	-11.8	-12.8	2.9	-----	9.6	15.8	41.6	0.33	0.037	2.50	-----	0.12
Std. Dev.		0.34	0.43	0.56	0.11	-----	0.05	0.19	0.97	0.00	-----	-----	-----	0.00
	8	71.1	-11.8	-12.9	2.9	-----	9.6	16.3	41.8	0.34	0.045	2.20	-----	0.12
Std. Dev.		0.33	0.28	0.42	0.09	-----	0.04	0.12	1.08	0.00	-----	-----	-----	0.00

	9	72.2	-11.0	-12.2	3.2	-----	9.6	16.2	41.6	0.34	0.056	1.80	-----	0.12
Std. Dev.		0.18	0.22	0.22	0.05	-----	0.05	0.17	0.59	0.00	-----	-----	-----	0.00
	10	70.9	-11.4	-12.8	2.8	-----	9.6	16.7	40.3	0.33	0.070	1.35	-----	0.12
Std. Dev.		0.11	0.32	0.32	0.00	-----	0.05	0.20	0.91	0.00	-----	-----	-----	0.00
	11	71.6	-10.8	-11.9	3.1	-----	9.7	16.8	40.4	0.34	0.085	1.10	-----	0.12
Std. Dev.		0.41	0.48	0.52	0.11	-----	0.05	0.23	1.11	0.00	-----	-----	-----	0.00

Date	Hour	RH	TRI	TRO	DPI	DPO	TAI	ΔT	CFM	RMF	ΔP	LL	PAM	X
051990	0	38.0	-10.5	-11.4	-9.2	-----	9.3	14.4	39.7	0.34	0.012	5.60	14.3	0.11
Std Dev.		0.22	0.50	0.64	0.12	-----	0.05	0.22	0.18	0.00	-----	-----	-----	0.00
	1	74.3	-10.1	-11.2	5.1	-3.5	11.0	14.9	39.5	0.34	0.015	5.30	-----	0.11
Std. Dev.		0.27	0.33	0.34	0.07	0.07	0.04	0.17	0.13	0.00	-----	-----	-----	0.00
	2	72.6	-9.7	-10.7	4.6	-3.7	10.9	14.7	39.8	0.34	0.020	4.90	-----	0.12
Std. Dev.		0.45	0.43	0.39	0.12	0.08	0.04	0.24	0.19	0.00	-----	-----	-----	0.00
	3	71.0	-10.2	-11.2	4.1	-3.5	10.8	14.9	40.5	0.33	0.026	4.60	-----	0.12
Std. Dev.		0.44	0.30	0.39	0.11	0.00	0.04	0.12	0.17	0.00	------	------	-----	0.00
	4	71.0	-9.4	-10.5	4.0	-3.3	10.8	14.7	40.2	0.33	0.033	4.30	-----	0.12
Std. Dev.		0.33	0.36	0.38	0.09	0.00	0.05	0.13	0.23	0.00	------	-----	-----	0.00
	5	72.2	-9.6	-10.7	4.4	-3.5	10.8	15.0	40.5	0.33	0.042	3.90	-----	0.13
Std. Dev.		0.29	0.23	0.22	0.90	0.01	0.05	0.17	0.26	0.00	-----	-----	-----	0.00
	6	71.4	-9.5	-10.7	4.1	-3.3	10.7	15.3	40.6	0.33	0.051	3.55	-----	0.13
Std. Dev.		0.31	0.30	0.31	0.08	0.09	0.04	0.16	0.16	0.00	-----	-----	-----	0.00
	7	70.6	-9.1	-10.1	3.8	-3.7	10.7	15.2	40.4	0.34	0.065	3.20	-----	0.10
Std. Dev.		0.26	0.27	0.29	0.07	0.01	0.04	0.13	0.13	0.00	-----	-----	-----	0.00
	8	73.0	-9.4	-10.4	4.5	-3.8	10.7	16.0	40.1	0.33	0.083	2.90	-----	0.13
Std. Dev.		0.28	0.24	0.21	0.07	0.08	0.03	0.14	0.22	0.00	-----	-----	-----	0.00
	9	72.9	-9.3	-10.3	4.5	-3.6	10.8	16.2	39.8	0.33	0.105	2.50	-----	0.14
Std. Dev.		0.24	0.27	0.23	0.08	0.09	0.05	0.17	0.16	0.00	-----	-----	-----	0.00
	10	70.9	-9.3	-10.4	3.8	-3.9	10.5	16.2	39.9	0.33	0.131	2.15	-----	0.14
Std. Dev.		0.12	0.36	0.37	0.00	0.05	0.05	0.15	0.27	0.00	-----	-----	-----	0.00

Date	Hour	RH	TRI	TRO	DPI	DPO	TAI	ΔT	CFM	RMF	ΔP	LL	PAM	X
052790	0	38.8	-10.6	-11.5	-7.7	------	10.4	15.3	39.9	0.34	0.013	5.60	14.3	0.11
Std. Dev.		0.28	0.30	0.38	0.14	------	0.03	0.15	0.31	0.00	-----	-----	-----	0.00
	1	73.3	-10.2	-11.2	4.3	-3.0	10.5	14.8	39.3	0.34	0.019	5.35	-----	0.12
Std. Dev.		0.32	0.58	0.62	0.08	0.13	0.04	0.26	0.16	0.00	-----	-----	-----	0.00
	2	71.8	-10.0	-11.0	3.8	-3.7	10.3	14.6	39.8	0.34	0.023	5.00	-----	0.11
Std. Dev.		0.08	0.32	0.36	0.00	0.08	0.03	0.15	0.24	0.00	-----	-----	-----	0.00
	3	72.0	-9.4	-10.4	3.8	-3.5	10.3	14.3	40.5	0.34	0.030	4.75	-----	0.11
Std. Dev.		0.28	0.24	0.27	0.07	0.05	0.04	0.10	0.19	0.00	-----	-----	-----	0.00
	4	72.1	-10.0	-11.0	3.7	-3.7	10.2	14.9	40.3	0.34	0.033	4.45	-----	0.11
Std. Dev.		0.30	0.46	0.51	0.08	0.09	0.05	0.20	0.13	0.00	-----	-----	-----	0.00

	5	71.9	-9.6	-10.7	3.7	-4.0	10.2	14.9	40.2	0.34	0.040	4.15	-----	0.11
Std. Dev.		0.35	0.38	0.36	0.09	0.08	0.03	0.22	0.11	0.00	-----	-----	-----	0.00
	6	72.8	-9.9	-11.1	3.9	-4.2	10.1	15.5	40.0	0.34	0.050	3.80	-----	0.12
Std. Dev.		0.30	0.32	0.31	0.08	0.14	0.03	0.18	0.17	0.00	-----	-----	-----	0.00
	7	72.7	-9.6	-10.8	3.7	-4.3	10.0	15.6	39.9	0.34	0.062	3.45	-----	0.12
Std. Dev.		0.34	0.26	0.32	0.09	0.09	0.03	0.11	0.20	0.00	-----	-----	-----	0.00
	8	72.4	-9.9	-11.1	3.6	-4.1	9.9	15.8	40.3	0.34	0.078	3.15	-----	0.11
Std. Dev.		0.07	0.27	0.26	0.00	0.12	0.03	0.18	0.20	0.00	-----	-----	-----	0.00
	9	71.6	-9.8	-10.9	3.4	-4.4	10.0	16.2	40.0	0.34	0.092	2.80	-----	0.12
Std. Dev.		0.09	0.15	0.19	0.00	0.10	0.03	0.06	0.24	0.00	-----	-----	-----	0.00
	10	71.8	-9.8	-10.9	3.4	-4.3	9.9	16.2	40.1	0.34	0.111	2.45	-----	0.12
Std. Dev.		0.27	0.22	0.21	0.08	0.07	0.04	0.14	0.16	0.00	-----	-----	-----	0.00
	11	71.8	-9.4	-10.5	3.3	-4.2	9.8	16.3	40.3	0.34	0.135	2.10	-----	0.12
Std. Dev.		0.34	0.21	0.18	0.09	0.07	0.03	0.13	0.23	0.00	-----	-----	-----	0.00
	12	72.9	-9.7	-10.8	4.4	-4.1	10.6	17.1	39.6	0.34	0.161	6.35/ 6.10	-----	0.12
Std. Dev.		0.34	0.29	0.27	0.09	0.14	0.02	0.12	0.09	0.00	-----	-----	-----	0.00
	13	72.2	-10.2	-11.2	4.1	-4.2	10.5	17.5	40.3	0.33	0.207	5.70	-----	0.10
Std. Dev.		0.25	0.38	0.38	0.07	0.05	0.03	0.16	0.17	0.00	-----	-----	-----	0.00
	14	72.3	-10.4	-11.5	4.1	-4.4	10.5	17.8	40.1	0.34	0.255	5.40	-----	0.10
Std. Dev.		0.08	0.12	0.12	0.00	0.08	0.03	0.10	0.13	0.00	-----	-----	-----	0.00
	15	72.4	-10.3	-11.3	4.1	-4.6	10.5	17.9	40.1	0.34	0.313	5.05	-----	0.10
Std. Dev.		0.46	0.33	0.29	0.14	0.08	0.04	0.18	0.18	0.00	-----	-----	-----	0.00
	16	72.1	-10.7	-11.7	4.1	-4.3	10.5	18.3	40.2	0.33	0.399	4.75	-----	0.11
Std. Dev.		0.25	0.24	0.28	0.07	0.07	0.04	0.09	0.28	0.00	-----	-----	-----	0.00
	17	72.3	-10.3	-11.4	4.3	-4.5	10.7	18.2	40.0	0.33	0.490	4.35	-----	0.11
Std. Dev.		0.47	0.07	0.07	0.12	0.07	0.02	0.01	0.19	0.00	-----	-----	-----	0.00
	18	72.1	-10.4	-11.5	4.2	-4.4	10.7	18.2	40.0	0.33	0.680	4.00	-----	0.11
Std. Dev.		0.30	0.22	0.21	0.08	0.11	0.03	0.13	0.26	0.00	-----	-----	-----	0.00
	19	73.2	-10.3	-11.3	4.6	-4.7	10.8	18.4	39.8	0.33	0.745	3.60	-----	0.11
Std. Dev.		0.32	0.30	0.28	0.07	0.07	0.03	0.14	0.26	0.00	-----	-----	-----	0.00
	20	72.1	-10.3	-11.4	4.3	-4.7	10.7	18.4	39.6	0.33	0.893	3.25	-----	0.11
Std. Dev.		0.13	0.16	0.14	0.00	0.07	0.04	0.05	0.15	0.00	-----	-----	-----	0.00
	21	72.4	-10.6	-11.6	4.1	-2.5	10.5	18.2	40.6	0.33	1.160	2.90	-----	0.12
Std. Dev.		0.09	0.12	0.13	0.00	0.09	0.03	0.04	0.13	0.00	-----	-----	-----	0.00
	22	71.5	-10.3	-11.4	4.0	-2.6	10.6	18.4	39.4	0.33	1.330	2.50	-----	0.12
Std. Dev.		0.41	0.19	0.23	0.12	0.10	0.03	0.06	0.33	0.00	-----	-----	-----	0.00
	23	72.2	-10.3	-11.3	4.3	-1.8	10.7	18.5	39.7	0.33	1.620	2.10	-----	0.12
Std. Dev.		0.27	0.20	0.18	0.07	0.08	0.03	0.11	0.30	0.00	-----	-----	-----	0.00
	24	72.4	-10.5	-11.6	4.3	-1.1	10.7	18.5	39.9	0.33	1.930	1.80	-----	0.12
Std. Dev.		0.10	0.20	0.22	0.00	0.19	0.04	0.13	0.33	0.00	-----	-----	-----	0.00

25 cfm

Date	Hour	RH	TRI	TRO	DPI	DPO	TAI	ΔT	CFM	RMF	ΔP	LL	PAM	X
052590	0	36.7	-10.7	-11.6	-8.9	-----	10.3	17.2	25.3	0.34	0.013	5.55	14.4	0.11
Std. Dev.		0.05	0.35	0.35	0.00	-----	0.03	0.26	0.09	0.00	-----	-----	-----	0.00
	1	55.7	-10.0	-10.8	-1.1	-5.7	10.3	16.7	25.3	0.34	0.013	5.45	-----	0.11
Std. Dev.		0.22	0.60	0.59	0.08	0.11	0.04	0.38	0.13	0.00	-----	-----	-----	0.01
	2	53.9	-9.9	-10.8	-1.5	-6.3	10.5	16.9	25.1	0.34	0.014	5.35	-----	0.12
Std. Dev.		0.21	0.23	0.25	0.08	0.00	0.03	0.13	0.07	0.00	-----	-----	-----	0.00
	3	52.6	-9.9	-10.8	-1.9	-6.2	10.5	17.0	25.1	0.33	0.014	5.25	-----	0.12
Std. Dev.		0.24	0.33	0.33	0.09	0.09	0.03	0.20	0.08	0.00	-----	-----	-----	0.00
	4	51.3	-10.1	-11.0	-2.4	-6.3	10.6	17.1	25.1	0.34	0.014	5.15	-----	0.12
Std. Dev.		0.25	0.20	0.22	0.08	0.00	0.04	0.12	0.13	0.00	------	-----	-----	0.00
	5	51.7	-9.9	-10.7	-2.3	-6.3	10.6	16.9	24.9	0.34	0.015	5.05	-----	0.12
Std. Dev.		0.31	0.18	0.18	0.11	0.08	0.03	0.12	0.12	0.00	-----	-----	-----	0.00
	6	51.4	-9.6	-10.5	-2.3	-6.3	10.6	16.9	24.8	0.34	0.015	5.00	-----	0.13
Std. Dev.		0.24	0.14	0.18	0.09	0.07	0.03	0.08	0.18	0.00	-----	-----	-----	0.00
	7	51.1	-10.3	-11.1	-2.6	-6.7	10.5	17.1	25.4	0.34	0.016	4.90	-----	0.12
Std. Dev.		0.38	0.11	0.17	0.15	0.08	0.03	0.06	0.11	0.00	-----	-----	-----	0.00
	8	52.3	-9.8	-10.7	-2.0	-6.4	10.6	16.9	25.4	0.34	0.016	4.80	-----	0.12
Std. Dev.		0.34	0.25	0.28	0.12	0.13	0.03	0.10	0.10	0.00	-----	-----	-----	0.00
	9	52.6	-9.8	-10.6	-1.7	-6.4	10.8	17.2	25.2	0.35	0.017	4.70	-----	0.11
Std. Dev.		0.07	0.40	0.38	0.00	0.07	0.04	0.22	0.14	0.00	-----	-----	-----	0.01
	10	52.3	-9.9	-10.8	-1.7	-6.4	10.9	17.4	25.2	0.35	0.017	4.60	-----	0.10
Std. Dev.		0.07	0.20	0.25	0.00	0.09	0.04	0.10	0.20	0.00	-----	-----	-----	0.01

80 cfm

Date	Hour	RH	TRI	TRO	DPI	DPO	TAI	ΔT	CFM	RMF	ΔP	LL	PAM	X
041190	0	55.4	-10.7	-13.4	-2.1	-----	9.3	12.2	79.7	0.46	0.035	5.65	14.5	0.12
Std. Dev.		1.67	0.68	0.75	0.60	-----	0.07	0.47	0.53	0.00	-----	-----	-----	0.00
	1	58.2	-8.4	-10.4	-0.7	-----	9.8	11.4	79.6	0.47	0.039	5.55	-----	0.11
Std. Dev.		0.41	0.15	0.19	0.14	-----	0.05	0.10	0.47	0.00	-----	-----	-----	0.00
	2	57.4	-8.4	-10.5	-1.1	-----	9.7	11.4	79.6	0.46	0.042	5.40	-----	0.12
Std. Dev.		0.26	0.19	0.27	0.08	-----	0.07	0.10	0.57	0.00	-----	-----	-----	0.00
	3	55.9	-8.5	-10.4	-1.7	-----	9.6	11.5	79.4	0.47	0.045	5.30	-----	0.11
Std. Dev.		0.29	0.41	0.40	0.08	-----	0.06	0.22	0.67	0.00	-----	-----	-----	0.00
	4	54.7	-8.2	-10.3	-2.1	-----	9.6	11.4	79.5	0.47	0.046	5.15	-----	0.11
Std. Dev.		0.07	0.21	0.25	0.00	-----	0.07	0.12	0.45	0.00	-----	-----	-----	0.00

	5	54.6	-8.6	-10.8	-2.1	-----	9.7	11.6	79.6	0.47	0.048	5.00	-----	0.11
Std. Dev.		0.52	0.10	0.08	0.21	-----	0.04	0.08	0.47	0.00	-----	-----	-----	0.00
	6	55.4	-8.7	-10.9	-1.8	-----	9.7	11.7	79.3	0.47	0.049	4.90	-----	0.11
Std. Dev.		0.16	0.17	0.17	0.05	-----	0.05	0.09	0.57	0.00	-----	-----	-----	0.00
	7	54.8	-8.5	-10.5	-1.8	-----	9.9	11.8	79.6	0.47	0.050	4.70	-----	0.11
Std. Dev.		0.17	0.34	0.41	0.07	-----	0.05	0.17	0.57	0.00	-----	-----	-----	0.00
	8	54.6	-8.5	-10.7	-1.8	-----	9.9	11.8	79.8	0.46	0.051	4.60	-----	0.11
Std. Dev.		0.25	0.19	0.31	0.08	-----	0.06	0.09	0.39	0.00	-----	-----	-----	0.00

Date	Hour	RH	TRI	TRO	DPI	DPO	TAI	ΔT	CFM	RMF	ΔP	LL	PAM	X
071090	0	35.0	-9.9	-10.9	-9.6	-----	10.5	12.0	80.4	0.47	0.038	5.75	14.4	0.10
Std. Dev.		0.13	0.23	0.29	0.07	-----	0.08	0.16	0.51	0.00	-----	-----	-----	0.00
	1	51.1	-10.4	-11.4	-2.9	-4.3	10.1	12.1	79.9	0.47	0.040	5.60	-----	0.09
Std. Dev.		0.19	0.19	0.24	0.08	0.12	0.08	0.08	0.64	0.00	-----	-----	-----	0.00
	2	51.4	-10.3	-11.4	-2.9	-4.4	10.0	12.0	79.9	-----	0.043	5.45	-----	0.10
Std. Dev.		0.27	0.30	0.21	0.09	0.05	0.06	0.10	0.72	-----	-----	-----	-----	0.00
	3	51.8	-10.1	-11.3	-2.6	-4.3	10.1	12.0	80.2	0.47	0.046	5.35	-----	0.11
Std. Dev.		0.04	0.26	0.35	0.00	0.09	0.08	0.15	0.48	0.00	-----	-----	-----	0.01
	4	51.6	-10.1	-11.1	-2.7	-4.3	10.2	12.0	79.9	0.47	0.049	5.15	-----	0.12
Std. Dev.		0.31	0.24	0.33	0.11	0.09	0.09	0.12	0.52	0.00	-----	-----	-----	0.00
	5	52.7	-9.8	-10.9	-2.3	-4.3	10.2	12.0	79.9	0.47	0.050	5.00	-----	0.12
Std. Dev.		0.33	0.17	0.22	0.12	0.08	0.08	0.09	0.44	0.00	-----	-----	-----	0.00
	6	51.9	-10.0	-11.1	-2.4	-3.9	10.3	12.1	79.7	0.47	0.052	4.90	-----	0.12
Std. Dev.		0.07	0.26	0.27	0.00	0.07	0.07	0.14	0.35	0.00	-----	-----	-----	0.01
	7	51.6	-9.8	-10.9	-2.4	-4.0	10.4	12.1	80.0	0.47	0.055	4.75	-----	0.11
Std. Dev.		0.10	0.18	0.23	0.00	0.07	0.08	0.09	0.55	0.00	-----	-----	-----	0.01
	8	51.5	-9.6	-11.0	-2.5	-3.9	10.4	12.1	80.1	0.47	0.057	4.60	-----	0.12
Std. Dev.		0.23	0.10	0.13	0.08	0.07	0.08	0.06	0.36	0.00	-----	-----	-----	0.00
	9	50.5	-10.2	-11.5	-3.0	-4.6	10.2	12.4	80.2	0.47	0.059	4.50	-----	0.11
Std. Dev.		0.25	0.22	0.22	0.09	0. 08	0.07	0.08	0.44	0.00	-----	-----	-----	0.00
	10	50.8	-10.3	-11.5	-2.9	-4.7	10.3	12.4	80.4	0.47	0.060	4.35	-----	0.09
Std. Dev.		0.23	0.22	0.23	0.08	0.06	0.08	0.09	0.44	0.00	-----	-----	-----	0.01

$T_{air,\ in}$ = 20 F

Date	Hour	RH	TRI	TRO	DPI	DPO	TAI	ΔT	CFM	RMF	ΔP	LL	PAM	X
041890	0	23.5	-9.8	-11.8	-8.1	-----	20.2	21.9	40.1	0.48	0.011	5.50	14.7	0.09
Std. Dev.		0.12	0.29	0.31	0.09	-----	0.06	0.17	0.92	0.00	-----	-----	-----	0.00

	1	51.9	-10.4	-12.6	6.6	-----	19.8	21.9	39.8	0.45	0.015	5.30	-----	0.11
Std. Dev.		0.06	0.31	0.29	0.00	-----	0.04	0.16	0.60	0.00	-----	-----	-----	0.00
	2	52.2	-9.1	-11.1	0.019	-----	20.1	21.4	40.0	0.46	0.019	4.80	-----	0.11
Std. Dev.		0.17	0.27	0.32	0.07	-----	0.06	0.16	0.84	0.00	-----	-----	-----	0.00
	3	51.8	-9.2	-11.2	6.6	-----	19.9	21.3	41.1	0.46	0.024	4.45	-----	0.11
Std. Dev.		0.50	0.15	0.21	0.19	-----	0.05	0.08	1.13	0.00	-----	-----	-----	0.00
	4	52.1	-8.8	-10.9	7.2	-----	20.4	21.5	40.7	0.46	0.029	4.00	-----	0.11
Std. Dev.		0.37	0.21	0.22	0.14	-----	0.07	0.17	0.82	0.00	-----	-----	-----	0.00
	5	51.5	-8.6	-10.8	6.9	-----	20.4	21.8	41.2	0.47	0.035	3.60	-----	0.11
Std. Dev.		0.69	0.12	0.15	0.28	-----	0.06	0.09	0.93	0.00	-----	-----	-----	0.00
	6	51.4	-8.6	-10.9	6.9	-----	20.4	22.2	40.8	0.47	0.041	3.20	-----	0.11
Std. Dev.		0.32	0.15	0.22	0.11	-----	0.06	0.09	1.04	0.00	-----	-----	-----	0.00
	7	50.2	-9.6	-12.0	6.4	-----	20.3	23.4	40.5	0.47	0.053	2.75	-----	0.11
Std. Dev.		0.23	0.18	0.21	0.07	-----	0.05	0.12	0.53	0.00	-----	-----	-----	0.00
	8	51.2	-9.8	-12.3	6.6	-----	20.2	24.0	41.0	0.47	0.068	2.30	-----	0.11
Std. Dev.		0.04	0.27	0.27	0.00	-----	0.05	0.16	1.04	0.00	-----	-----	-----	0.00
	9	50.5	-9.7	-12.1	6.3	-----	20.1	24.5	40.8	0.47	0.085	1.90	-----	0.11
Std. Dev.		0.27	0.19	0.25	0.08	-----	0.05	0.09	0.67	0.00	-----	-----	-----	0.00
	10	52.1	-9.8	-12.0	6.9	-----	20.1	24.9	40.6	0.47	0.110	1.50	-----	0.11
Std. Dev.		0.19	0.31	0.32	0.08	-----	0.05	0.19	0.69	0.00	-----	-----	-----	0.00

Date	Hour	RH	TRI	TRO	DPI	DPO	TAI	ΔT	CFM	RMF	ΔP	LL	PAM	X
052190	0	25.6	-10.0	-11.9	-6.8	-----	19.9	22.2	40.0	0.46	0.013	5.60	14.4	0.11
Std. Dev.		0.04	0.37	0.51	0.00	-----	0.04	0.22	0.16	0.00	-----	-----	-----	0.00
	1	53.1	-9.9	-12.1	7.2	-2.4	20.0	22.0	39.9	0.46	0.018	5.30	-----	0.12
Std. Dev.		0.23	0.15	0.23	0.07	0.00	0.03	0.10	0.15	0.00	-----	-----	-----	0.00
	2	52.3	-10.1	-12.2	7.0	-2.4	20.1	22.4	39.8	0.45	0.021	4.90	-----	0.12
Std. Dev.		0.23	0.30	0.41	0.09	0.07	0.03	0.17	0.19	0.00	-----	-----	-----	0.00
	3	52.8	-9.4	-11.4	7.3	-2.5	20.2	22.3	39.8	0.45	0.028	4.55	-----	0.12
Std. Dev.		0.13	0.31	0.31	0.06	0.08	0.02	0.23	0.22	0.00	-----	-----	-----	0.00
	4	52.6	-9.3	-11.4	7.1	-2.7	20.1	22.6	40.1	0.45	0.037	4.10	-----	0.12
Std. Dev.		0.05	0.24	0.23	0.00	0.09	0.03	0.15	0.27	0.00	-----	-----	-----	0.00
	5	51.3	-9.7	-11.9	6.5	-2.5	20.0	23.1	40.1	0.45	0.049	3.70	-----	0.13
Std. Dev.		0.23	0.18	0.22	0.09	0.07	0.03	0.17	0.28	0.00	-----	-----	-----	0.00
	6	50.6	-9.1	-11.2	6.1	-2.4	19.9	23.1	40.1	0.45	0.059	3.30	-----	0.12
Std. Dev.		0.22	0.25	0.28	0.09	0.00	0.03	0.15	0.09	0.00	-----	-----	-----	0.00
	7	51.3	-9.7	-11.9	6.4	-2.8	19.9	23.9	40.1	0.45	0.072	2.95	-----	0.13
Std. Dev.		0.21	0.14	0.21	0.08	0.12	0.03	0.13	0.17	0.00	-----	-----	-----	0.00
	8	51.9	-9.4	-11.7	6.7	-2.6	20.0	24.3	39.9	0.45	0.094	2.55	-----	0.13
Std. Dev.		0.20	0.26	0.30	0.08	0.07	0.03	0.14	0.27	0.00	-----	-----	-----	0.00
	9	51.5	-9.3	-11.5	6.7	-2.6	20.1	24.9	39.7	0.45	0.124	2.15	-----	0.13
Std. Dev.		0.42	0.20	0.20	0.16	0.07	0.03	0.13	0.25	0.00	-----	-----	-----	0.00

	10	52.0	-9.6	-11.8	6.8	-2.8	20.1	25.3	40.0	0.45	0.164	1.70	-----	0.13
Std. Dev.		0.30	0.17	0.14	0.12	0.00	0.03	0.08	0.27	0.00	-----	-----	-----	0.00

Date	Hour	RH	TRI	TRO	DPI	DPO	TAI	ΔT	CFM	RMF	ΔP	LL	PAM	X
071590	0	28.3	-9.7	-10.4	-5.3	-----	19.5	20.8	39.9	0.46	0.016	5.70	14.3	0.09
Std. Dev.		0.13	0.31	0.32	0.08	-----	0.06	0.23	0.24	0.00	-----	-----	-----	0.00
	1	50.5	-9.8	-10.9	6.7	1.5	20.5	21.2	40.1	0.46	0.021	5.30	-----	0.10
Std. Dev.		0.23	0.44	0.45	0.08	0.18	0.08	0.24	0.16	0.00	-----	-----	-----	0.00
	2	53.3	-10.1	-11.0	7.2	0.7	19.9	21.3	40.1	0.46	0.026	4.85	-----	0.11
Std. Dev.		0.35	0.14	0.14	0.12	0.00	0.07	0.05	0.19	0.00	-----	-----	-----	0.00
	3	48.9	-9.6	-10.8	6.3	0.8	20.7	22.0	40.1	0.46	0.033	4.45	-----	0.12
Std. Dev.		0.20	0.23	0.24	0.08	0.10	0.07	0.10	0.12	0.00	-----	-----	-----	0.00
	4	50.1	-10.2	-11.3	6.6	1.1	20.5	22.7	40.0	0.46	0.041	4.05	-----	0.11
Std. Dev.		0.06	0.21	0.26	0.01	0.00	0.06	0.15	0.18	0.00	-----	-----	-----	0.00
	5	51.4	-10.2	-11.3	7.0	0.7	20.5	23.6	40.0	0.45	0.053	3.55	-----	0.11
Std. Dev.		0.23	0.24	0.31	0.08	0.05	0.05	0.12	0.26	0.00	-----	-----	-----	0.00
	6	52.4	-9.9	-11.2	7.0	0.4	20.0	23.7	39.8	0.45	0.069	3.10	-----	0.12
Std. Dev.		0.35	0.26	0.32	0.13	0.00	0.06	0.13	0.22	0.00	-----	-----	-----	0.00
	7	50.7	-9.7	-10.9	6.6	1.0	20.3	24.3	40.1	0.45	0.089	2.60	-----	0.12
Std. Dev.		0.07	0.20	0.16	0.00	0.11	0.06	0.13	0.21	0.00	-----	-----	-----	0.00
	8	51.5	-10.0	-11.2	6.4	0.4	19.8	24.5	40.1	0.45	0.116	2.60	-----	0.12
Std. Dev.		0.21	0.14	0.18	0.09	0.05	0.04	0.10	0.25	0.00	-----	-----	-----	0.00
	9	49.9	-10.0	-11.2	6.3	0.2	20.3	25.3	40.0	0.45	0.145	2.20	-----	0.13
Std. Dev.		0.43	0.24	0.32	0.16	0.14	0.04	0.11	0.20	0.00	-----	-----	-----	0.00
	10	50.4	-10.3	-11.5	6.3	0.0	20.1	25.6	39.8	0.45	0.185	1.30	-----	0.13
Std. Dev.		0.52	0.20	0.26	0.20	0.07	0.05	0.08	0.21	0.00	-----	-----	-----	0.00

Date	Hour	RH	TRI	TRO	DPI	DPO	TAI	ΔT	CFM	RMF	ΔP	LL	PAM	X
071990	0	29.4	-10.4	-11.3	-5.1	-----	19.0	20.8	39.9	0.46	0.018	5.70	14.5	0.09
Std. Dev.		0.25	0.42	0.43	0.16	-----	0.08	0.24	0.21	0.00	-----	-----	-----	0.00
	1	50.8	-9.9	-10.8	6.4	1.8	20.1	21.2	39.8	0.46	0.021	5.40	-----	0.10
Std. Dev.		0.42	0.29	0.27	0.16	0.00	0.09	0.17	0.19	0.00	-----	-----	-----	0.00
	2	49.0	-9.9	-10.7	5.5	0.6	19.9	21.0	40.2	0.46	0.025	5.00	-----	0.10
Std. Dev.		0.05	0.24	0.26	0.00	0.11	0.08	0.13	0.22	0.00	-----	-----	-----	0.00
	3	50.0	-10.1	-10.9	6.0	0.5	20.0	21.4	40.3	0.46	0.030	4.65	-----	0.11
Std. Dev.		0.20	0.18	0.23	0.07	0.11	0.10	0.05	0.19	0.00	-----	-----	-----	0.00
	4	50.3	-9.9	-10.8	6.2	0.0	20.1	21.6	40.1	0.46	0.035	4.30	-----	0.11
Std. Dev.		0.12	0.17	0.20	0.05	0.00	0.08	0.11	0.28	0.00	-----	-----	-----	0.00
	5	50.3	-9.9	-10.9	6.0	0.6	20.0	22.0	40.2	0.46	0.043	3.85	-----	0.12
Std. Dev.		0.06	0.18	0.16	0.00	0.00	0.04	0.11	0.17	0.00	-----	-----	-----	0.00
	6	49.9	-9.9	-11.0	5.9	0.5	19.9	22.5	40.2	0.45	0.053	3.40	-----	0.12
Std. Dev.		0.19	0.15	0.18	0.08	0.08	0.08	0.13	0.21	0.00	-----	-----	-----	0.00

	7	50.9	-9.6	-10.7	6.4	0.4	20.0	23.0	40.2	0.47	0.067	2.95	-----	0.10
Std. Dev.		0.09	0.24	0.29	0.00	0.07	0.10	0.10	0.25	0.00	-----	-----	-----	0.01
	8	49.9	-9.8	-10.9	6.1	0.6	20.2	23.8	39.9	0.46	0.088	2.55	-----	0.10
Std. Dev.		0.26	0.23	0.27	0.09	0.05	0.09	0.11	0.19	0.00	-----	-----	-----	0.00
	9	50.8	-10.0	-11.1	6.5	0.3	20.2	24.5	40.2	0.46	0.113	2.10	-----	0.11
Std. Dev.		0.28	0.17	0.17	0.09	0.09	0.10	0.09	0.20	0.00	-----	-----	-----	0.00
	10	50.4	-9.8	-10.9	6.3	0.8	20.2	24.7	39.8	0.46	0.149	1.65	-----	0.11
Std. Dev.		0.40	0.24	0.26	0.17	0.14	0.10	0.10	0.15	0.00	-----	-----	-----	0.00

$T_{ref.\ in}$ = -20 F

Date	Hour	RH	TRI	TRO	DPI	DPO	TAI	ΔT	CFM	RMF	ΔP	LL	PAM	X
042390	0	24.9	-19.3	-22.0	-15.8	-----	10.3	21.5	40.2	0.46	0.015	5.70	14.4	0.10
Std. Dev.		0.13	0.37	0.33	0.08	-----	0.06	0.26	0.78	0.00	-----	-----	-----	0.00
	1	50.0	-19.7	-22.7	-3.8	-----	9.6	21.3	39.9	0.46	0.019	5.40	-----	0.11
Std. Dev.		0.22	0.42	0.47	0.07	-----	0.06	0.26	1.32	0.00	-----	-----	-----	0.00
	2	54.6	-19.6	-22.8	-1.4	-----	10.4	21.8	40.1	0.46	0.022	5.20	-----	0.11
Std. Dev.		0.20	0.27	0.32	0.07	-----	0.06	0.17	1.16	0.00	-----	-----	-----	0.00
	3	52.1	-18.8	-21.7	-2.3	-----	10.4	21.6	39.5	0.47	0.027	4.90	-----	0.11
Std. Dev.		0.36	0.46	0.54	0.13	-----	0.06	0.27	0.87	0.00	-----	-----	-----	0.00
	4	51.4	-19.4	-22.5	-2.8	-----	10.2	21.9	40.3	0.46	0.031	4.65	-----	0.11
Std. Dev.		0.07	0.18	0.20	0.00	-----	0.06	0.15	1.09	0.00	-----	-----	-----	0.00
	5	51.0	-19.4	-22.4	-2.9	-----	10.2	22.4	39.8	0.46	0.036	4.35	-----	0.11
Std. Dev.		0.23	0.30	0.52	0.08	-----	0.06	0.16	0.70	0.00	-----	-----	-----	0.00
	6	52.0	-18.8	-21.6	-2.5	-----	10.1	22.2	40.0	0.46	0.040	4.10	-----	0.10
Std. Dev.		0.22	0.25	0.29	0.08	-----	0.05	0.18	0.93	0.00	-----	-----	-----	0.00
	7	53.6	-18.6	-21.8	-1.8	-----	10.3	22.7	39.5	0.46	0.050	3.80	-----	0.11
Std. Dev.		0.04	0.22	0.27	0.00	-----	0.06	0.13	0.72	0.00	-----	-----	-----	0.00
	8	52.6	-18.7	-21.8	-2.0	-----	10.4	23.2	40.5	0.46	0.065	3.50	-----	0.11
Std. Dev.		0.10	0.21	0.28	0.00	-----	0.06	0.16	0.80	0.00	-----	-----	-----	0.00
	9	52.2	-18.9	-21.9	-2.4	-----	10.2	23.6	40.9	0.46	0.076	3.20	-----	0.11
Std. Dev.		0.24	0.17	0.30	0.07	-----	0.05	0.11	0.97	0.00	-----	-----	-----	0.00
	10	47.5	-19.0	-22.0	-4.3	-----	10.1	23.9	41.2	0.45	0.090	3.00	-----	0.11
Std. Dev.		0.04	0.21	0.32	0.00	-----	0.05	0.11	0.71	0.00	-----	-----	-----	0.00

Date	Hour	RH	TRI	TRO	DPI	DPO	TAI	ΔT	CFM	RMF	ΔP	LL	PAM	X
052390	0	24.9	-20.1	-23.0	-15.8	-----	10.4	22.3	40.0	0.45	0.011	5.60	14.4	0.10
Std. Dev.		0.09	0.28	0.30	0.05	-----	0.03	0.20	0.17	0.00	-----	-----	-----	0.00

	1	55.7	-19.9	-22.8	-0.9	-11.6	10.5	22.1	39.8	0.46	0.014	5.35	-----	0.10
Std. Dev.		0.29	0.32	0.63	0.09	0.00	0.04	0.19	0.13	0.00	-----	-----	-----	0.00
	2	52.5	-19.5	-22.4	-1.7	-11.4	10.8	22.3	39.9	0.46	0.019	5.05	-----	0.10
Std. Dev.		0.05	0.52	0.69	0.00	0.05	0.03	0.26	0.18	0.00	-----	-----	-----	0.00
	3	51.9	-19.0	-22.0	-1.9	-11.7	10.9	22.1	40.0	0.45	0.023	4.80	-----	0.10
Std. Dev.		0.06	0.25	0.38	0.00	0.07	0.03	0.13	0.15	0.00	-----	-----	-----	0.00
	4	52.3	-19.2	-22.2	-1.8	-11.9	10.9	22.7	39.8	0.46	0.027	4.55	-----	0.11
Std. Dev.		0.23	0.25	0.21	0.08	0.09	0.03	0.17	0.21	0.00	-----	-----	-----	0.00
	5	53.2	-19.0	-22.0	-1.4	-11.6	10.9	22.9	39.7	0.46	0.033	4.30	-----	0.11
Std. Dev.		0.28	0.20	0.21	0.09	0.05	0.04	0.17	0.22	0.00	-----	-----	-----	0.00
	6	52.5	-19.1	-22.1	-1.7	-11.6	10.8	23.5	39.6	0.46	0.041	4.00	-----	0.11
Std. Dev.		0.05	0.51	0.55	0.00	0.08	0.02	0.32	0.16	0.00	-----	-----	-----	0.00
	7	52.3	-18.7	-21.8	-2.0	-11.8	10.6	23.5	40.2	0.46	0.050	3.70	-----	0.11
Std. Dev.		0.32	0.20	0.30	0.10	0.09	0.03	0.14	0.21	0.00	-----	-----	-----	0.00
	8	52.8	-18.5	-21.8	-1.7	-11.9	10.8	23.9	40.0	0.46	0.061	3.40	-----	0.11
Std. Dev.		0.27	0.38	0.52	0.08	0.09	0.03	0.19	0.20	0.00	-----	-----	-----	0.00
	9	51.9	-19.0	-22.1	-1.9	-12.0	10.8	24.7	40.3	0.46	0.073	3.10	-----	0.11
Std. Dev.		0.26	0.26	0.47	0.09	0.09	0.03	0.12	0.26	0.00	-----	-----	-----	0.00
	10	50.6	-18.6	-21.9	-2.4	-12.1	10.9	24.7	40.1	0.45	0.086	2.85	-----	0.12
Std. Dev.		0.20	0.33	0.46	0.07	0.07	0.03	0.16	0.17	0.00	-----	-----	-----	0.00

APPENDIX C.

C.1 Sample Data Summary Sheet

Test Number:051790.1
Notes: Frost
Date: 5/17/90
Time: 11:23 AM

********** Evaporator Parameters **********

Sample Number: 1.0
Number of Fins: 106
Tube Diameter: 0.375 in.
Tube Wall Thickness: 0.0280 in.
Fin Thickness: 0.0075 in.
Evaporator Weight: 2.30 lbs.

********** Test Conditions **********

1/2 in. nozzle: Open
1 in. nozzle: Open
2 in. nozzle: Closed
Atmospheric P (psia): 14.33
Room T (F): 73.53
Freezer T (F): 0.98
DP Nozzles (in.H2O): 2.57
Air In (F): 10.59
Air Flow (CFM): 40.13

********** Evaporator Performance Summary **********

Effectiveness: 0.720
Superheat: 2.80 F
Qref: 1227 Btu/hr
Air Outlet Temperature: -4.5 F
Qair: 709 Btu/hr
Air Inlet Temperature: 10.6 F
Q Difference: 42.2 %
Refrigerant Inlet Temperature: -10.5 F
UA: 59.4 Btu/hr/F
Refrigerant Outlet Temperature: -11.4 F
Air Mass Flow: 3.24 lbm/min
Delta T Air: 15.2 F
Refrigerant Mass Flow: 0.329 lbm/min
Refrigerant Quality: 0.110

********** Recorded Test Data **********

	Average:	Standard Deviation:
Air Flow (CFM)	40.1	0.19
Refrigerant Flow (lbm/min)	0.329	0.00
Relative Humidity (%)	35.0	0.29
Dew point (F)	-9.5	0.15
Evaporator Press. Drop (in WC)	0.015	0.00
Air Inlet Average (F)	10.6	0.03
Air Outlet (F)	-4.5	0.06
Refrigerant Inlet (F)	-10.5	0.31
Refrigerant Outlet (F)	-11.4	0.30
Superheat (F)	2.8	0.21
Refrigerant Inlet (psia)	19.8	0.12
Refrigerant Outlet (psia)	17.6	0.14
Refrigerant before TEV (F)	26.8	0.38
Refrigerant before TEV (psia)	89.6	0.12
Refrigerant Quality	0.110	0.00
Return Air (F)	4.7	0.03
Air Delta P (in.)	2.57	0.02
Air Delta T (F)	15.2	0.17
Freezer T (F)	1.0	0.05

Air Flow (CFM):	40.0	40.5	40.2	40.2	39.9	39.8	40.3	40.0	40.3	40.2
Refrigerant Flow (lbm/min):	0.327	0.327	0.328	0.332	0.329	0.329	0.329	0.329	0.329	0.328
Relative Humidity (%):	35.3	35.4	35.3	35.1	35.0	35.0	34.7	34.7	34.6	34.7
Dew Point (F):	-9.3	-9.3	-9.3	-9.5	-9.5	-9.5	-9.6	-9.6	-9.7	-9.7
Evap. Press. Drop (in WC):	0.016	0.012	0.014	0.010	0.012	0.010	0.016	0.018	0.014	0.024
Air Inlet Average (F):	10.6	10.6	10.6	10.6	10.6	10.6	10.6	10.6	10.6	10.6
Refrigerant Inlet (F):	-10.6	-10.4	-10.3	-10.1	-10.2	-10.4	-10.7	-10.7	-10.9	-11.1

Refrigerant Outlet (F):	-11.6	-11.3	-11.2	-11.0	-11.0	-11.3	-11.2	-11.5	-11.7	-12.0
Superheat (F):	3.0	3.0	3.0	2.6	2.9	2.8	2.3	2.8	2.9	2.6
Refrigerant Inlet (psia):	19.8	19.9	19.9	20.0	19.9	19.9	19.8	19.7	19.7	19.6
Refrigerant Outlet (psia):	17.5	17.6	17.6	17.8	17.7	17.6	17.8	17.5	17.4	17.4
Refrigerant before TEV (F):	26.3	26.7	27.2	27.0	27.4	26.9	26.7	26.4	26.4	26.4
Refrigerant Quality:	0.109	0.110	0.111	0.110	0.112	0.111	0.110	0.110	0.110	0.111
Return Air (F):	4.7	4.7	4.7	4.7	4.7	4.7	4.8	4.7	4.7	4.7
Air Delta P (in.):	2.6	2.6	2.6	2.6	2.5	2.5	2.6	2.6	2.6	2.6
Air Delta T (F):	15.1	15.1	15.0	15.0	15.1	15.2	15.3	15.4	15.4	15.5
Freezer T (F):	0.9	0.9	1.0	1.0	1.1	1.0	1.0	0.9	1.0	1.0

C.2 Sample ImageWriter Output

In the output shown below, the values for the ten parameters listed are given at each minute of testing. The time of day is shown in hours and minutes.

Definition on Abbreviations

Tairin:	Inlet Air Temperature [F]	TTEV:	Refrigerant Temperature Before the Main Expansion Valve [F]
UA:	Overall Evaporator Heat Transfer Coefficient [Btu/hr-F]	CFM:	Airflow Rate [cfm]
Trefin:	Refrigerant Inlet Temperature [F]	Qair:	Heat Transfer from the Air [Btu/hr]
relh:	Inlet Air Relative Humidity [%]	mdotr:	Refrigerant Flow Rate [lb_m/hr]
dewpt:	Inlet Air Dew Point [F]	X:	Inlet Refrigerant Quality

Date: 5/21/90

Time	Tairin	UA	Trefin	relh	dewp	TTEV	CFM	Qair	mdotr	X
12:02	20.17	60.50	-9.31	47.51	7.10	30.58	39.663	958.26	0.453	0.118
12:03	20.19	59.81	-9.71	47.60	7.27	30.69	39.682	966.14	0.450	0.119
12:04	20.11	60.27	-9.42	47.58	7.09	29.82	39.623	957.58	0.453	0.115
12:05	20.17	60.48	-9.98	47.61	7.09	31.10	40.852	995.06	0.455	0.121
12:06	20.16	61.48	-9.02	47.41	7.09	33.17	40.116	961.25	0.452	0.125
12:07	20.17	58.91	-10.21	47.64	6.74	32.18	39.577	973.59	0.449	0.125
12:08	20.16	61.27	-8.84	47.54	7.09	30.56	39.814	949.74	0.452	0.116
12:09	20.19	60.91	-9.81	47.67	7.27	31.68	40.349	986.79	0.451	0.123
12:10	20.12	60.94	-9.18	47.64	7.10	30.67	40.037	960.16	0.453	0.118
12:11	20.12	61.05	-9.90	47.62	7.27	33.30	40.189	986.67	0.452	0.128
12:12	20.13	61.22	-9.42	47.64	6.92	31.32	40.496	975.86	0.451	0.120
12:13	20.13	61.35	-9.63	47.66	7.09	31.12	40.228	980.99	0.453	0.121
12:14	20.11	60.69	-9.62	47.85	7.27	32.13	40.303	975.43	0.451	0.123
12:15	20.16	61.22	-9.44	47.74	7.27	32.02	40.241	974.05	0.452	0.122
12:16	20.14	60.71	-9.69	47.91	7.09	31.77	40.199	977.10	0.452	0.123
12:17	20.12	61.70	-9.02	47.77	7.09	31.10	39.936	958.80	0.453	0.118
12:18	20.16	60.12	-9.80	47.97	7.09	31.39	39.863	972.70	0.452	0.122
12:19	20.17	60.86	-9.04	47.75	7.27	31.44	39.730	952.01	0.453	0.120
12:20	20.12	61.55	-9.87	47.73	6.92	33.51	40.149	988.44	0.451	0.128
12:21	20.19	60.22	-9.49	47.71	6.75	31.14	40.041	966.98	0.452	0.120
12:23	20.11	62.03	-9.38	47.66	6.92	31.32	40.030	974.26	0.451	0.120
12:24	20.13	60.92	-9.72	47.79	7.27	31.46	40.117	978.80	0.451	0.122
12:25	20.16	62.00	-9.24	47.61	7.27	33.01	40.110	971.69	0.448	0.125
12:26	20.16	60.96	-9.89	47.89	7.09	30.97	40.317	987.57	0.451	0.121
12:27	20.18	61.16	-9.02	47.78	7.09	31.12	39.918	956.34	0.451	0.119
12:28	20.17	60.95	-9.76	47.88	7.27	31.55	40.311	983.69	0.450	0.121
12:29	20.15	62.65	-8.82	47.77	7.27	32.43	40.068	961.37	0.451	0.123
12:30	20.14	61.64	-10.10	47.85	7.09	33.03	40.371	1000.16	0.447	0.127
12:31	20.21	60.62	-9.18	47.81	4.82	30.65	39.784	956.85	0.451	0.118